Modeling and Manufacturing of Vocal Folds: First Steps Towards the Development of an Active Voice-Box Prosthesis

W. Garret Burks

Dissertation submitted to the Faculty of the
Virginia Polytechnic Institute and State University
in partial fulfillment of the requirements for the degree of

Doctor of Philosophy
in
Mechanical Engineering

Alexander Leonessa, Chair
Raffaella De Vita, Co-Chair
Blake Johnson
Rolf Mueller
Pablo A. Tarazaga

December 13, 2019
Blacksburg, Virginia

Keywords: Vocal Folds, Larynx, Elastic Modulus, Phonation

Modeling and Manufacturing of Vocal Folds: First Steps Towards the Development of an Active Voice-Box Prosthesis

W. Garret Burks

(ABSTRACT)

The movement and control of the vocal folds within the laryngeal cavity enables three crucial physiological functions: 1) allowing respiration by opening, 2) aiding in airway protection by closing, and 3) regulating sound production during phonation. Although treatment options have improved, many of the estimated 7.5 million individuals in the United States who are annually affected by voice-related disorders still face serious challenges related to dysphonia and dysphagia. The need for improved voice-disorder treatments has motivated the work presented in this dissertation which focuses on modeling and manufacturing the vocal folds and aims to answer three main questions: 1) what are the mechanical properties of the vocal folds and how do they change across the full vocal range? 2) how do those properties influence the dynamic behavior of the tissue? and 3) can we manufacture a synthetic vocal fold model that exhibits a desired and controllable dynamic behavior? First, the elastic properties of sixteen porcine vocal folds were evaluated through uniaxial tensile tests on a custom built experimental setup. Stress-strain data was analyzed using an optimization method to yield continuous model parameters which described the linear and nonlinear elastic regions as well as transition points between those regions. Next, the impact of the vocal fold elastic properties on the frequencies of vibration was evaluated through dynamic tests on excised porcine larynges. Sound data was analyzed via a spectrogram and through the use of fast Fourier transforms to study changes in the frequency of vibration while the vocal folds were stretched. Additionally, a mathematical aeroelastic model of phonation was implemented to further evaluate the changing elastic properties on vocal fold dynamics. Next, eight synthetic vocal fold models were created, each with varying mechanical properties and a geometry based on reported anatomical measurements of porcine vocal folds. The synthetic models were then dynamically tested to further study the impact of changes in mechanical properties on the dynamic behavior of the synthetic vocal folds.

Modeling and Manufacturing of Vocal Folds: First Steps Towards the Development of an Active Voice-Box Prosthesis

W. Garret Burks

(GENERAL AUDIENCE ABSTRACT)

The movement and control of the vocal folds within the voice-box enables three crucial physiological functions: 1) allowing respiration by opening, 2) aiding in airway protection and swallowing by closing, and 3) regulating sound production during vocalization. Although treatment options have improved, many of the estimated 7.5 million individuals in the United States who are annually affected by voice-related disorders still face serious challenges related to speech production and swallowing which often results in significant detrimental impacts to quality of life. The need for improved treatments is most easily observed in the evaluation of treatment options following a total laryngectomy, which is a procedure where the entire voice-box is removed often due to cancer. Following a laryngectomy, all three of the vital functions of the vocal folds are immediately impacted as patients adjust to breathing through and protecting a redirected airway and are forced to use alternative methods of speech production which often result in monotone or robotic-sounding speech. The need for improved voice-disorder treatments has motivated the work presented in this dissertation which focuses on modeling and manufacturing the vocal folds and aims to answer three main questions: 1) what are the mechanical properties of the vocal folds? 2) how do those properties influence the dynamic behavior of the tissue during sound production? and 3) can we manufacture synthetic vocal folds that produce a desired and controllable dynamic behavior? Sixteen porcine vocal fold samples were mechanical tested to evaluate the elastic properties of the tissue. Next, porcine voice-box samples were experimentally tested in a way that simulated sound production by subjecting the samples to a heated and humidified air flow, similar to the air flow conditions coming out of the lungs. In this way, the relationship between the tissue properties and the frequencies of sound was investigated. Lastly, the synthetic vocal fold samples were evaluated using a similar experimental protocol to further investigate the impact of changing structural properties on the dynamics of the vocal folds during sound production.

Dedication

This work is dedicated to my wife, Rachel, for her endless love and encouragement, her patience and support, and the daily inspiration that she provides me, to my parents, Ben and Sandra Burks, for their unconditional love and unwavering support, and to my advisor, Dr. Alexander Leonessa for investing in me with his time and energy, for imparting his knowledge, and offering guidance throughout my educational endeavors.

Acknowledgments

First, I would like to thank my advisors, Dr. Alexander Leonessa and Dr. Raffaella De Vita, for the vital role they have played in this work and in my education. Since early in my undergraduate studies, Dr. Leonessa has supported, guided, and encouraged me in my academic pursuits. I am incredibly thankful for his mentorship, his insight and feedback which has improved the quality of my work, and for his friendship. Similarly, throughout my time as a graduate student, Dr. De Vita has generously offered her time, provided assistance when I needed help, and aided me in finding the space or resources necessary to complete much of my experimental work. Together, they have enhanced my ability as a researcher and as an engineer and I am very grateful for their support, guidance, and mentorship. I would also like to thank Keri Swaby for the role she played in first introducing me to research opportunities around Virginia Tech. Additionally, Dr. Blake Johnson has been instrumental in helping to ensure that the portion of this work related to the manufacturing of synthetic vocal folds was successful. Dr. Johnson graciously allowed me access to his lab space and has provided valuable feedback that helped guide the manufacturing process and ultimately helped improve the design. I am very thankful for his help and support as well as the support and feedback from my other committee members, Dr. Rolf Mueller and Dr. Pablo Tarazaga. I would also like to thank all of the friends and lab-mates who have made my graduate experiences significantly more enjoyable through their encouragement and companionship. Lastly, I am extremely grateful for my family, especially my wife, Rachel, and my parents for their patience, encouragement, and unending love.

Contents

List of Figures

List of Tables

Chapter 1

Introduction

The movement and control of the vocal folds within the laryngeal cavity enables three crucial physiological functions: 1. opening the vocal folds helps regulate the flow of air into or out of the lungs during respiration, 2. closing the vocal folds aids in airway protection from food, drink, or saliva and during swallowing, and 3. the coordination and movement of the vocal folds enables vocalization and helps regulate sound production. Conditions such as vocal fold paralysis, head, neck or throat cancer, and instances of trauma that damage the vocal fold or larynx affect millions of individuals each year and often adversely impact quality of life. Damage to an individual's vocal folds or the surrounding tissue that help to coordinate their movement can result in a variety of significant challenges such as difficulty with sound vocalization, airway problems such as shortness of breath or ineffective coughing, as well as complications related to swallowing. Considerable research efforts have been made to better understand vocal fold mechanics and voice disorders and to improve the treatment options for individuals suffering from voice related impairments. These efforts, which have focused on understanding and evaluating glottal airflow dynamics [10, 11, 12], the anatomy of the vocal folds and surrounding tissue [4, 13], and the mechanics of vocal fold tissue properties [14, 15], have led to improved treatments for a variety of voice disorders. In particular, treatment for individuals requiring a total laryngectomy, a procedure in which the larynx is removed often due to laryngeal cancer, has improved through the development of the electrolarynx and tracheosophageal (TEP) prosthesis as well as improved voice therapy techniques [16, 17, 18, 19, 20]. Although progress has been made in the treatment and rehabilitation of individuals requiring a laryngectomy, patients still face significant challenges associated with general dysphagia, learning how to communicate using alternative methods for sound production, and new complications related

to protecting a redirected airway [21, 22, 23, 24].

This dissertation focuses on taking the first steps toward an active vocal fold prosthesis which can restore full vocal function to patients requiring a laryngectomy. In order to develop a functional vocal fold prosthesis that can recreate the dynamics of functions of healthy vocal fold tissue, it was first necessary to understand the mechanical properties of the vocal folds. Therefore, experimental work was first conducted to quantifying the elastic properties of the vocal folds through quasi-static mechanical testing of porcine vocal fold tissue. The elastic properties of porcine vocal folds were evaluated due to the common use of porcine larynges as a model for phonation. Uniaxial mechanical tensile tests were conducted on porcine inferior vocal fold samples and the resulting stress-strain data was analyzed using an optimization method to yield continuous elastic parameters which describe both the linear and nonlinear modulus regions. In addition to studying the vocal fold tissue elasticity, the relationship between the tissue properties and the dynamic response of the vocal folds during sound production was also explored. The effect of the varying elastic properties (due to anterior-posterior strain) on the dynamics of the vocal fold tissue during sound production was first investigated through the implementation of a 2D mathematical aeroelastic model of phonation which incorporated the previously described mechanical properties of the tissue, tissue geometry, and air flow conditions found in the trachea. The mathematical model based on the proposed framework in [9] provides insight into how the elastic properties impact the frequency of sounds produced by the vocal folds and also sheds light on the flow conditions required for phonation onset as previously studied in [9]. Additional experimental work was also conducted using full excised porcine larynx samples to further understand the impact of anterior-posterior strain and, consequently, the changing elastic modulus on vocal fold dynamics. Finally, synthetic vocal fold models were created based on porcine vocal fold geometry and the measured tissue properties. Similar dynamic experiments were conducted with the synthetic vocal folds while changes to the vocal fold geometry and mechanical properties of the synthetic models were made in order to better approximate the dynamic response of the porcine vocal folds. Ultimately, the work presented in this dissertation supports the long-term goal which is to use the improved knowledge of vocal fold

tissue properties and their impact on vocal fold dynamics during sound production to manufacture an improved synthetic vocal fold prosthesis with a desired and controllable dynamic response that can restore full vocal function to patients requiring a laryngectomy.

1.1 The Complexity of the Vocal Folds

The important role of the vocal folds in respiration, airway protection, and sound production has prompted numerous researchers to study the anatomy and physiology of the vocal folds and the surrounding tissue. Additionally, the prevalence of voice-related disorders has furthered the desire to understand how the vocal folds function and enable those crucial physiological tasks with the goal of improving treatment options for a wide range of voice complications. According to recent studies by the National Institute on Deafness and Other Communication Disorders (NIDCD), approximately 18 million US adults reported dealing with a voice-related problem in 2012 while approximately 10% of those individuals sought medical treatment [25, 26]. While treatment options and outcomes vary significantly depending on the pathology of the voice-disorder, many of the individuals seeking treatment continue to struggle with complications related to swallowing, voice production, or shortness of breath [27, 28, 29]. The need for improved treatment options can be most easily observed in the available treatments for individuals requiring a total laryngectomy, which is a procedure in which the entire voice-box is removed often due to cancer or trauma. According to the American Cancer Society there are approximately 60,000 total laryngectomees currently living in the United States with over 13,000 new cases of laryngeal cancer, the most common cause for a total laryngectomy, being diagnosed every year. The following sections focus on first describing the anatomy and physiology of the vocal folds and surrounding tissue. Next, this report will highlight the current available treatment options for individuals requiring a laryngectomy while explaining the limitations of each of those options in relation to the three primary physiological functions enabled by the vocal folds: respiration, airway protection, and sound production.

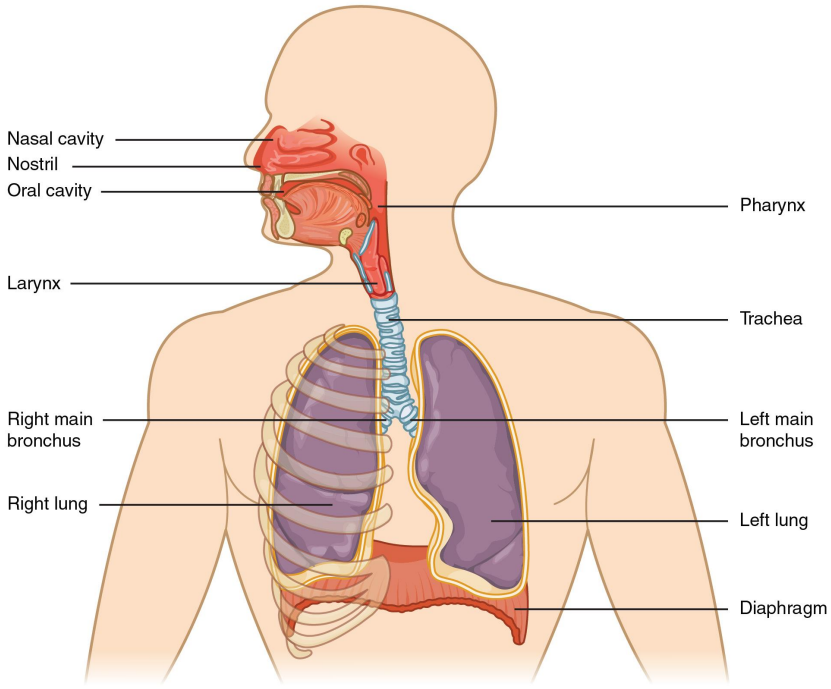

Figure 1.1: Overview of vocal system from lungs to oral and nasal cavities [1].

1.1.1 Vocal Fold Anatomy and Physiology

During respiration, air enters the body through either the oral or nasal cavities and travels through the larynx and trachea before residing in the lungs. Conversely, during speech production, air is expelled from the lungs through the trachea and laryngeal cavity before leaving the body through the oral or nasal cavities. As illustrated in Figure 1.1, the larynx or voice-box is situated between the lungs and oral and nasal cavities which requires it to serve several critical functions related to respiration and voice production.

The larynx, which forms the voice box, is composed of cartilage, muscle, nerve and the vocal folds as can be seen in more detail in Figure 1.2. The vocal folds, which are a pair of mucosal membranes that span the diameter of the laryngeal cavity, play an especially critical role in the mechanics of respiration and phonation. A transverse plane cross-sectional view of the laryngeal cavity, which can also be seen on the right side of Figure 1.2, shows the superior surface of the vocal folds and further highlights the significance of the vocal fold tissue. As mentioned previously, during

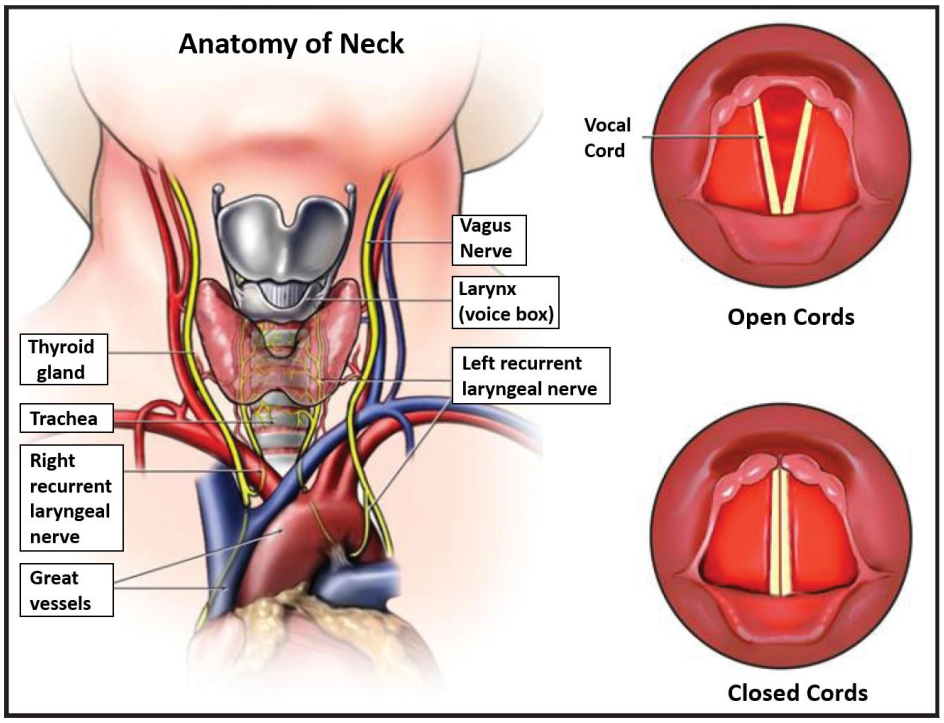

Figure 1.2: Anatomy of neck and transverse cross-section of vocal fold tissue [2].

respiration, the vocal folds are pulled open laterally to allow air to pass freely through the trachea and into or out of the lungs. During swallowing, the vocal folds are closed, which protects the airway from any unwanted debris or particles.

In order to perform the critical functions related to respiration, airway protection, and voice production, the vocal folds are actuated and controlled by numerous muscle groups located within and around the larynx. Figure 1.3, highlights the intrinsic laryngeal muscles that help to control the position and movement of the vocal folds through both a saggital plane and transverse plane cross-section of the laryngeal cavity. It is important to note that the movement and control of the vocal folds is complex and, as can be seen in the figure, there are numerous intrinsic muscle groups as well as several extrinsic muscles that are involved in positioning the vocal fold tissue during each of the physiological functions (respiration, airway protection, and phonation) described previously. The following descriptions of muscle functions highlight some of the important laryngeal muscles used to accomplish the previously mentioned vocal fold physiological functions. The thyroarytenoid

(TA) muscle contracts to cause the vocal folds to be shortened and thickened due to the arytenoids being pulled toward the thyroid cartilage. Contraction of the cricothyroid (CT) muscles, results in the thyroid cartilage being pulled down and rotated toward the cricoid cartilage. The contraction of this muscle group tightens the thyroarytenoid muscle and the lamina propria which, in turn, modulates the fundamental frequency of vibration by stretching the tissue in the anterior-posterior direction [30]. The ability to modulate the frequency of sound produced by the vocal folds by stretching the tissue in the anterior-posterior direction will be discussed in more detail in later sections of this dissertation. Additionally, the lateral cricoarytenoid muscle functions as an adductor by drawing the arytenoids together medially and closing the vocal folds [30] which helps to protect the airway.

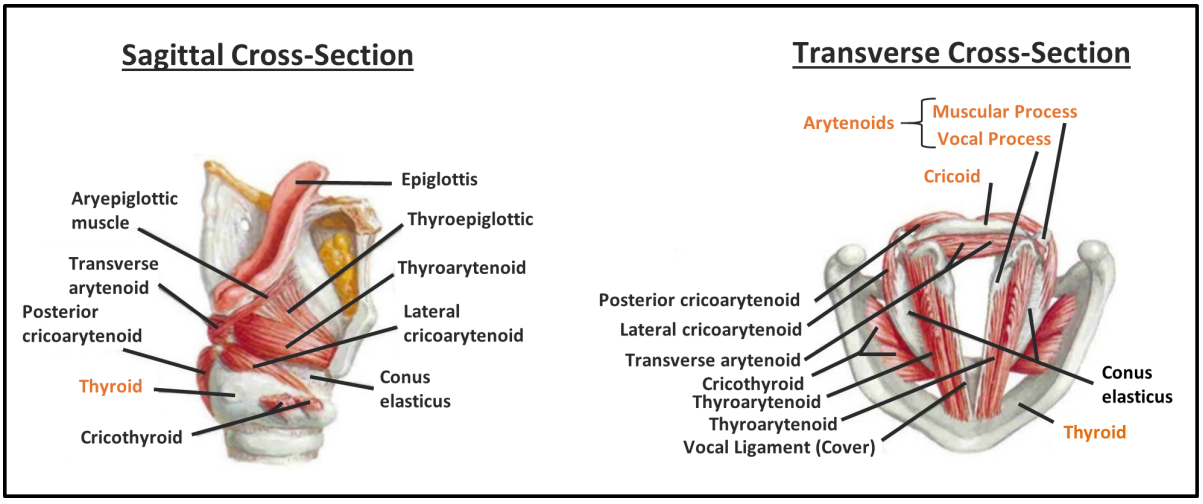

Figure 1.3: Transverse and sagittal plane cross-sections of the laryngeal cavity which highlight the intrinsic muscles used to coordinate the movement of the vocal folds [3]. Orange text is used to label cartilage while black text is used to label soft tissue such as muscle or ligaments.

Early studies of vocal fold anatomy and physiology reported in [4], proposed a cover-body division of vocal fold tissue which is shown in Figure 1.4 and has since been commonly used in the analysis of vocal fold vibrations. The authors in [13], further describe the composition of each layer of the vocal fold lamina propria as follows: the superficial layer being comprised of mostly interstitial fluid and a few elastin fibers, the intermediate layer composed of more elastin fibers organized in the

anterior-posterior direction, and the deep layer consisting primarily of collagen type I and type III fibers which are also oriented in the anterior-posterior direction and help to maintain the structure while adding stiffness to the vocal folds. More recently, [6, 7] presented a study to highlight interspecies similarities and differences in extracellular matrix composition which highlighted the similarities between porcine and human vocal fold tissue. The authors of [31] also studied and compared interspecies anatomy and composition of vocal folds and determined that the density of collagen and elastin fibers found in porcine samples was most similar to that of human vocal folds.

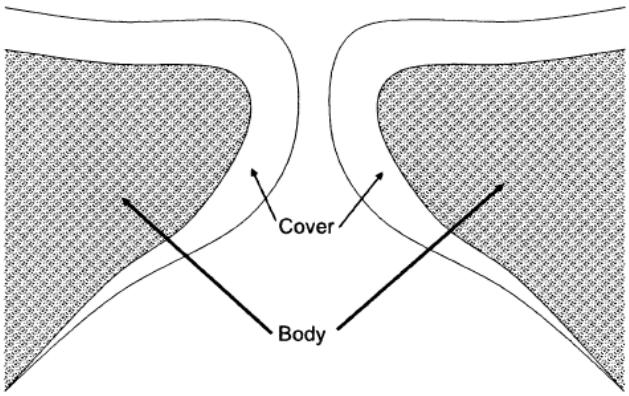

Figure 1.4: Sagittal plane cross-section of vocal folds highlighting cover-body model of vocal folds as proposed by [4]. Image from [5].

1.1.2 Laryngectomy Rehabilitation

Laryngeal carcinoma is the second-most common malignancy of the head and neck and the eleventh most common form of cancer in men world-wide with approximately 13,000 new cases of laryngeal cancer occurring each year in the United States alone [32, 33, 34]. After diagnosis through direct laryngoscopy, imaging, and ultimately a biopsy of the impacted tissue, physicians are faced with limited choices on the best treatment option for each patient [32]. Radiotherapy and surgery are the most common treatments for individuals with laryngeal cancer with surgery either in the form of a partial or total laryngectomy often being required for patients with more advanced T3 or T4 lesions

[32]. While the cure rates for laryngeal cancer have experienced minimal changes since the 1970s with an approximately 60% cure rate outlook for a T3/4 diagnosis, significant strides have been made to improve patient quality of life through a variety of laryngectomy rehabilitation options [35]. Although a total laryngectomy may leave a patient cancer free and despite significant advances in laryngectomy rehabilitation, the procedure will often still have a significantly detrimental impact on one's quality of life.

Following a total laryngectomy, all three of the vital functions of the larynx are immediately impacted as patients adjust to breathing through a redirected airway, suffer from dysphagia and other complications related to airway protection, and learn how to communicate using alternative methods of speech production. As can be seen in Figure 1.3, the removal of the larynx requires the airway to be redirected through a surgical hole called a stoma in the neck. While the stoma allows air to enter and exit the lungs, the redirection of the air bypasses humidification in the upper airway and prevents the movement of air over sensory organs such as the tongue that contribute to the senses of taste and smell. Figure 1.5, further highlights the three most common forms of alternative speech production following a total laryngectomy: esophageal speech, using an electrolarynx, and using a tracheoesophageal prosthesis (TEP). Through rehabilitation with speech therapists, some laryngectomy patients can learn to produce esophageal speech through insufflation of the esophagus and controlled air release to vibrate tissue in the pharynx and upper esophagus [35, 36]. Despite esophageal speech requiring no additional surgery or external devices, a study in [37] shows that relatively few laryngectomy patients (6%) develop usable esophageal speech with most opting to use an electrolarynx, as shown in Figure 1.3, instead. The electrolarynx works by transmitting vibrated electronic sound through the neck tissue which is then modulated in the oral cavity by the patient to create speech [16, 38]. Although the electrolarynx is widely used, patients still have the inconvenience of the device requiring manual control. In addition, despite recent advances, electrolarynx generated speech is still reported as sounding unnatural and robotic due to limited frequency modulation [16, 18, 36, 38, 39, 40, 41, 42]. Tracheoesophageal speech is produced through a tracheoesophageal prosthesis (TEP) which serves as a one-way valve allowing air to be directed

into the esophagus after manually closing the stoma. Speech is then produced by modulating the airflow in the oral cavity. Although the use of a TEP often results in higher satisfaction with speech quality and the ability to communicate, patients still face complications around protecting an open airway, reduced vocal range, and the inconvenience of needing to occlude the stoma when wanting to speak [43].

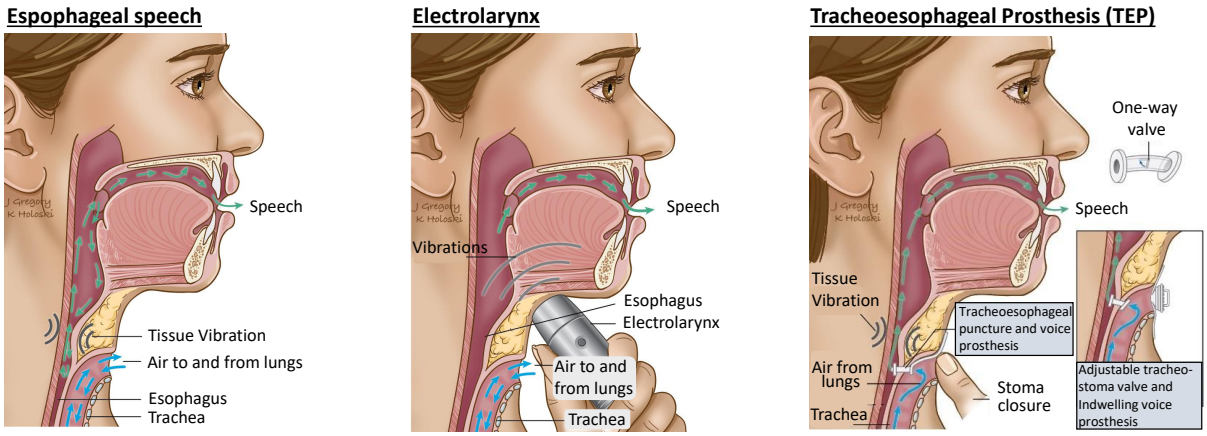

Figure 1.5: Current rehabilitation options following total laryngectomy include esphophageal speech, the use of an electrolarynx, and the use of a tracheoesophageal prosthesis.

1.2 Prior Literature on Vocal Folds Mechanics and Dynamics

The following section highlights some of the significant research findings related to mechanical testing of the vocal fold tissue as well as work focused on modeling and experimentally measuring vocal fold tissue dynamics. The work discussed in this section provides a foundation for further investigating vocal fold tissue properties and the impact those properties have on the tissue dynamics during sound production.

1.2.1 Mechanical Testing

Due to the importance of the mechanical properties of the vocal fold on the tissue dynamics during sound production, numerous researchers have conducted studies to try and quantify the tissue elasticity. During these efforts, a variety of techniques have been to quantify the mechanical properties of the vocal fold tissue. In a prior study [14], the authors measured the elastic properties of canine vocal fold tissue through uniaxial traction testing. The results of their tests showed that the stress-strain behavior of canine vocal folds exhibited linear behavior at low strains and nonlinear behavior at higher strain values. The authors reported a low strain ($< 15\%$) secant modulus of 42 kPa and used a third-order polynomial to describe the higher strain nonlinear behavior for the canine vocal fold cover layer [14]. Other authors [44] presented results which built on this work by studying the elastic behavior of sheep, cow, and porcine vocal folds and compared them to the stress-strain results of the canine vocal folds. These tests were conducted using a similar experimental protocol as the study mentioned previously [14] and subjected the samples to approximately 40 percent elongation while measuring the displacement of a Dual-Servo ergometer. The initial marked length of the vocal fold samples was used to determine strain values. Similar to the results of the canine vocal fold study [14], the authors [44] reported an average low strain ($< 15\%$) secant modulus for the linear region of the stress-strain data for each species. The results of the interspecies study [44] indicated that the porcine vocal folds exhibited greater nonlinearity in higher strains than the other species that were tested, but the parameters describing the nonlinear behavior were not defined. The authors suggested that the greater nonlinear behavior could be an attribute of the porcine vocal folds that yield wider ranges of oscillation frequencies and make porcine samples a more suitable model for phonation. In another study [45], researchers presented results of uniaxial traction tests on a single cadaveric vocal fold sample while using Digital Image Correlation (DIC) techniques to determine the spatial deformation field for the entire sample. The authors in this study highlighted variations in the anterior-posterior direction and found the elastic modulus to be an order of magnitude larger at the midpoint of the human vocal fold than towards the thyroid and arytenoid cartilaginous attachment points [45]. Generally, biaxial mechanical testing of the

biological tissue is preferred as it can often more similarly represent physiological conditions and loading. Preforming biaxial mechanical testing on the vocal fold tissue has been challenging due to difficulties in clamping or securing the sample given the small width (usually less than 1 cm) of the tissue. More recently, one study [46] was able to collect biaxial data on two human cadaver samples which showed that vocal folds were nearly isotropic at rest but became exhibited more anisotropic behavior at higher strains. While the studies described above have investigated the mechanical properties of the vocal folds, additional studies are still required to provide a more comprehensive understanding of vocal fold elasticity across the the full vocal range (approximately 0-40% strain) as well as to better understand anisotropic and viscoelastic properties of the tissue.

1.2.2 Excised Larynx and Synthetic Vocal Fold Dynamic Testing

In addition to performing uniaxial traction and other testing on the mechanical properties of the vocal fold, some dynamic tests have been conducted to further study vocal fold mechanics and phonation. While some research has been conducted to study voice production *in vivo*, these studies are often limited by the the ability to accurately measure or observe vocal fold movement in a safe and noninvasive manner. Cadaver tissue has also been used in some research, such as in [47], however, cost and availability has lead many researchers to explore the use of excised canine, sheep, porcine, or bovine larynges when experimentally investigating vocal fold dynamics. In several early studies [48, 49, 50, 51], researchers used excised canine larynges as models of phonation due to their relative ease of accessibility over cadaveric tissue. In one study [51], researchers varied canine vocal fold tension and length while photoglottography (PGG) and electroglottography (EGG) measurements were collected during sound production tests. The EGG and PGG measurements provided insight into the flow characteristics and movement of the canine vocal fold tissue during phonation. Other studies using canine larynges have investigated vocal fold impact stresses [48], the effect of different muscle activation on the fundamental frequency and subglottal pressure in canine vocal folds [50], and even the phonatory characteristics of canine hemilaryngeal samples [49].

More recently, researchers have conducted tests using pig, cow, and sheep fully excised larynges in addition to canine larynx samples to further study the dynamics of phonation [10, 11, 12, 52]. In one prior study [52], researchers used DIC techniques to study the kinematics of porcine vocal folds during self-oscillation and reported on the contact stresses and strain values that were observed. Through analyzing the images taken by two high-speed cameras, the authors of [52] measured and illustrated the vocal fold tissue strain and tracked the displacement of the tissue in the medial-lateral, inferior-superior, and anterior-posterior directions throughout testing. During the tests presented in [52], the vocal folds oscillated at a constant 245 Hz due to a flow rate of 0.236 cm^3/s. In other studies [10, 11], researchers evaluated the phonatory characteristics of pig, sheep, and cow larynges when subjected to varied airflow and pressures. While the researchers found that all three species could be used as potential models for phonation, they noted that pig larynges could be especially useful due to their larger possible range of phonation frequencies.

In addition to conducting tests on excised canine, porcine, bovine, or sheep larynges, some researchers have investigated the use of synthetic vocal fold models to simulate speech production. While canine, porcine, or other species larynx samples are more easily obtained and less expensive than cadaveric samples, they are also limited by a relatively short time frame (after thawing) during which the samples are usable for experimental testing and it is often more difficult to account for changes in mechanical properties in geometry between samples. In early synthetic vocal fold studies, researchers in [53] used polyester resin models of a simplified rectangular glottal channel to better understand and compare results to a mathematical models describing the fluid flow through the larynx. Building on that work, researchers in [54], identified phonation onset threshold pressures using a synthetic vocal fold cover layer made of silicone that was attached to a rigid (metal) body layer. In other studies such as in [55, 56, 57], researchers have used rubber models to represent an isotropic cover layer of the vocal folds and investigate how vocal fold dynamics change with varying air flow characteristics and vocal fold geometry. More recently, researchers in [58], described the methodology used to produce a multi-layer synthetic vocal fold model which could more closely approximate the spatially varying mechanical properties of human vocal folds. In the study presented

in [58], the researchers showed that the multi-layer vocal fold model exhibited a lower phonation onset pressure than single-layer synthetic models and, in turn, more closely approximated human vocal fold dynamics. Additionally, researchers used the synthetic vocal fold models to study the effect of stiffness asymmetry in [59] and to investigate the impact of different materials used in vocal fold augmentation injections [60]. While progress has been made by the researchers highlighted above and others to improve the manufacturing of synthetic vocal fold models, there is still a work need to more closely approximate vocal fold dynamics across the full vocal range. Specifically, there are limited studies that have investigated the impact of the varying elastic properties across the full vocal range on vocal fold dynamics and the frequencies of vibration during sound production. Further, there are even fewer studies that have investigated actuation methods which could be used to control the dynamic response of the synthetic vocal folds during sound production.

1.2.3 Mathematical Models of Vocal Fold Sound Production

While excised vocal fold studies provide an opportunity for researchers to measure vocal fold characteristics under specific and measurable conditions, they are often limited by sample availability or cost, tissue variability, as well as sample preservation as most larynx samples have a short time period (minutes) following dissection during which they are viable and appropriate for experimental work. Due to these reasons, other authors have developed and investigated mathematical models which can be used to describe speech production and vocal fold dynamics based on vocal fold tissue properties, such as the elastic modulus, tissue density, and in situ length of the tissue [61, 62, 63]. In early models, researchers used the simple equations for a vibrating string to start describing the motion of the vocal folds during phonation [64]. In other studies, researchers used ribbon or Euler-Bernoulli beam and even Timoshenko beam models of vibration which was necessary to account for motion in more degrees of freedom and to take into consideration phase delays in the motion of the vocal fold tissue during self-oscillation [45, 65, 66]. In other studies, researchers have investigated aeroelastic models of phonation which evaluate the role of glottal aerodynamics

in the vibration of the vocal folds [9, 61, 67, 68]. In many early models of vocal fold vibration, the parameters used to describe the physical quantities of the vocal folds varied between models and specifically between point-mass and distributed-mass systems. Recently, the author of [69] argued for the use of distributed-mass models which can be more easily related to the physical tissue properties. In particular, the model presented in [9], incorporates the vocal fold geometry, vocal fold biomechanical properties such as the elastic modulus and Poisson's ratio of the tissue as well as the airflow characteristics such as the air density, flow rate, and pressure. Because of the incorporation of fluid dynamics into the model, the presented work in [9] is not only able to illustrate changes in frequency caused by varying tissue properties but also has the ability to shed light on the onset of phonation which is indicated by a bifurcation in the real component of the model's eigenvalues determined under varying flow conditions. Through the incorporation of tissue properties, these models highlight the importance of the nonlinear elastic modulus on frequency changes during sound production.

1.3 Summary of Work

Building off of the work of Drs. Titze, Alipour, Thomson, Zhang, and other researchers highlighted in the previous sections, the work presented in this dissertation focuses on quantifying the elastic parameters which describe the vocal fold tissue, investigating the role of vocal fold elasticity due to anterior-posterior strain on vocal fold dynamics during phonation, and exploring manufacturing techniques used to produce synthetic vocal folds and modify their dynamic flow-induced behavior.

The second chapter describes the experimental work focused on identifying quasi-static continuous model parameters for the elastic properties of porcine vocal folds using DIC methods to calculate strain values during uniaxial tension tests. 16 porcine inferior vocal fold (IVF) samples were extricated after identifying and marking the cartilaginous attachment points and carefully removing extraneous muscle fibers from the folds. The samples were mechanical clamped and mounted on a custom built uniaxial tensile setup. After applying a preload, the samples were stretched to

approximately 40% strain while force data was collected via a load cell and images of the speckled superior surface of the samples were captured throughout testing. Engineering strain values were determined by tracking the deformation of the speckle points on the surface of the vocal fold using a digital image correlation (DIC) protocol implemented in MATLAB. The stress-strain results were then modeled by finding the optimized continuous elastic parameters using a similar method as described in [70].

The third and fourth chapters detail the 2D mathematical fluid-structure model used to better understand the role of vocal fold mechanical properties on the dynamics of tissue during sound production as well as the results of experimental dynamic tests using excised porcine larynges. The 2D aeroelastic model of phonation was based on the work presented in [9] which investigates how changes in the the vocal fold geometry, tissue properties, and flow characteristics impact vocal fold dynamics. The dynamic experimental tests studied the impact of applying an anterior-posterior strain on porcine larynx samples on the vocal fold dynamic response and especially on the frequency of produced sounds. These tests involved subjecting the porcine larynx samples to a heated and humidified air source which was adjusted to simulate airflow through the trachea and laryngeal cavity. The superior surface of the vocal fold tissue was exposed through dissection while two high-speed cameras (4000 FPS) and a microphone (44100 Hz) were used to continuously record data throughout the tests. The results of the dynamic testing was then compared to the simulated results produced by the aeroelastic model with the goal of better understanding the correlation between varying vocal fold stiffness or elastic modulus (changing with anterior-posterior strain) and the dynamic behavior of the vocal folds during phonation.

The fifth chapter describes the process used to manufacture of synthetic vocal fold models and highlights the dynamic experimental test results using those models. The synthetic models were mounted on the same experimental setup and be subjected to an air source with similar flow characteristics. Manufacturing parameters were iteratively adjusted to span the elastic modulus or stiffness range of the porcine vocal folds as found in the mechanical tensile testing described in Chapter 2. The dynamic results of the synthetic models were also discussed in relation to the

porcine vocal folds and the simulated results from the aeroelastic model of phonation.

1.3.1 Significance of Work

While some prior work has been conducted to investigate porcine vocal fold elasticity [44], the quasi-static elastic parameters in the anterior-posterior direction have not yet been fully described for both the low and higher strain regions. Further, no studies have identified the location of transition points between linear and nonlinear elastic regions of vocal fold properties. Through the uniaxial tension testing, it was found that the stress-strain results indicated that the elastic modulus of the tissue could be closely modeled by a low-strain linear region followed by an exponential nonlinear region and then a higher strain linear region. The results obtained from this work further the available information on porcine vocal fold elasticity and can be incorporated into models of phonation where the frequency of sound produced changes with strain in the anterior-posterior direction and, as a result, with the vocal fold tissue properties. Additionally, the dynamic experimental work using excised porcine larynges provides valuable insight into the impact of the nonlinear elastic properties of porcine vocal fold tissue on the frequencies of sound produced during phonation. While other researchers have used porcine and other species larynx samples to investigate vocal fold impact stresses or airflow characteristics which correspond to vocal fold vibration onset, the study presented in this dissertation focuses primarily on the frequency changes produced by porcine vocal folds and sheds new light on relationship between changes in the frequency of vocal fold vibration and changes in elastic properties due to anterior-posterior tissue strain. Furthermore, the experimental results were compared to the simulated vocal fold dynamics using the previously proposed aeroelastic model of phonation in an effort to determine the model's effectiveness at predicting frequency changes across the full vocal range. Also, this work utilizes additive manufacturing techniques to produce synthetic vocal fold models with the goal of achieving a desired dynamic response across the vocal range of the porcine vocal folds. While progress has been made by other researchers to improve the manufacturing of synthetic vocal fold models, there is still a need to more closely approximate vocal

fold dynamics across the full vocal range. The studies presented in this dissertation investigate the impact of the varying elastic properties across the full range of vocal fold elasticity on the frequencies of vibration during sound production and also begin exploring potential actuation methods which could be used to control the dynamic response of the synthetic vocal folds during phonation. While there is still much work need to continue refining the design and control, an improved synthetic vocal fold model has the potential to increase the understanding and possible treatments of numerous voice-related disorders. Finally, the work in this dissertation continues taking steps toward the long-term goal of developing a synthetic vocal fold model that can fully recreate the dynamics of healthy tissue and can be used as an improved vocal fold prosthesis for total laryngectomy patients.

Chapter 2

Mechanical Properties of Porcine Vocal Folds

Garret Burks, Raffaella De Vita, Alexander Leonessa. Characterization of the Continuous Elastic Parameters of Porcine Vocal Folds. Journal of Voice (2018).

Abstract

This paper presents an evaluation of the elastic properties of porcine vocal folds through uniaxial tensile tests. Inferior vocal fold tissue samples were subjected to tension in the longitudinal direction while digital image correlation techniques were employed to determine strain values throughout the tests. The stress-strain results showed a low-strain linear region, followed by both a nonlinear exponential and then a higher strain linear region. Data from 16 porcine vocal fold samples were analyzed following a similar optimization method as proposed in prior studies [70] to yield continuous model parameters which describe the elastic properties of the tissue. The average low and high strain linear modulus values were found to be 17.86 kPa and 609.27 kPa, respectively. The model also identified the location of two transition points: p_1, describing the transition from the low-strain linear region to an exponential region at 0.122 ± 0.058 mm/mm and p_2, describing the transition from the exponential to the high strain linear region at 0.308 ± 0.069 mm/mm. The exponential region of the averaged data set was found to be described by the relationship $\sigma_{\mathrm{m}}(\epsilon_{xx}) = 0.083e^{19.32\epsilon_{xx}} + 2.0951$ kPa. In addition to locating transition points, the optimization

method maintained modulus continuity across all strain values. Averaged elastic modulus values across strain from 0 to 0.40 mm/mm were compared to representative low and high strain linear modulus which were measured at 0.05 and 0.35 mm/mm, respectively. Statistically significant differences were found among all strain intervals between the two transition points and the linear modulus values. These results indicate the need to consider the location of transition points and further highlight the nonlinearity and changes in elastic modulus which are especially important when using excised porcine vocal folds as a model for phonation. The results quantify continuous linear and nonlinear parameters describing the elastic properties which can be used as a framework for future excised larynx tests and while evaluating the dynamics of sound production, which rely heavily on the elastic properties of the tissue.

2.1 Introduction

According to the American Speech-Language-Hearing Association (ASHA), approximately 60,000 total laryngectomy patients live in the United States alone. These individuals requiring a laryngectomy, a procedure in which a patients' larynx is removed often due to laryngeal cancer or severe trauma, must significantly adjust their lifestyle to compensate for their lack of vocal folds. In addition to laryngectomy patients, ASHA estimates that another 7.5 million individuals in the United States suffer from other voice related disorders often as a result of damage to the vocal folds or surrounding tissue. The movement and control of the vocal folds within the laryngeal cavity allows for three vital functions: 1. Enabling respiration and breathing by opening the vocal folds, 2. Regulating sound production and vocalization and 3. Aiding in airway protection and enabling individuals to swallow. Due to the importance of the vocal fold tissue in numerous physiological processes and in an effort to try and improve treatment options for voice related disorders, there have been considerable research efforts to better understand vocal fold tissue properties, vocal fold anatomy and physiology, and vocal fold dynamics during speech production. In particular, understanding tissue elasticity is crucial when studying the oscillatory behavior of the vocal folds

during phonation. Due to their relative ease of availability over human cadaveric tissue, prior studies have utilized canine and porcine larynges in fully excised larynx studies while evaluating the dynamics and studying vocal fold fundamental frequencies during speech production [10, 11, 52]. While some prior studies have also been conducted to quantify tissue geometry and collect data for canine, porcine, cadaveric, and other species' vocal fold tissue elasticity, these studies have often either contained small sample sizes (≤ 6) or focused on reporting low strain secant modulus values [14, 44, 47].

In early studies [4] of vocal fold anatomy and physiology, a cover-body division was proposed to describe human vocal folds, as illustrated in Figure 2.1. Additional studies [13] were conducted which further evaluated the composition of the cover layer and classified the superficial, intermediate, and deep layers in vocal fold tissue. Hahn et al. presented findings in earlier studies [6, 7] which highlight interspecies similarities and differences in extracellular matrix composition. Based on those reported findings [6, 7], Figure 2.1.B illustrates the location of the superficial, intermediate, and deep layers of porcine vocal folds in comparison to human vocal folds. Notably, the porcine vocal folds have a wider superficial layer and more inferior deep layer in comparison to human vocal folds. In addition, Figure 2.1 shows a comparison of extracellular matrix volume fractions in human and porcine vocal fold cover layers based on the results reported in the same study [6, 7, 8]. Other authors [31] also studied and compared the anatomy and composition of sheep, dog, pig, and human vocal folds. Through their work, the authors determined that the density of collagen and elastin fibers found in the in porcine vocal folds was most similar to that of human vocal folds [31]. These studies also highlighted that the fibers were oriented in the longitudinal direction for each of the species tested.

A variety of techniques have been used in previous studies to quantify the mechanical properties of the vocal fold tissue. In an prior study [14], the authors measured the elastic properties of canine vocal fold tissue through uniaxial traction testing. The results of their tests showed that the stress-strain behavior of canine vocal folds exhibited linear behavior at low strains and nonlinear behavior at higher strain values. The authors reported a low strain ($< 15\%$) secant modulus of 42 kPa and

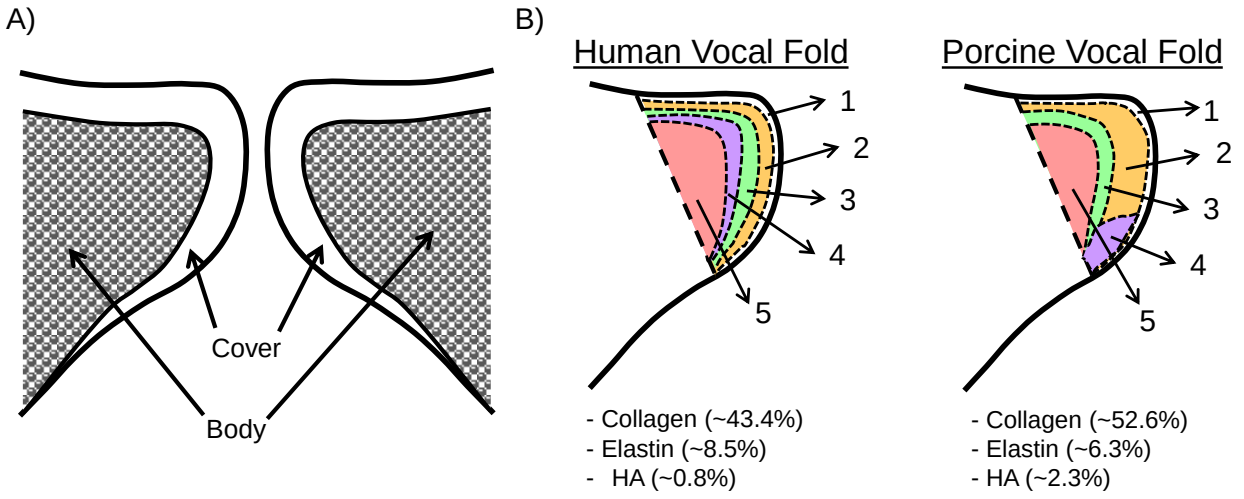

Figure 2.1: A) Vocal fold coronal cross section illustrating cover body theory [4, 5]; B) Numbers 1-5 represent the following tissue layers in order from lowest to highest based on the findings in [6, 7]: Epithelium, Superficial Layer, Intermediate Layer, Deep Layer, Muscle. The cover layer composition of human and porcine vocal folds is represented by the volume fractions of collagen, elastin, and hyaluronic acid (HA) [6, 7, 8].

used a third-order polynomial to describe the higher strain nonlinear behavior for the canine vocal fold cover layer [14]. Other authors [44] presented results which built on this work by studying the elastic behavior of sheep, cow, and porcine vocal folds and compared them to the stress-strain results of the canine vocal folds. These tests were conducted using a similar experimental protocol as the study mentioned previously [14] and subjected the samples to approximately 40 percent elongation while measuring the displacement of a Dual-Servo ergometer. The initial marked length of the vocal fold samples was used to determine strain values. Similar to the results of the canine vocal fold study [14], the authors [44] reported an average low strain ($< 15\%$) secant modulus for the linear region of the stress-strain data for each species. The results of the interspecies study [44] indicated that the porcine vocal folds exhibited greater nonlinearity in higher strains than the other species that were tested, but the parameters describing the nonlinear behavior were not defined. The authors suggested that the greater nonlinear behavior could be an attribute of the porcine vocal folds that yield wider ranges of oscillation frequencies and make porcine samples a more suitable model for phonation. In another study [45], researchers presented results of uniaxial

traction tests on a single cadaveric vocal fold sample while using Digital Image Correlation (DIC) techniques to determine the spatial deformation field for the entire sample. The authors in this study highlighted variations in the anterior-posterior direction and found the elastic modulus to be an order of magnitude larger at the midpoint of the human vocal fold than towards the thyroid and arytenoid cartilaginous attachment points [45].

In addition to performing uniaxial traction tests, some tests have been conducted using pig, cow, sheep, or canine fully excised larynges to further study the dynamics of phonation [10, 11, 12, 52]. In one prior study [52], researchers used DIC techniques to study the kinematics of porcine vocal folds during self-oscillation and reported on the contact stresses and strain values that were observed. Other authors have investigated biomechanical models used to predict the fundamental frequencies of speech production based on vocal fold tissue properties, such as the elastic modulus, tissue density, and in situ length of the tissue [61, 62, 63]. These models highlight the importance of the nonlinear modulus behavior on frequency changes during sound production. Due to the impact of the changing vocal fold elastic modulus on the oscillatory behavior exhibited during sound production, there is need for additional work to quantify elastic parameters at all strain values and to more accurately identify the location of transition points between the low strain linear region and higher strain modulus values.

The work detailed in this paper will highlight the results of testing 16 porcine vocal fold samples while using DIC techniques to determine strain values and collect a more complete set of tissue elasticity data during uniaxial tensile tests. Using an optimized linear-exponential model, transition points between linear and exponential regimes were determined as well as the nonlinear parameters for those regions while maintaining continuity in both the modeled stress-strain curves and resulting modulus. The continuous modulus functions can be used in future work when evaluating the effect of changes in porcine vocal fold tissue strain and modulus on the fundamental frequencies observed during excised larynx testing.

2.2 Methodology

The following section outlines the steps used to prepare the tissue samples as well as the experimental testing methods used on the porcine vocal fold samples ($n = 16$).

2.2.1 Sample Preparation

Sample preparation was conducted by following similar procedure to Alipour et al. as described in prior studies [14, 44]. Porcine larynges were obtained from adult swine through an on-campus abattoir in the Virginia Tech Department of Animal and Poultry Sciences and transported to the laboratory while immersed in a phosphate-buffered saline (PBS, pH 7.4, Fisher Scientific, USA) solution. A 2×2 inch sterile gauze pad was folded in half and placed between the left and right vocal folds while the excised larynges were submerged in a PBS solution which saturated the gauze to prevent tissue dehydration. The use of saturated gauze has been previously used as a method of tissue storage in prior studies [71] and is assumed to mitigate the adverse effects of crystallization and cracking during freezing. Each of the larynx samples was then frozen in its own container. The samples were stored at a temperature of -20 °C for a maximum duration of 6 weeks prior to testing. On the day of the experiment, the excised larynges were thawed at room temperature before removing and discarding connective tissue surrounding the thyroid cartilage as well as the epiglottis. The porcine larynx was then divided into two hemilarynges by making careful incisions from the superior region of the arytenoid cartilage down to the tracheal rings and similarly through the midline of the thyroid cartilage as shown in Figure 2.2. Great care was taken during incisions to avoid damage to the vocal fold tissue through punctures or excessive loading of the tissue.

After identifying the cartilaginous attachment points, incisions were made through the thyroid cartilage around the anterior attachment points of the inferior vocal folds and around the posterior attachment point through the arytenoid process. Incisions were made laterally along edges of the inferior vocal folds in order to separate the folds from surrounding tissue. After extricating

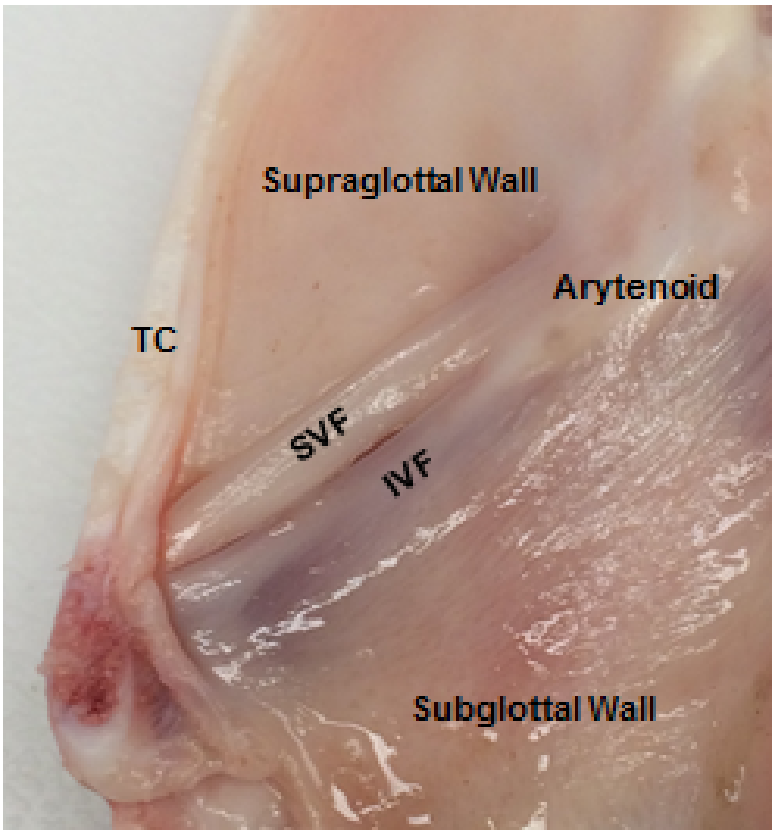

Figure 2.2: Porcine hemilarynx sample showing the arytenoid and thyroid cartilage (TC), the inferior vocal fold (IVF), superior vocal fold (SVF), subglottal wall, and supraglottal wall.

the sample, extraneous muscle fibers were carefully removed from the folds. The width, length, thickness, and mass were measured using a digital caliper (accuracy ± 0.05 mm, Mitutoyo Absolute Low Force Calipers Series 573, Japan) and scale and recorded for each sample. A total of 5 measurements for both the width and thickness were collected and were used to compute an average cross-sectional area for each sample. The in situ length was measured by identifying and marking the arytenoid and thyroid cartilaginous attachment points before removing the inferior vocal fold (IVF) sample.

In previous studies, the inferior porcine vocal folds have been described as the true vocal folds while the superior folds were described as the ventricular folds [31]. However, more recent excised larynx tests using porcine larynges indicate that both the inferior and superior folds vibrate during

phonation [11]. Due to the new information regarding the function of each vocal fold, other authors [44] have questioned the use of the labels ”true” and ”false” vocal folds for porcine larynges. Because of the lack of consensus on the use of the ”true” and ”false” labels, the authors chose to use the nomenclature ”inferior” and ”superior” which describe the vocal folds anatomical position rather than their function.

2.2.2 Experimental Methods

After recording the sample measurements, the IVF samples were submerged for 5 minutes in a solution of PBS and methylene blue, 1% aqueous solution (Fisher Science Education, USA) following methods described by Lionello et al. [72]. After 5 minutes, the samples were removed and speckled using a using an aerosol fast dry gloss white paint (McMaster-Carr, USA). Sand paper strips with a 200 grit were then cut approximately 1 cm in length and 5 mm in width and folded over the cartilaginous ends. The dyed and speckled samples were then clamped over the folded sandpaper and secured on the experimental setup as shown in Figure 2.3. Custom L-shaped clamps were 3D printed using a PLA plastic that were $30 \times 24 \times 20$ mm in height, width and depth, respectively, and were used to mechanically tighten the grip on the folded sandpaper over the cartilaginous ends. In addition, the clamps were secured to both a microscale linear actuator (Zaber T-NA) which was used to control displacement rates and a load cell (accuracy of 0.002 N, Omega 2 lbf) used to record force measurements during testing and were centrally placed in a custom built $3 \times 10 \times 10$ cm bath made of polycarbonate which allowed the sample to be submerged in a PBS solution during testing. While securing the clamped sample to the load cell and actuator, effort was made to position the sample in the center of the field of view of a camera (Thorlabs Inc., DCC1645C) that was placed directly above the testing setup. Displacement controlled tests were conducted using the microscale linear actuator, which operated at a displacement rate of 0.033 mm/s during all tension tests. The load cell was then zeroed after obtaining a desired preload of 0.02 N. Displacement controlled tensile tests were performed while stretching the sample to approximately 40% strain (displacement was

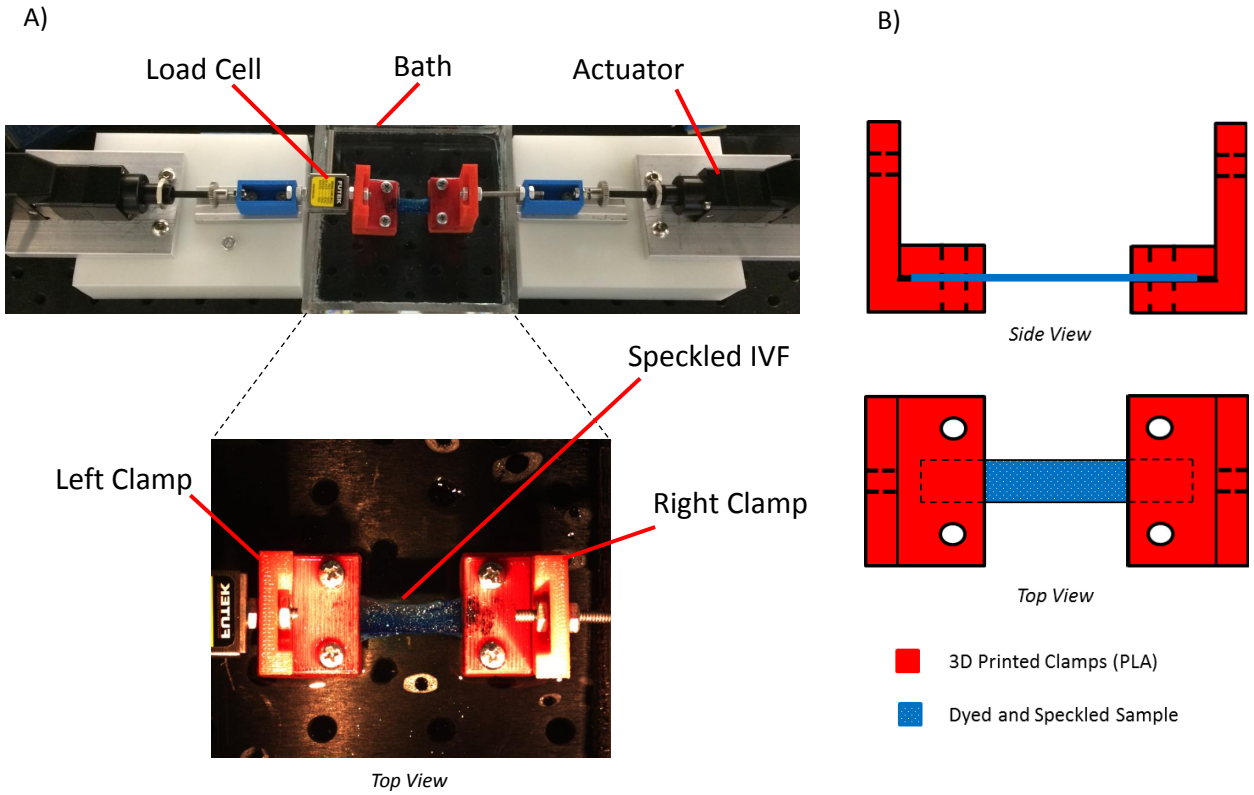

Figure 2.3: A) Picture of the dyed and speckled sample clamped in the experimental setup. B) Schematic of the clamps used to secure the IVF sample.

limited by maximum actuator stroke distance) while recorded images of 1280×1024 pixels were taken at a rate of 4 Hz with a field of view of 8.0×8.0 cm. Actuator position, force, and video data were recorded synchronously to a desktop computer via a data acquisition module (National Instruments NI cDAQ-9172) using LabVIEW (National Instruments).

All stress and strain values were calculated referenced from the preloaded configuration. Engineering strain of the IVF sample was calculated using DIC methods implemented in MATLAB [73]. Previous studies have demonstrated the successful implementation of this non-contact strain measurement method in biological materials [74]. For each of our samples, we chose to compute strain values based on a rectangular grid of 25 points in the center region of the IVF sample. The engineering strain was then found by taking the average of the engineering strain values computed

from each of the 25 points. The nominal stress, σ, was calculated using the following relationship

$$\sigma = \frac{F}{wt}, \tag{2.1}$$

where F, is the measured tensile force, and w and t are the average width and thickness, respectively, of the IVF sample.

2.2.3 Model Optimization

The calculated stress and strain values were then analyzed through a combination of optimized linear and exponential continuous functions. The continuous model was based on the methodology presented by Tanaka et al. [70] in a previous study, which highlighted its benefits over using conventional curve-fitting techniques when computing linear and exponential parameters for soft biological materials. As pointed out in the prior study, efforts to model soft biological data using traditional piecewise methods often lead to discontinuities between the linear and exponential regions or result in a discontinuous modulus. The continuous method by Tanaka [70] minimizes the mean square error (MSE) while simultaneously calculating the linear parameters, exponential parameters, and the location of a transition point between the two regions. Our model employed a similar method to determine the location of a transition point between a low strain linear region and an exponential region as well as a secondary transition point between the exponential region and a high strain linear region. The model minimized both the MSE and the percent error while calculating all linear and exponential parameters as well as the location of the two transition points.

The following equations describe the continuous model

$$\sigma_{\mathrm{m}}(\epsilon_{xx}) = \begin{cases} m_1\epsilon_{xx}, & \epsilon_{xx} < p_1, \\ ae^{b\epsilon_{xx}} + q_1, & p_1 \leq \epsilon_{xx} < p_2, \\ m_2\epsilon_{xx} + q_2, & p_2 \leq \epsilon_{xx}, \end{cases} \tag{2.2}$$

where σ_{m} is the model calculated stress, ϵ_{xx} is the engineering strain in the longitudinal direction, and (p_1, q_1) and (p_2, q_2) are transition points between the linear and exponential regions of the stress-strain data. In addition, m_1, m_2 and a, b, are model parameters of the linear and exponential regions, respectively. In order to ensure continuity at the transition points, the slopes of the linear regions m_1 and m_2, and the stress values at the transition points, q_1 and q_2 are defined in terms of a and b using the following relationships,

$$m_1 = abe^{b\epsilon_{xx}(p_1)}, \tag{2.3}$$

$$m_2 = abe^{b\epsilon_{xx}(p_2)}, \tag{2.4}$$

$$q_1 = ab\epsilon_{xx}(p_1)e^{b\epsilon_{xx}(p_1)} \tag{2.5}$$

$$q_2 = ae^{b\epsilon_{xx}(p_2)} + q_1. \tag{2.6}$$

The continuous model utilized the MATLAB® function *fmincon* to calculate parameters a, b, p_1 and p_2 while minimizing the MSE and percent error which were defined by

$$\mathrm{MSE} = \frac{1}{n}\sum_{i=1}^{n}(\sigma_{\mathrm{m}}(i) - \sigma(i))^2, \tag{2.7}$$

$$\%\mathrm{Error}(i) = \frac{\sigma(i) - \sigma_{\mathrm{m}}(i)}{\sigma(i)}, \tag{2.8}$$

where i is the index number that corresponds to each data point and n is the total number of data points being analyzed. Figure 2.4 illustrates the continuous model fit to data collected from a representative sample.

2.2.4 Statistical Analysis

Elastic model parameters were determined for each of the 16 samples using the continuous optimization method described previously. Modulus values were recorded for each sample from 0 to 0.40 mm/mm strain at an interval of 0.05 mm/mm. A student's t–test was then used to compare

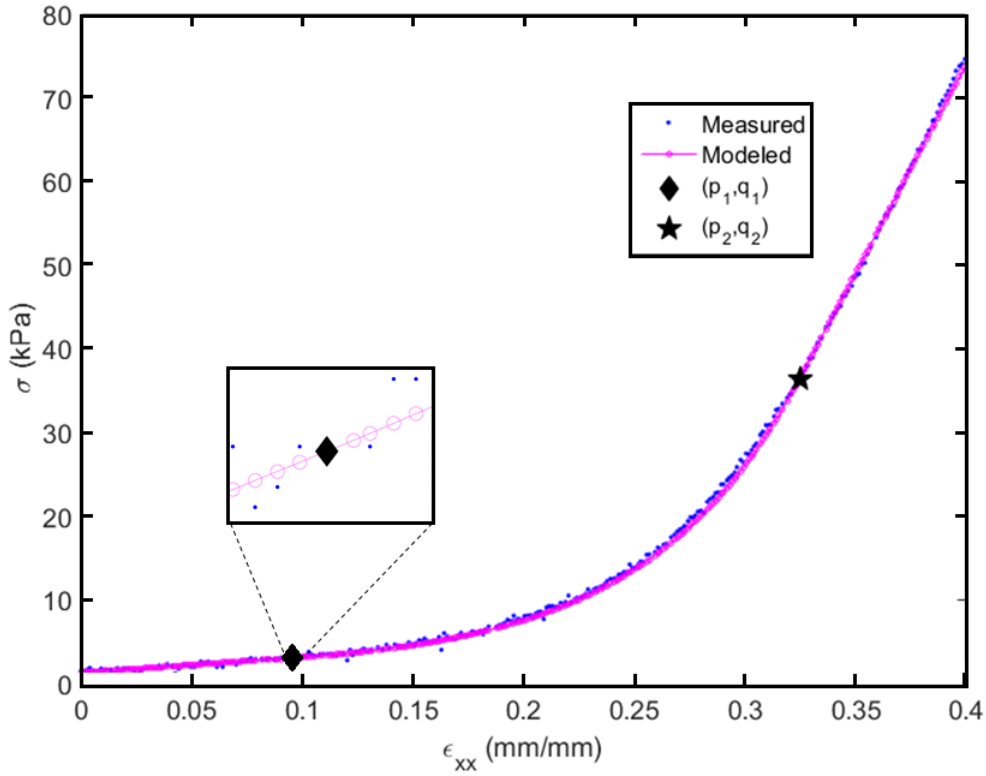

Figure 2.4: Continuous model analyzed for porcine IVF sample

the modulus values at various strain values to an average low strain modulus (mean modulus at 0.05 mm/mm) and a high strain modulus (0.35 mm/mm). The threshold chosen for statistical significance was 0.05. Data were analyzed using the JMP statistical software (JMP, Version 10, SAS Institute Inc.).

2.3 Results

The average recorded length, width, and thickness for the porcine vocal fold samples was found to be 25.69 ± 4.8 mm, 5.57 ± 1.31 mm, and 1.91 ± 0.62 mm, respectively. Data from each of the 16 IVF samples was analyzed individually to obtain model parameters. Analyzing the sample

data individually enabled the calculation of standard deviation values for the transition points, which can be found in Table 2.1. Figure 2.5 displays the average stress, σ_{mean}, for the total data set of all 16 porcine IVF tension tests along with the shaded regions representing $\pm$ standard deviation across all strain values for the samples tested. Results of all linear and exponential parameters calculated from the continuous model can be seen in Table 2.1. The slope of the low-strain linear region ($\epsilon_{xx} < p_1$) was found to be 17.86 ± 7.91 kPa while the slope in the high-strain region ($\epsilon_{xx} > p_2$) was 609.27 ± 236.73 kPa. The transition points p_1 and p_2 were found to be 0.122 ± 0.058 and 0.308 ± 0.069 mm/mm, respectively. The standard deviation for the transition points were calculated by evaluating the values of p_1 and p_2 for each of the 16 IVF samples. The parameters a and b were determined from the averaged data set to describe the nonlinear region between transition points p_1 and p_2 and can be found in Table 2.1. The exponential equation, $\sigma_{\text{m}}(\epsilon_{xx}) = 0.083e^{19.32\epsilon_{xx}} + 2.0951$ kPa, follows the form of $\sigma_{\text{m}}(\epsilon_{xx}) = ae^{b\epsilon_{xx}} + q_1$ to describe the stress-strain relationship between the transition points where $q_1 = \sigma(p_1)$.

Table 2.1: Mean and Standard Deviation Model Parameter Values

	m_1	a	b	m_2	p_1	p_2
σ_{mean}	17.86	.083	19.32	609.27	0.122	0.308
STD	7.91	-	-	236.73	0.058	0.069

The elastic modulus, E, was calculated from the continuous model, where $E = \frac{\mathrm{d}\sigma_m}{\mathrm{d}\epsilon_{xx}}$. The resulting modulus can be seen in Figure 2.6 plotted with respect to the strain. As described previously, the continuous model maintains continuity throughout the transitions points. The modulus of low and high strain linear regions can be represented by the constants m_1 and m_2, while the nonlinear region, which is evaluated at strain values, ϵ_{xx}, between p_1 and p_2, can be described by $abe^{b\epsilon_{xx}}$ where a and b are constants as shown in Table 2.1.

Modulus values were calculated for each of the tests individually and recorded at engineering strain values from 0 to 0.40 mm/mm at an interval of 0.05 mm/mm. Table 2.2 highlights the average modulus, E_{mean}, and standard error of the mean (SEM) values for each of the recorded strain values. A student t–test was conducted to compare each set of modulus values to a low and high

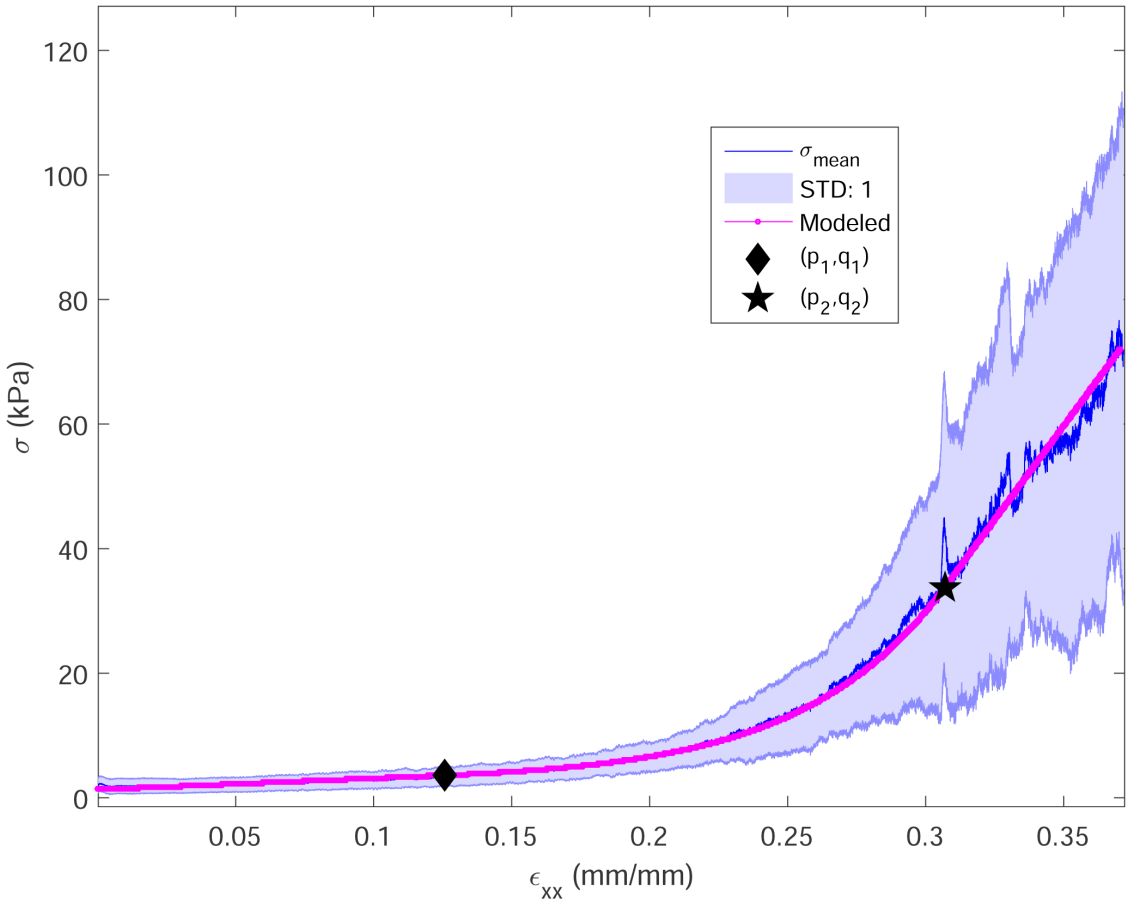

Figure 2.5: Mean and standard deviation of stress-strain data collected from 16 IVF porcine samples (parameters for continuous model can be found in Table 1)

strain modulus value evaluated at 0.05 mm/mm and 0.35 mm/mm respectively. The resulting p–values highlighting differences in the compared modulus values can be see in Table 2.2. A comparison between the low-strain modulus value evaluated at 0.05 mm/mm and recorded values at 0.10 mm/mm showed no statistically significant differences ($p = 0.173$). All other strain intervals greater than 0.10 mm/mm, however, indicated significant differences ($p < 0.05$) from the recorded values at 0.05 mm/mm. Conversely, all strain intervals lower than 0.30 mm/mm were found to have significant differences when compared to the recorded high strain modulus values at 0.35 mm/mm. These results are found to be in agreement with the location of the transition points, where all of the strain intervals between p_1 and p_2 have statistically significant differences when compared to

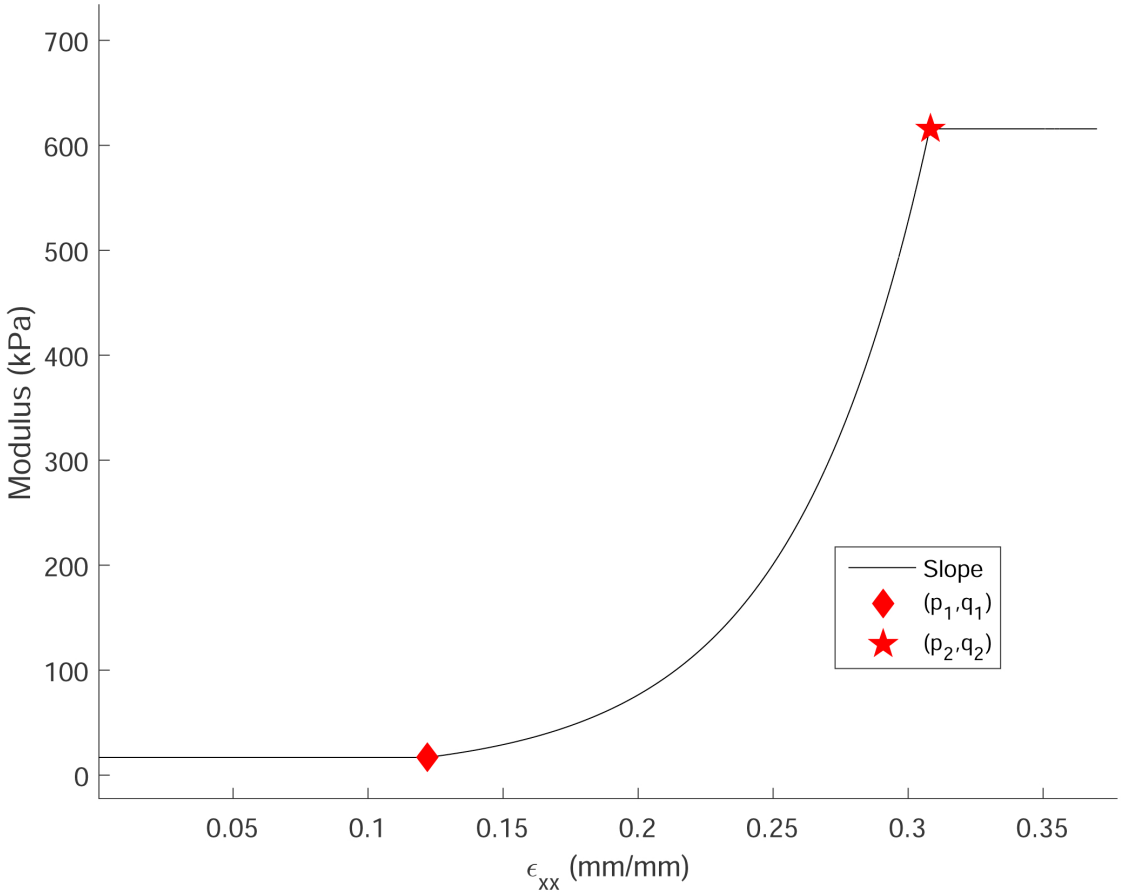

Figure 2.6: Continuous model modulus highlighting transition points and linear and exponential regions

the low and high strain linear modulus values.

2.4 Discussion

The average low-strain modulus was compared to the results reported in a prior study [44] of porcine inferior vocal folds where a value of 16.3 ± 1.9 kPa was determined. The results in this study are found to be in agreement with no statistically significant differences (p–value = 0.486) in the reported finding and a 8.73% difference in the average low-strain modulus. In addition, the modulus results were compared to prior studies which reported findings on human true vocal folds

Table 2.2: Mean and standard error of the mean modulus values for different engineering strain as well as the resulting p–values from individual Student t–tests to compare the modulus at each strain interval to the low and high strain modulus values of 0.05 and 0.35 mm/mm, respectively.

ϵ_{xx}	0.05	0.10	0.15	0.20	0.25	0.30	0.35
E_{mean}	17.68	21.68	39.00	87.44	224.14	517.15	651.97
SEM	1.56	2.32	7.04	19.45	51.17	123.99	111.04
Low: p	-	**0.173**	0.011	0.002	< 0.001	< 0.001	< 0.001
High: p	< 0.001	< 0.001	< 0.001	< 0.001	0.003	**0.483**	-

samples and prior tests of canine vocal fold cover layer samples [14, 47]. At low-strains, Alipour et al. [14] reported an average canine cover vocal fold modulus of 41.9 ± 7.1 kPa while a high strain modulus evaluated at 35% strain was determined to be 132 kPa based off the reported third-order polynomial. In a different study, the authors [47] determined a low-strain modulus value of 28 kPa for human vocal fold samples while a high strain modulus value was found to be 390 kPa between 30% and 35% strain. The low strain modulus for the porcine IVF was found to be lower than the reported findings for both the human vocal fold samples [47] and the canine vocal fold cover samples [14]. The porcine IVF samples, however, exhibited higher modulus values at higher strains than the canine or human results presented [14, 47].

As Figures 2.5 and 2.6 illustrate, the results demonstrate the nonlinear elasticity of the porcine vocal folds. The nonlinearity of the tissue is thought to be a result of collagen fiber recruitment occurring as the sample is stretched, while the low-strain linear region occurs before the collagen fibers are under tension and bear load [75]. At low strains, collagen fibers may exist in a crimped or wavy state. As the vocal folds are elongated, the collagen fibers can begin to straighten and eventually become taut and load bearing. An increasing number of collagen fibers may be recruited under tension as the tissue stretches which could contribute to the nonlinear stress-strain response. The linear low-strain modulus can be assumed to be a result of the elastin content in the tissue before the collagen recruitment occurs around the transition point p_1.

This study focused on only uniaxial elastic tensile tests of porcine inferior vocal folds, which have

been previously used in excised larynx testing [52]. Although biaxial tension tests are typically preferred to characterize tissue responses to varying loads, geometric constraints requiring tissue sample sizes of at least 3×3 cm prevented these tests from occurring using the porcine vocal fold samples. Prior studies have indicated that the composition of pig vocal folds is more similar to humans than canine, cow, or sheep vocal folds and could be a particularly useful model of phonation [6, 7]. The nonlinear stress-strain relationship found in porcine vocal folds could be especially helpful when evaluating frequency changes during vocal fold vibration. As indicated in previous studies [44], porcine vocal folds may be likely strain rate dependent and the nonlinear stress-strain curves, including the elastic parameters of the proposed model, may change at different strain rates. For this reason, future experiments should be conducted to further explore the viscoelasticity of the tissue with regard to the nonlinear elastic properties.

In a prior study [45], researchers investigated the spatially-varying elastic properties of one human vocal ligament. It is possible that porcine vocal folds also exhibit spatially varying elasticity. To our knowledge, there have not been investigations on the spatial variations in elasticity of the porcine vocal fold cover layer. The authors of the prior study [45], also posed questions and investigated how the spatially varying elasticity would impact the eigenfrequency response of the tissue during phonation. Similarly, it would be of interest to investigate the spatial variations in porcine vocal folds and also investigate how those variations impact the dynamic response of the tissue during sound production. In addition, it is important to note that the strain values were computed in this study by tracking 25 points in center region of the tissue. Thus, spatial variations in the porcine tissue elasticity could lead to differences in the recorded strain values when using different methods to compute the tissue strain such as clamp displacement.

Non-contact means of measuring strain, such as DIC, are typically more appropriate when evaluating the tissue strain during excised larynx tests and have been used in prior studies [52]. The use of DIC methods in our study to help produce the continuous model parameters can be used as a foundation for future tests using excised porcine vocal folds to evaluate sound production. In particular, our results indicate the need to consider the location of transition points p_1 and p_2 and

the corresponding change in elastic modulus between the low and high strain linear regions during excised larynx testing.

As mentioned previously, models of vocal fold vibration rely heavily on the elastic properties of the tissue [61]. When studying the vibration of vocal folds during excised larynx tests and, in particular, evaluating frequency changes produced by the tissue, it is necessary to have a clear understanding of how the modulus changes with tissue strain. Thus, the development of a comprehensive continuous modulus model that evaluates transition points between the linear and exponential regions while also employing the use of non-contact DIC methods for measuring strain values can be particularly useful in future studies to evaluate phonation dynamics using excised porcine vocal folds.

Chapter 3

Vocal Fold Dynamic Modeling and Testing

Garret Burks, Raffaella De Vita, Alexander Leonessa. Evaluation of excised porcine larynx frequencies due to vocal fold elastic properties. (2019).

Abstract

The work presented in this study investigates the impact of changing vocal fold elastic properties on the frequencies of vibration during phonation. Excised porcine larynx tests were conducted to examine the relationship between porcine vocal fold anterior-posterior strain and the resulting changes in phonation frequency. During each test, two high speed cameras (4000 FPS) and a microphone (44100 Hz) were used to record changes in vocal fold dynamics while a servo motor stretched the tissue in the anterior-posterior direction. A digital image correlation tracking method was then used to measure anterior-posterior strain. Strain measurements were related to changes in vocal fold elasticity based on previously reported mean elastic parameters which describe porcine vocal fold elasticity from $0 - 40\%$. Additionally, an aeroelastic model of phonation which incorporates the measured vocal fold geometry, elastic properties, and air flow characteristics was implemented to further study the impact of changing porcine vocal fold elasticity on vibration frequency. Phonation was first observed at a strain of 0.18 mm/mm with a fundamental frequency of 247 Hz and increased to 404 Hz at a strain of 0.35 mm/mm.

3.1 Introduction

The vocal folds, which are housed within the laryngeal cavity, serve several important physiological functions. First, the vocal folds play a important role in respiration by opening and allowing air to flow between the lungs and oral and nasal passageways. Secondly, the vocal folds help to protect the airway and lungs and assist in swallowing by closing medially. Lastly, the vocal folds serve a critical role during phonation and in the modulation of sound frequencies during singing or speaking. Due to the importance of the vocal folds, individuals who suffer from voice-related disorders such as vocal fold paralysis, vocal nodules, or laryngeal cancer can experience significant complications with one or more of those functions which, as a result, can often lead to detrimental impacts on quality of life. In an effort to improve treatment options for individuals suffering from laryngeal cancer or other voice-related disorders, many researchers have studied vocal fold anatomy and physiology as well as vocal fold tissue dynamics under varying conditions.

While some researchers have conducted studies focused on understanding vocal fold anatomy and physiology [4, 6, 7, 13, 31] or investigating the elastic properties of vocal fold tissue [14, 15, 44, 47, 76, 77], other tests have been conducted to better understand vocal fold dynamics during sound production and the mechanics of phonation. In several early excised larynx studies [48, 49, 50, 51], researchers used canine larynges as models of phonation due to their relative ease of accessibility over cadaveric tissue. In one study [51], researchers varied canine vocal fold tension and length while photoglottography (PGG) and electroglottography (EGG) measurements were collected as air passed through the laryngeal cavity to investigate flow characteristics and canine vocal fold position during phonation. Other studies using canine larynges have investigated vocal fold impact stresses [48], the effect of different muscle activation on the fundamental frequency and subglottal pressure in canine vocal folds [50], and the phonatory characteristics of canine hemilaryngeal samples [49]. More recently, researchers have conducted tests using porcine, bovine, and sheep fully excised larynges in addition to canine larynx samples to further study the dynamics of phonation [10, 11, 12, 52]. In addition to the relative ease of availability of porcine or bovine larynges over cadaveric or even canine

voice-boxes, the use of porcine larynges as models of phonation is further supported by previously reported human and porcine similarities in vocal fold structure [6, 7] as well as similarities in vocal fold elasticity across the full vocal range [15, 44]. Prior studies using porcine larynx samples have reported on vocal fold contact stresses and strains during self-oscillation [52], as well as other phonatory characteristics and changes in vocal fold kinematics when subjected to varied airflow and pressures [10, 11]. While some of these studies have reported on the measured frequencies during changing airflow conditions or vocal fold adduction and abduction levels [10, 11], to our knowledge there have not been comprehensive studies reporting on changes in frequency in relation to changes in porcine vocal fold elasticity due to anterior-posterior strain.

While excised larynx studies provide an opportunity for researchers to measure and study phonation, they are often limited by sample availability or cost, tissue variability, as well as sample preservation as most larynx samples have a short time period (minutes) following dissection during which they are viable and appropriate for experimental work. Due to these reasons, other authors have developed mathematical models which can be used to describe speech production and vocal fold dynamics based on vocal fold tissue properties, such as the elastic modulus or tissue density, as well as geometric parameters describing the width, thickness, or length of the tissue [61, 62, 63]. In early mathematical models, researchers used the simple equations for a vibrating string to start describing the motion of the vocal folds during phonation [64]. In other studies, researchers used ribbon or Euler-Bernoulli beam as well as Timoshenko beam models of vibration to account for the motion of the vocal folds in multiple degrees of freedom during self-oscillation [45, 65, 66]. Additionally, several researchers have implemented coupled fluid-structure models of phonation which evaluate the role of glottal aerodynamics in the vibration of the vocal folds [9, 61, 67, 68, 78]. In particular, the aeroelastic model first presented in [9] incorporates the vocal fold geometry, vocal fold tissue properties such as the elastic modulus and Poisson's ratio as well as the airflow characteristics such as the air density, flow rate, and pressure. This model is in not only able to illustrate changes in frequency caused by varying tissue properties but also has the ability to shed light on the onset of phonation due to varying flow conditions.

The work presented in this paper investigates the change in measured phonation frequencies during excised porcine larynx testing due to changes in strain in the anterior-posterior direction. The changes in vocal fold strain were related to changes in changes in elastic modulus using the continuous elastic model parameters reported in [15] in an effort to study the correlation between vocal fold elastic modulus and phonation frequencies. Additionally, the aeroelastic model of phonation proposed in [9] was implemented to further study the impact of the changing porcine vocal fold elastic parameters across the full vocal range (0-40% strain) on the measured vocal fold dynamics.

3.2 Aeroelastic Model Description

The mathematical model highlighted in this section is based off the work presented in [9] which employs the Ritz method [79] to approximate displacement fields of the vocal folds and ultimately to describe the coupled fluid-structure interaction occurring inside the voice-box. The model reported in [9] was chosen since it accounts for geometric and elastic parameters of the vocal folds unlike other lumped-element models [80, 81, 82] in which the mass and stiffness parameters cannot be easily related to the physical properties of the tissue [69]. While the work in [9] and more recently in [68, 78], were primarily interested in studying phonation onset due to varying flow conditions, our work is most interested in understanding the relationship between changing tissue elastic parameters and the frequencies of vibration. The following section describes the structural and fluid components of the model before explaining how we have used the model to better understand the impact of the changing tissue properties on vocal fold dynamics.

3.2.1 Structural Model

In order to numerically model the dynamics of the vocal fold tissue, we can first consider vocal folds with geometrical parameters defined in Fig 2.1. In this figure, the two-dimensional model represents a frontal plane cross-section of the vocal folds which are assumed to be an isotropic,

elastic layer. As the figure shows, the cross-section is symmetric about the center of the glottal channel and the vocal folds can be described by having a depth, D, in the medial-lateral direction and a thickness in the inferior-superior direction defined by the parameters, z_{inf} and z_{sup}. For this study, only one side of the glottal channel was evaluated due to the assumption of symmetry about the center of the channel. Additionally, for all simulated results presented in this study, the geometric parameters were defined as: $D = 10$ mm, $z_{sup} = 7$ mm, $z_{inf} = -7$ mm, and the glottal half width, $g = 0.5$ mm, based on the anatomical measurements of the porcine vocal folds as reported in [15, 83].

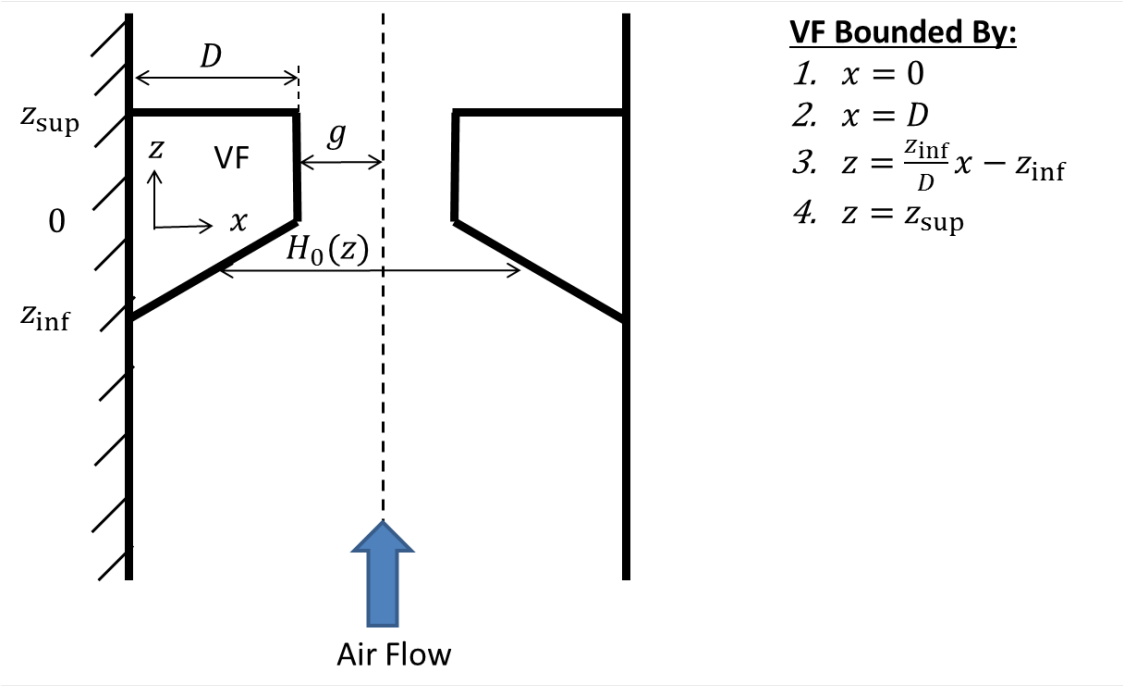

Figure 3.1: 2D frontal plane cross-section of vocal folds and glottal channel. The vocal fold geometry is described has having a depth, D, and a thickness based on the parameters, z_{inf} and z_{sup}. Ref: [9]

The geometric parameters were nondimensionalized and written in the following form,

$$\begin{aligned} \overline{D} &= \frac{D}{l_s}, \\ \bar{z}_{\text{sup}} &= \frac{z_{\text{sup}}}{l_s}, \\ \bar{z}_{\text{inf}} &= \frac{z_{\text{inf}}}{l_s}, \end{aligned}$$

where the nondimensionalized vocal fold depth and thickness parameters, $\overline{D}$, $\bar{z}_{\text{sup}}$, and $\bar{z}_{\text{inf}}$, respectively, were based on the length scale, l_s, which was set equal to the thickness parameter, z_{sup}. In the example which will be highlighted in this section, the nondimensional vocal fold depth and thickness values of

$$\bar{D} = 1.4,$$

$$\bar{z}_{\text{sup}} = 1,$$

$$\bar{z}_{\text{inf}} = -1,$$

were based on the physical vocal fold depth and thickness of $D = 10$ cm, $z_{\text{inf}} = -7$ mm, and $z_{\text{sup}} = 7$ mm and a length scale of $l_s = 7$ mm. To begin modeling the dynamics of the vocal fold tissue, the displacement fields of the vocal folds, ξ and η, which describe the motion in the x and z directions, respectively, were approximated by the decomposition of spatial and temporal variables containing $I \times (K+1)$ terms and expressed as

$$\xi(\bar{x}, \bar{z}, t) = \sum_{i=1}^{I} \sum_{k=0}^{K} A_{ik}(t) \bar{x}^i \bar{z}^k, \tag{3.1}$$

$$\eta(\bar{x}, \bar{z}, t) = \sum_{i=1}^{I} \sum_{k=0}^{K} B_{ik}(t) \bar{x}^i \bar{z}^k, \tag{3.2}$$

where A_{ik} and B_{ik} are time-varying variables and $\bar{x}$ and $\bar{z}$ describe nondimensionalized points within the two-dimensional vocal fold model. Because the spatially-varying points, $(\bar{x}, \bar{z})$, are in a nondimensional form, the resulting displacement fields, ξ and η, will also be calculated as dimensionless values. The time-varying variables A_{ik} and B_{ik} used in the approximations of the displacement fields can be grouped together to form a state vector of generalized coordinates, q_r, where

$$q_r = [A_{10}, A_{11}, ..., A_{IK}, B_{10}, B_{11}, ..., B_{IK}], \tag{3.3}$$

and has a length of $N = 2 \times I \times (K+1)$ based on the summation indices. To illustrate how ξ, η, and q_r will be used later, the expansion for case when $I = 1$ and $K = 1$, is shown below,

$$\begin{aligned} \xi(\bar{x}, \bar{z}, t) &= A_{10}\bar{x} + A_{11}\bar{x}\bar{z}, \\ \eta(\bar{x}, \bar{z}, t) &= B_{10}\bar{x} + B_{11}\bar{x}\bar{z}, \\ q_r &= [A_{10}, A_{11}, B_{10}, B_{11}]. \end{aligned}$$

The displacement fields, ξ and η, can then be related to the strains and stresses in the vocal fold model by the following expressions,

$$\epsilon = \begin{bmatrix} \epsilon_x \\ \epsilon_z \\ \gamma_{xz} \end{bmatrix} = \begin{bmatrix} \frac{\partial \xi}{\partial \bar{x}} \\ \frac{\partial \eta}{\partial \bar{z}} \\ \frac{\partial \xi}{\partial \bar{z}} + \frac{\partial \eta}{\partial \bar{x}} \end{bmatrix}, \tag{3.4}$$

$$\tau = [\tau_x, \tau_z, \tau_{xz}] = G\epsilon, \tag{3.5}$$

where ϵ and τ represent the strains and stresses, respectively, and G is the stress-strain matrix. The stress-strain matrix, G [84], can be expressed as,

$$G = \frac{\bar{E}(1-\nu)}{(1+\nu)(1-2\nu)} \begin{bmatrix} 1 & \frac{\nu}{1-\nu} & 0 \\ \frac{\nu}{1-\nu} & 1 & 0 \\ 0 & 0 & \frac{1-2\nu}{2(1-\nu)} \end{bmatrix} \tag{3.6}$$

where ν is the Poisson's ratio of the vocal fold tissue and $\bar{E}$ is a nondimensional modulus based on

$$\bar{E} = \frac{E}{E_s},$$

where E is the elastic modulus of the vocal fold tissue and E_s is a scaling modulus. Following the previous example when $I = 1$ and $K = 1$, the expressions for $\frac{\partial \xi}{\partial \bar{x}}$, $\frac{\partial \eta}{\partial \bar{z}}$, $\frac{\partial \xi}{\partial \bar{z}}$, and $\frac{\partial \eta}{\partial \bar{x}}$, can be evaluated

as

$$\begin{aligned}
\frac{\partial \xi}{\partial \bar{x}} &= A_{10} + A_{11}\bar{z}, \\
\frac{\partial \eta}{\partial \bar{z}} &= B_{11}\bar{x}, \\
\frac{\partial \xi}{\partial \bar{z}} &= A_{11}\bar{x}, \\
\frac{\partial \eta}{\partial \bar{x}} &= B_{10} + B_{11}\bar{z},
\end{aligned}$$

in terms of the generalized coordinates, q_r. Next, the kinetic and potential energy can be written in terms of the vocal fold displacement fields, strains, and stresses, and expressed as,

$$V(t) = \frac{1}{2}\iint_{\mathrm{VF}} (\dot{\xi}^2 + \dot{\eta}^2)\rho_{vf}\mathrm{d}\bar{z}\mathrm{d}\bar{x}, \tag{3.7}$$

$$U(t) = \frac{1}{2}\iint_{\mathrm{VF}} (\epsilon_x\tau_x + \epsilon_z\tau_z + \gamma_{xz}\tau_{xz})\mathrm{d}\bar{z}\mathrm{d}\bar{x}, \tag{3.8}$$

where $V(t)$ is the kinetic energy, $U(t)$ is the potential energy, ρ_{VF} is the density of the vocal fold model, and the integrals are evaluated over the entire bounded region, VF, describing the vocal fold geometry. The expanded expressions for $\dot{\xi}^2$ and $\dot{\eta}^2$ can be written as

$$\begin{aligned}
\dot{\xi}^2(\bar{x},\bar{z},t) &= \sum_{i,s=1}^{I}\sum_{k,q=0}^{K} \dot{A}_{ik}\dot{A}_{sq}\bar{x}^{i+s}\bar{z}^{k+q}, \\
\dot{\eta}^2(\bar{x},\bar{z},t) &= \sum_{i,s=1}^{I}\sum_{k,q=0}^{K} \dot{B}_{ik}\dot{B}_{sq}\bar{x}^{i+s}\bar{z}^{k+q},
\end{aligned}$$

where $\dot{\xi}^2$ and $\dot{\eta}^2$ are now evaluated over summation indices i, k, s, and q to accommodate the variables being squared. After substituting the expressions for $\dot{\xi}^2$ and $\dot{\eta}^2$ as well as the expressions for $\frac{\partial \xi}{\partial \bar{x}}$, $\frac{\partial \eta}{\partial \bar{z}}$, $\frac{\partial \xi}{\partial \bar{z}}$, and $\frac{\partial \xi}{\partial \bar{z}}$ into (7) and (8) for the case when $I = 1$ and $K = 1$, we can obtain the

following expressions for the kinetic and potential energy,

$$V(t) = \frac{\bar{\rho}_{\text{vf}}}{2} \iint_{\text{VF}} \Big(\dot{A}_{10}^2 \bar{x}^2 + 2\dot{A}_{10}\dot{A}_{11}\bar{x}^2\bar{z} + \dot{A}_{11}^2 \bar{x}^2\bar{z}^2 + \dot{B}_{10}^2 \bar{x}^2 + 2\dot{B}_{10}\dot{B}_{11}\bar{x}^2\bar{z} + \dot{B}_{11}^2 \bar{x}^2\bar{z}^2 \Big) \mathrm{d}\bar{z}\mathrm{d}\bar{x},$$

$$U(t) = \frac{1}{2} \iint_{\text{VF}} (U_x + U_z + U_{xz}) \mathrm{d}\bar{z}\mathrm{d}\bar{x},$$

in terms of the generalized coordinates, where,

$$U_x = G_{11} \left(\frac{\partial \xi}{\partial \bar{x}} \right)^2 + G_{12} \left(\frac{\partial \xi}{\partial \bar{x}} \right) \left(\frac{\partial \eta}{\partial \bar{z}} \right),$$

$$U_z = G_{21} \left(\frac{\partial \xi}{\partial \bar{x}} \right) \left(\frac{\partial \eta}{\partial \bar{z}} \right) + G_{22} \left(\frac{\partial \eta}{\partial \bar{z}} \right)^2,$$

$$U_{xz} = G_{33} \left(\frac{\partial \xi}{\partial \bar{z}} + \frac{\partial \eta}{\partial \bar{x}} \right)^2.$$

Integrating over the bounds of the vocal fold model as illustrated in Figure 3.1 and applying nondimensional values for the parameters described earlier, $\bar{D} = 1.4$, $\bar{z}_{\text{inf}} = 1$, $\bar{z}_{\text{sup}} = 1$, , $\nu = 0.47$, and $\bar{E} = 1$, as well as a nondimensional vocal fold density of $\bar{\rho}_{vf} = 1.03$ yields

$$V(t) = 0.59\dot{A}_{10}^2 + 0.42\dot{A}_{10}\dot{A}_{11} + 0.16\dot{A}_{11}^2 + 0.59\dot{B}_{10}^2 + 0.42\dot{B}_{10}\dot{B}_{11} + 0.16\dot{B}_{11}^2,$$

$$U(t) = U_1 + U_2 + U_3,$$

where,

$$\begin{aligned} U_1 &= 12.6A_{10}^2 + 5.61A_{10}A_{11} + 6.96A_{11}^2 + 3.51B_{11}A_{10} + 2.18B_{11}A_{11}, \\ U_2 &= 6.96A_{10}B_{11} + 2.18A_{11}B_{11} + 6.87B_{11}^2, \\ U_3 &= 0.39A_{11}^2 + 0.89A_{11}B_{10} + 0.28A_{11}B_{11} + 0.71B_{10}^2 + 0.32B_{10}B_{11} + 0.20B_{11}^2. \end{aligned}$$

The kinetic and potential energy expressions can be used to determine the Lagrangian, $L = V - U$,

which can then be substituted into the Lagrange's equation,

$$\frac{d}{dt}\left(\frac{\partial L}{\partial \dot{q}_r}\right) - \frac{\partial L}{\partial q_r} = Q_r, \tag{3.9}$$

where Q_r is the Lagrangian force acting on the generalized coordinate, q_r, due to the airflow through the glottal channel. Lagrange's equation can then be rewritten and organized in the form,

$$M\ddot{q}_r + Kq_r = Q_r, \tag{3.10}$$

where M and K are the mass and stiffness matrices based on the coefficients of the Lagrangian where each element is defined by,

$$\begin{aligned} M_{ij} &= \frac{\partial}{\partial \ddot{q}_j}\left(\frac{d}{dt}\left(\frac{\partial L}{\partial \dot{q}_i}\right)\right), \\ K_{ij} &= \frac{\partial}{\partial q_j}\left(-\frac{\partial L}{\partial q_i}\right). \end{aligned} \tag{3.11}$$

From the earlier example, the mass and stiffness matrices, M and K can be written as

$$M = \begin{bmatrix} 1.18 & 0.42 & 0 & 0 \\ 0.42 & 0.33 & 0 & 0 \\ 0 & 0 & 1.18 & 0.42 \\ 0 & 0 & 0.42 & 0.33 \end{bmatrix},$$

$$K = \begin{bmatrix} 12.62 & 2.80 & 0 & 6.96 \\ 2.80 & 3.89 & 0.44 & 2.31 \\ 0 & 0.44 & 0.71 & 0.16 \\ 6.96 & 2.31 & 0.16 & 7.07 \end{bmatrix},$$

respectively. Note that both M and K have the dimensions $N \times N$ which is based on the length of the generalized coordinate vector and both matrices are symmetric. Next, we can apply a

coordinate transformation,

$$q_r(t) = M^{-1/2}s(t), \tag{3.12}$$

which can be substituted into (10). For the *in vacuo* case where $Q_r = 0$, the resulting equation can be premultiplied by $M^{-1/2}$ to yield,

$$M^{-1/2}MM^{-1/2}\ddot{s} + M^{-1/2}KM^{-1/2}s = 0, \tag{3.13}$$

which can be reduced to,

$$\ddot{s} + \tilde{K}s = 0, \tag{3.14}$$

where $\tilde{K} = M^{-1/2}KM^{-1/2}$ is a mass-normalized stiffness matrix. Because both M and K are symmetric matrices, the resulting mass-normalized stiffness matrix, $\tilde{K}$, is also symmetric. The symmetric eigenvalue problem can then be solved to find the eigenvalues, λ and corresponding eigenvectors, $\mathbf{v}$, in the form of the equation below,

$$\tilde{K}\mathbf{v} = \lambda\mathbf{v},$$

where $\lambda = \omega^2$ for the *in vacuo* case. Following the example using the nondimensional parameters described earlier, the resulting first three natural frequencies are $\omega_1 = 0.117$, $\omega_2 = 0.308$, and $\omega_3 = 0.710$. In terms of the following physical parameters, $D = 10$ mm, $z_{inf} = -7$ mm, $z_{sup} = 7$ mm, $\rho_{vf} = 1030\ \frac{\text{kg}}{\text{m}^3}$, and $E = 3$ kPa, the first three eigenfrequencies were found to be 28.4, 74.8, and 172.7 Hz when the summation indices $I = 1$ and $K = 1$. In order to plot the modeshapes which describe the vocal fold displacement, the eigenvectors, $\mathbf{v}$ were normalized following

$$\bar{\mathbf{v}} = \frac{1}{\sqrt{\mathbf{v}^{\mathrm{T}}\mathbf{v}}}\mathbf{v},$$

where $\bar{\mathbf{v}}$, is then the normalized vector. The transformation from (13) can then be applied to the normalized eigenvectors to yield,

$$\mathbf{v}_{\text{mode}} = M^{-1/2}\bar{\mathbf{v}},$$

which can then be plotted to describe both the x and z components (ξ and η, respectively) of the vocal fold motion. Lastly, a structural damping term can be constructed as a matrix proportional to the mass matrix in the following form,

$$C = \sigma M,$$

where, σ is a structural damping constant.

3.2.2 Flow Model

The vibrations and sound waves produced by the vocal folds are created by air flow coming from the lungs through the glottal channel. The air flow used in the simulations presented in this report can be assumed to have a constant flow rate at beginning of the glottal channel, $z = z_{inf}$, and to be incompressible. Due to the displacement of the vocal fold tissue in the x-direction, the changing glottal width can be described by the following equation [9],

$$h = -2\xi(f(\bar{z}), \bar{z}), \tag{3.15}$$

where $f(\bar{z})$ represents the surface of the vocal fold where the fluid and structure interact. The fluid structure interface at the mean state can be described by the following expressions which are based on the geometry of the model presented in Figure 1,

$$f(\bar{z}) = \begin{cases} \bar{D}, & 0 \leq \bar{z} \leq \bar{z}_{\text{sup}}, \\ \frac{\bar{D}(\bar{z}_{\text{inf}} - \bar{z})}{\bar{z}_{\text{inf}}}, & \bar{z}_{\text{inf}} \leq \bar{z} \leq 0, \end{cases} \tag{3.16}$$

where $f(\bar{z})$ represents the fluid structure interface. It is important to note that (3.15) is based on the equation for the vocal fold displacement in the x-direction, ξ, at the medial edge of the vocal fold with the coefficient of -2 accounting for the displacement of both folds where a positive displacement indicates a constricting glottal channel. Using the same nondimensional values as presented in the example in the previous section and evaluated when $I = 1$ and $K = 1$, the following expressions for the glottal width, h, can be written to highlight a similar expansion,

$$h(t,\bar{z}) \quad = \quad \begin{cases} -2.8A_{10} - 2.8A_{11}\bar{z}, & 0 \leq \bar{z} \leq \bar{z}_{\text{sup}}, \\ -2.8A_{10}\bar{z} - 2.8A_{10} - 2.8A_{11}\bar{z}^2 - 2.8A_{11}\bar{z}, & \bar{z}_{\text{inf}} \leq \bar{z} \leq 0, \end{cases}$$

where the top and bottom equations represent the changing glottal width in the superior and inferior sections of the model, respectively. Using the principle of conservation of momentum, the velocity distribution through the glottal channel at the mean state can be related to the changing glottal width by

$$w_0(\bar{z}) \quad = \quad \frac{2\bar{g}w_{\text{j}}}{H_0(\bar{z})},$$

where $\bar{g}$ is the dimensionless mean glottal half width, w_{j} is the jet velocity, and $H_0(\bar{z})$ is the changing width of the glottal channel at the mean state based on $f(\bar{z})$. Therefore, we can also write the following expressions,

$$w_0(\bar{z}) \quad = \quad \begin{cases} w_{\text{j}}, & 0 \leq \bar{z} \leq \bar{z}_{\text{sup}}, \\ \frac{2\bar{g}w_{\text{j}}}{2(\bar{D}+\bar{g})-2\bar{D}\left(\frac{\bar{z}_{\text{inf}}-\bar{z}}{\bar{z}_{\text{inf}}}\right)} & \bar{z}_{\text{inf}} \leq \bar{z} \leq 0, \end{cases}$$

where the velocity in the superior and inferior regions at the mean state are based on a total channel width of $2(\bar{D} + \bar{g})$. Following the example from before yields,

$$w_0(\bar{z}) \quad = \quad \begin{cases} 1, & 0 \leq \bar{z} \leq \bar{z}_{\text{sup}}, \\ \frac{-0.14}{2.8\bar{z}-0.14} & \bar{z}_{\text{inf}} \leq \bar{z} \leq 0, \end{cases}$$

when applying a nondimensional jet velocity, $w_{\mathrm{j}} = 1$, and a nondimensional glottal half width, $\bar{g} = 0.0714$ which corresponds to a physical glottal half width, $g = 0.5$ mm when using the same length scale as discussed in the structural model. Using Bernoulli's equation, the changing pressure around the mean state can also be represented by

$$P_0(\bar{z}) \quad = \quad \frac{1}{2}\bar{\rho}_{\mathrm{f}} w_{\mathrm{j}}^2 \left(1 - \frac{4g^2}{H_0(\bar{z})^2}\right),$$

where, $\bar{\rho}_{\mathrm{f}}$ is the nondimensionalized fluid density, and $P_0(\bar{z})$ is the pressure distribution through the glottal channel. The linearized forms of the continuity equation and Bernoulli's equation can then be written as

$$\frac{\partial h}{\partial t} + \frac{\partial w_0 h}{\partial \bar{z}} + \frac{\partial w H_0}{\partial \bar{z}} \quad = \quad 0, \tag{3.17}$$

$$\frac{\partial w}{\partial t} + w_0 \frac{\partial w}{\partial \bar{z}} + w \frac{\partial w_0}{\partial \bar{z}} + \frac{1}{\rho_{\mathrm{f}}} \frac{\partial p}{\partial \bar{z}} \quad = \quad 0, \tag{3.18}$$

respectively, where w is the fluctuating flow velocity and p is the fluctuating pressure which are characterized by the changing glottal width, h, the initial velocity distribution around the mean state, w_0, and initial glottal width at the mean state, H_0. The linearized Bernoulli's equation can be rewritten to solve for the fluctuating pressure within the glottal channel,

$$\frac{p(\bar{z}, t)}{\bar{\rho}_{\mathrm{f}}} \quad = \quad \int_{\bar{z}_{\mathrm{sup}}}^{\bar{z}} \left(\frac{\partial w}{\partial t} + w_0 \frac{\partial w}{\partial \bar{z}} + w \frac{\partial w_0}{\partial \bar{z}}\right) \mathrm{d}\bar{z}, \tag{3.19}$$

which is obtained by first integrating (18) with respect to $\bar{z}$ and then applying the boundary condition $p(\bar{z}_{\mathrm{sup}}) = 0$, which describes the fixed point of flow separation at the superior edge of the vocal folds. The linearized continuity equation can also be reorganized to solve for the fluctuating flow velocity,

$$w \quad = \quad \frac{1}{H_0} \int_{\bar{z}_{\mathrm{inf}}}^{\bar{z}} \left(\frac{\partial h}{\partial t} + h \frac{\partial w_0}{\partial \bar{z}} + w_0 \frac{\partial h}{\partial \bar{z}}\right) \mathrm{d}\bar{z}, \tag{3.20}$$

which is obtained by integrating with respect to $\bar{z}$, dividing by H_0, and applying the condition of $w(\bar{z}_{\text{inf}}) = 0$ due an assumed constant flow rate at the vocal fold inlet. The fluctuating flow velocity, w, can then be substituted into the previous expression for the changing flow pressure which can then be reorganized and ordered in terms of h, h_t, and h_{tt}, where h_t and h_{tt} are the first and second time derivatives of h, respectively. In this way, the fluctuating pressure can be expressed as,

$$\frac{p(z,t)}{\rho_{\text{f}}} = p_0(h) + p_1(h_t) + p_2(h_{tt}) \tag{3.21}$$

and the individual pressure components can be written as

$$\begin{aligned}
p_0 &= \int_{\bar{z}_{\text{sup}}}^{\bar{z}} \left(w_0 \frac{\partial}{\partial \bar{z}} + \frac{\partial w_0}{\partial \bar{z}} \right) \left[\frac{1}{H_0} \int_{\bar{z}_{\text{inf}}}^{\bar{z}} \left(w_0 \frac{\partial h}{\partial \bar{z}} + h \frac{\partial w_0}{\partial \bar{z}} \right) \mathrm{d}\bar{z} \right] \mathrm{d}\bar{z}, \\
p_1 &= \int_{\bar{z}_{\text{sup}}}^{\bar{z}} \left(w_0 \frac{\partial}{\partial \bar{z}} + \frac{\partial w_0}{\partial \bar{z}} \right) \left[\frac{1}{H_0} \int_{\bar{z}_{\text{inf}}}^{\bar{z}} h_t \mathrm{dz} \right] \mathrm{d}\bar{z} \\
&\quad + \int_{\bar{z}_{\text{sup}}}^{\bar{z}} \left[\frac{1}{H_0} \int_{\bar{z}_{\text{inf}}}^{\bar{z}} \left(w_0 \frac{\partial}{\partial \bar{z}} + \frac{\partial w_0}{\partial \bar{z}} \right) h_t \mathrm{d}\bar{z} \right] \mathrm{d}\bar{z}, \\
p_2 &= \int_{\bar{z}_{\text{sup}}}^{\bar{z}} \frac{1}{H_0} \int_{\bar{z}_{\text{inf}}}^{\bar{z}} h_{tt} \mathrm{d}\bar{z} \mathrm{d}\bar{z},
\end{aligned}$$

where the pressure terms, p_0, p_1, and p_2 are made up of the combined zero-order, first-order, and second-order pressure and velocity terms, respectively, from (3.19) and (3.20). Following the earlier example, the pressure term, p_0, can be written in the following form,

$$p_0(t,\bar{z}) = \begin{cases} 0.02A_{11} - 0.02A_{11}\bar{z}, & 0 \le \bar{z} \le \bar{z}_{\text{sup}}, \\ \frac{2.4\times10^{-5}(A_{10}(2.8\bar{z}+2.8)+A_{11}\bar{z}(2.8\bar{z}+2.8))}{(2.8\bar{z}-0.14)^3} + & \\ \qquad +0.02A_{10} + 0.02A_{11}, & \bar{z}_{\text{inf}} \le \bar{z} \le 0, \end{cases}$$

where the pressure p_0 contains only the the time-varying constants $A_{ik}(t)$ from the expression for the fluctuating glottal width, h, and the spatially varying locations $\bar{z}$. Similarly, the pressure terms p_1 and p_2 can be written as functions of the spatially varying points, $\bar{z}$, and the constants $\dot{A}_{ik}(t)$ in the expression of p_1 and $\ddot{A}_{ik}(t)$ in the expression of p_2. The pressure terms can then be related to the force, Q_r which acts on the vocal fold surface through the Lagrangian force equation in the

form,

$$Q_r = -\int_{l_{\mathrm{FSI}}} \left(p\frac{\partial \xi}{\partial q_r} n_x + p\frac{\partial \eta}{\partial q_r} n_z \right) \mathrm{d}l_{\mathrm{FSI}}, \tag{3.22}$$

where l_{FSI} represents the interface between the vocal fold and fluid, the negative sign ensures that a positive pressure exerts a force directed into the vocal fold, and n_x and n_z represent the x and z components of a normal vector to vocal fold and fluid interface. Using the dimensions of the vocal fold model in Figure 3.1, the unit normal vector components were found to be

$$n_x = \begin{cases} 0, & 0 \leq \bar{z} \leq \bar{z}_{\mathrm{sup}}, \\ \frac{-\overline{D}}{\sqrt{\bar{z}_{\mathrm{inf}}^2 + \overline{D}^2}} & \bar{z}_{\mathrm{inf}} \leq \bar{z} \leq 0, \end{cases}$$

$$n_z = \begin{cases} 1, & 0 \leq \bar{z} \leq \bar{z}_{\mathrm{sup}}, \\ \frac{\bar{z}_{\mathrm{inf}}}{\sqrt{\bar{z}_{\mathrm{inf}}^2 + \overline{D}^2}} & \bar{z}_{\mathrm{inf}} \leq \bar{z} \leq 0, \end{cases}$$

where the direction of the normal vector was chosen so that it always points outward from the vocal fold structure. In order to perform the line integral along l_{FSI}, the equations were parameterized using the following substitutions

$$\bar{x} = \begin{cases} \overline{D}, & 0 \leq \bar{z} \leq \bar{z}_{\mathrm{sup}}, \\ \overline{D}\alpha & \bar{z}_{\mathrm{inf}} \leq \bar{z} \leq 0, \end{cases}$$

$$\bar{z} = \begin{cases} \bar{z}_{\mathrm{sup}}\alpha, & 0 \leq \bar{z} \leq \bar{z}_{\mathrm{sup}}, \\ \bar{z}_{\mathrm{inf}} - \bar{z}_{\mathrm{inf}}\alpha & \bar{z}_{\mathrm{inf}} \leq \bar{z} \leq 0, \end{cases}$$

and then integrated with respect to α from 0 to 1. Each of the inferior and superior pressures terms p_0, p_1, and p_2 were substituted into (3.22) to determine the force acting in each region. The total

force acting on the vocal folds, Q_r, can then be written as

$$Q_r = Q_0 q_r + Q_1 \dot{q}_r + Q_2 \ddot{q}_r. \tag{3.23}$$

Following the example described earlier the force terms can be written in matrix form as,

$$Q_0 = \begin{bmatrix} -0.016 & -0.033 & 0 & 0 \\ 0.006 & 3.03 \times 10^{-6} & 0 & 0 \\ 0.022 & 0.023 & 0 & 0 \\ -0.007 & -0.008 & 0 & 0 \end{bmatrix},$$

$$Q_1 = \begin{bmatrix} -0.074 & -0.044 & 0 & 0 \\ 0.003 & -0.001 & 0 & 0 \\ 0.059 & 0.031 & 0 & 0 \\ -0.019 & -0.010 & 0 & 0 \end{bmatrix},$$

$$Q_2 = \begin{bmatrix} -0.021 & -0.008 & 0 & 0 \\ -5.0 \times 10^{-4} & -3.0 \times 10^{-4} & 0 & 0 \\ 0.015 & 0.006 & 0 & 0 \\ -0.005 & -0.001 & 0 & 0 \end{bmatrix},$$

where Q_0, Q_1, and Q_2 are obtained by integrating p_0, p_1, and p_2 in (22). Note that each matrix only consists of terms in first two columns as a result of the expressions being comprised of only A_{ik}, $\dot{A}_{ik}$, or $\ddot{A}_{ik}$ terms due to the expression for the changing glottal width in (15) containing no B_{ik} terms.

3.3 Aeroelastic Vocal Fold Model Results

Before using the aeroelastic model to simulate the vocal fold dynamics, it is first necessary to determine the required values for the summation indices I and K. The first three eigenfrequencies, ω

were determined for varying summation indices I and K while using the same geometric parameter values as described in the previous sections. Figure 3.2, illustrates how the eigenfrequencies converge as the size of the mass and stiffness matrices are increased with the summation indices, I and K. When $I = K = 4$, the calculated values for the first three eigenfrequencies are all within 1% of their converged value. Therefore, unless otherwise stated, the results highlighted in the following section will be determined when $I = K = 4$ and the resulting q_r vector is composed of 40 terms.

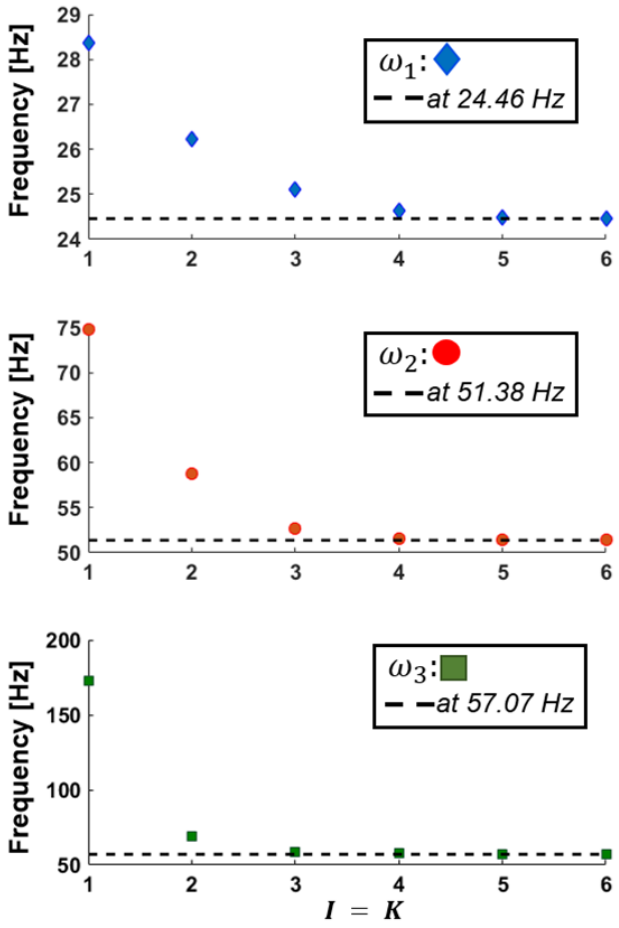

Figure 3.2: This figure illustrates how the calculated values for the first 3 eigenfrequencies change as the number of eigenmodes is increased with the summation variables I and K. When $I = K = 4$, the approximations for ω_1, ω_2, and ω_3 are all within 0.5 Hz of their converged values.

After determining the minimum values of the summation indices I and K, it was then possible

to plot the modeshapes based on the eigenvectors calculated following the previously described method. Figure 3.3 illustrates modeshapes based on the first, second, and third eigenvectors for the *in vacuo* case when $Q_r = 0$. The top row illustrates the x component of the displacement based on the displacement field, $\xi(\bar{x}, \bar{z}, t)$, while the bottom row shows the z component of displacement based on the displacement field $\eta(\bar{x}, \bar{z}, t)$. It is important to note that due to the fixed boundary condition, there is no motion in either direction along the lateral edge of the vocal fold model. As can be seen the figure, the first eigenmode is primarily characterized by movement in inferior-superior direction along the medial edge of the vocal fold. The second eigenmode shows greater displacement in medial-lateral direction along the superior edge of the vocal fold model. Similarly, the third eigenmode contains significant medial-lateral movement slightly inferior on the vocal fold surface. In addition to evaluating the eigenfrequencies and eigenmodes for the *in vacuo* case, it

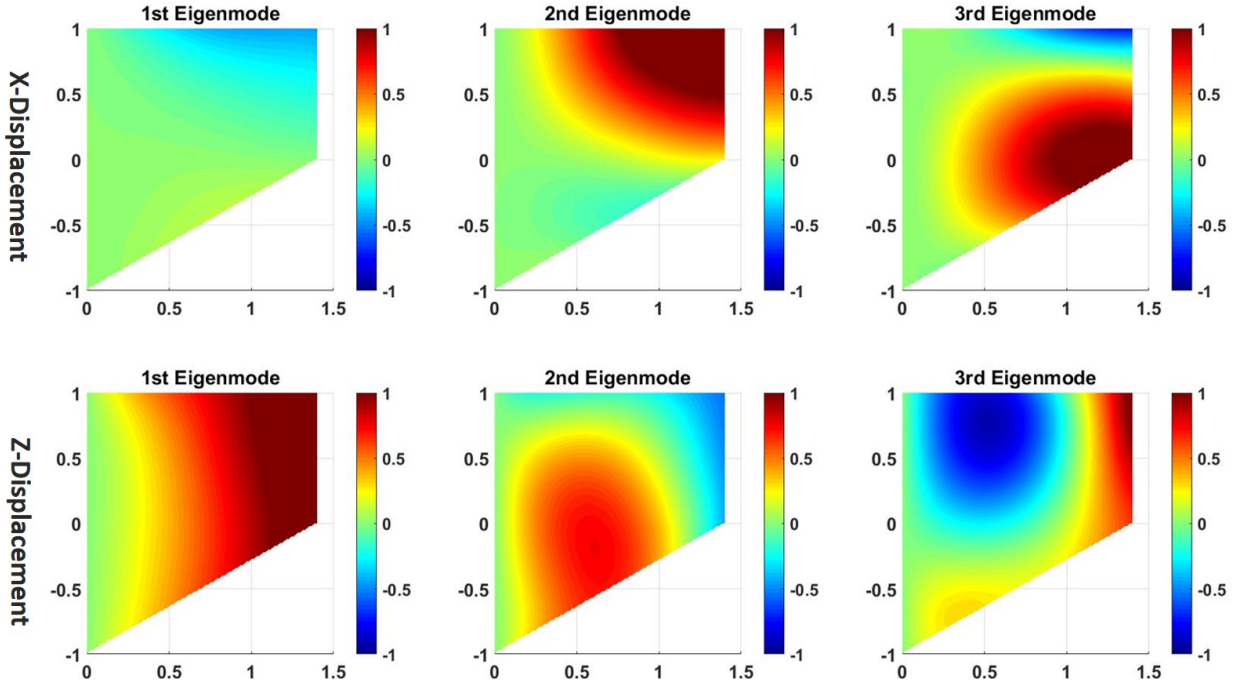

Figure 3.3: This figure illustrates the 1st, 2nd, and 3rd *in vacuo* eigenmodes of the vocal fold. The top row shows the x-component and the bottom row shows z-component of the vocal fold displacement.

was also important to evaluate the dynamic response when airflow was present. After solving for

all structural and force matrices due to the airflow, a new differential equation can be written as

$$M\ddot{q}_r + C\dot{q}_r + Kq_r \quad = \quad Q_2\ddot{q}_r + Q_1\dot{q}_r + Q_0 q_r,$$

which can be reorganized in the form,

$$(M - Q_2)\ddot{q}_r + (C - Q_1)\dot{q}_r + (K - Q_0)q_r \quad = \quad 0. \tag{3.24}$$

The new differential equation can then be expressed in state space form as,

$$\begin{bmatrix} \dot{q}_r \\ \ddot{q}_r \end{bmatrix} = \begin{bmatrix} 0 & I \\ -(M - Q_2)^{-1}(K - Q_0) & -(M - Q_2)^{-1}(C - Q_1) \end{bmatrix} \begin{bmatrix} q_r \\ \dot{q}_r \end{bmatrix}. \tag{3.25}$$

The eigenvalue problem can then be written as

$$A\mathbf{v} = \lambda\mathbf{v}, \tag{3.26}$$

where A is a matrix comprising all of the fluid and structural terms as shown in (25). Because the matrix A will generally be asymmetric, the resulting eigenvalues will likely be complex with imaginary components providing information on the frequencies of vibration and the real components providing information on the growth rates and ultimately on phonation onset. As mentioned previously, while other groups such as [9] have focused on understanding phonation onset due to varying flow conditions or structural loss parameters, this study is primarily interested on understanding the impact of changing physical properties of the vocal fold on the frequencies produced by the tissue. In order to determine the impact of the physical properties of the vocal fold on the the dynamic response, simulations were run to calculate the eigenvalues and eigenvectors of (26) while varying the Poisson ratio, ν from 0.22 to 0.49 and the elastic modulus, E from 15 to 750 kPa. The range for the elastic modulus and Poisson ratio values were selected to span the entire vocal range of porcine vocal folds as determined from uniaxial tensile tests reported in [15]. In addition, a jet

velocity, $U_j = 11.85$ m/s was used based on the measured flow rate from excised dynamic vocal fold experiments described in the following section and the calculated prephonation vocal fold opening area. Lastly, a structural loss constant of $\sigma = 0.1$ was kept constant for all cases. Figure 3.4 highlights the change in frequencies due to changes in both the Poisson's ratio and elastic modulus. The change is frequency (in Hz) is indicated by a change in color for each of the combinations of modulus and Poisson's ratio values. As can be seen in the figure, changes in the the elastic modulus (over the range of the porcine vocal folds) was found to have a significantly larger impact on the frequency response than changes in the Poisson ratio with the calculated fundamental frequency spanning from 60 Hz to 432 Hz across the full elastic range of the tissue.

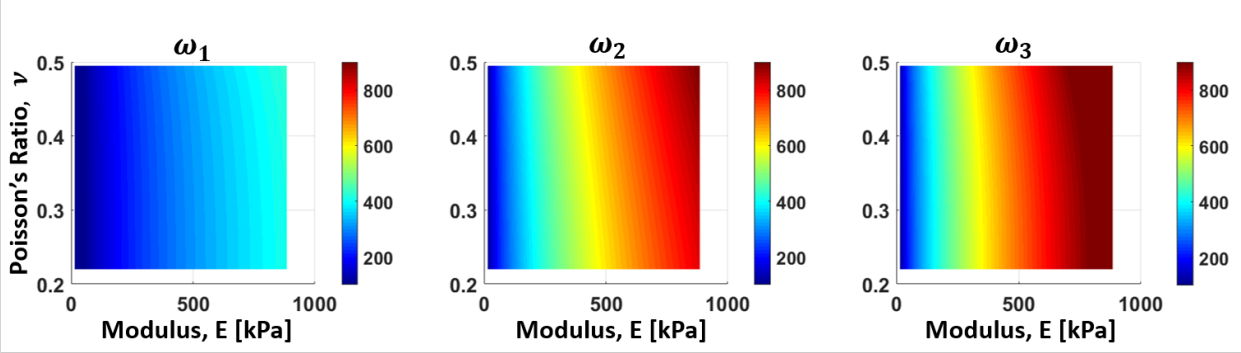

Figure 3.4: This figure illustrates the changing 1st, 2nd, and 3rd eigenfrequencies of the vocal fold due to varying physical properties (ν and E [kPa]). The change in color represents the calculated frequencies in Hz based on equation 26.

Contour plots were also generated, as displayed in Figure 3.5, to further illustrate the impact of changing physical properties on the calculated frequency. Figure 3.5 shows contour lines ranging from 260–370 Hz for the first eigenfrequency, ω_1, over a range of vocal fold modulus values of 250 to 700 kPa and a range of Poisson ratio values from 0.22 to 0.49. As can be seen in the figure, as the modulus increases the frequency increases significantly. Further, as the Poisson's ratio increases the frequency, ω_1, also increases albeit in a significantly smaller manner over the calculated range of Poisson ratios. The information displayed in both of these figures, which show the impact of changes physical properties on the frequency of vocal fold vibration, can be used as a guide in the

manufacturing of the synthetic vocal fold models with a desired frequency response and used as a reference when comparing the measured frequencies during the excised porcine larynx tests.

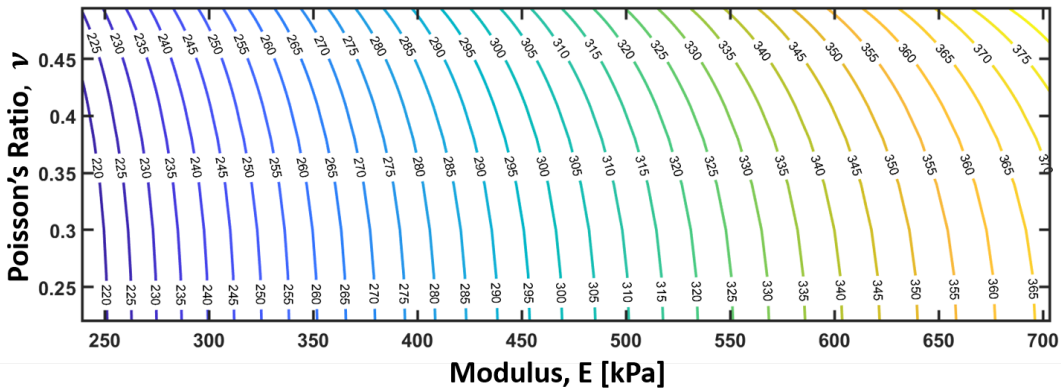

Figure 3.5: Contour plot showing changes in the first eigenfrequency, ω_1, from 320–365 Hz for different elastic modulus values in kPa and different Poisson's ratios.

In addition to evaluating the frequency changes of vocal fold vibration, the change in growth rates which result in phonation onset due to varying structural parameters were also investigated. Phonation onset and self-sustaining vocal fold oscillation is thought to occur when the structural and flow induced force terms are roughly equivalent. As Figure 3.6 illustrates, the flow velocity which resulted in phonation onset (as indicated by the bifurcation) increased with increasing vocal fold modulus values. Prior to the bifurcation, the flow rates are thought to be insufficient or too low to result in phonation. Similarly, at flow velocity values significantly greater than the bifurcation or critical flow velocity, the vocal folds would likely be pushed open laterally due to the vocal fold structural stiffness values being too low (in comparison to the flow induced forces) to return to the mean state. As demonstrated in previous studies, the vocal fold modulus changes significantly as the tissue is stretched. Thus, the required flow velocity for phonation onset would also significantly change. Further exploration of varying flow rates and varying physical parameters will be needed to better understand how the changing modulus and Poisson ratios impact phonation onset over the entire vocal range.

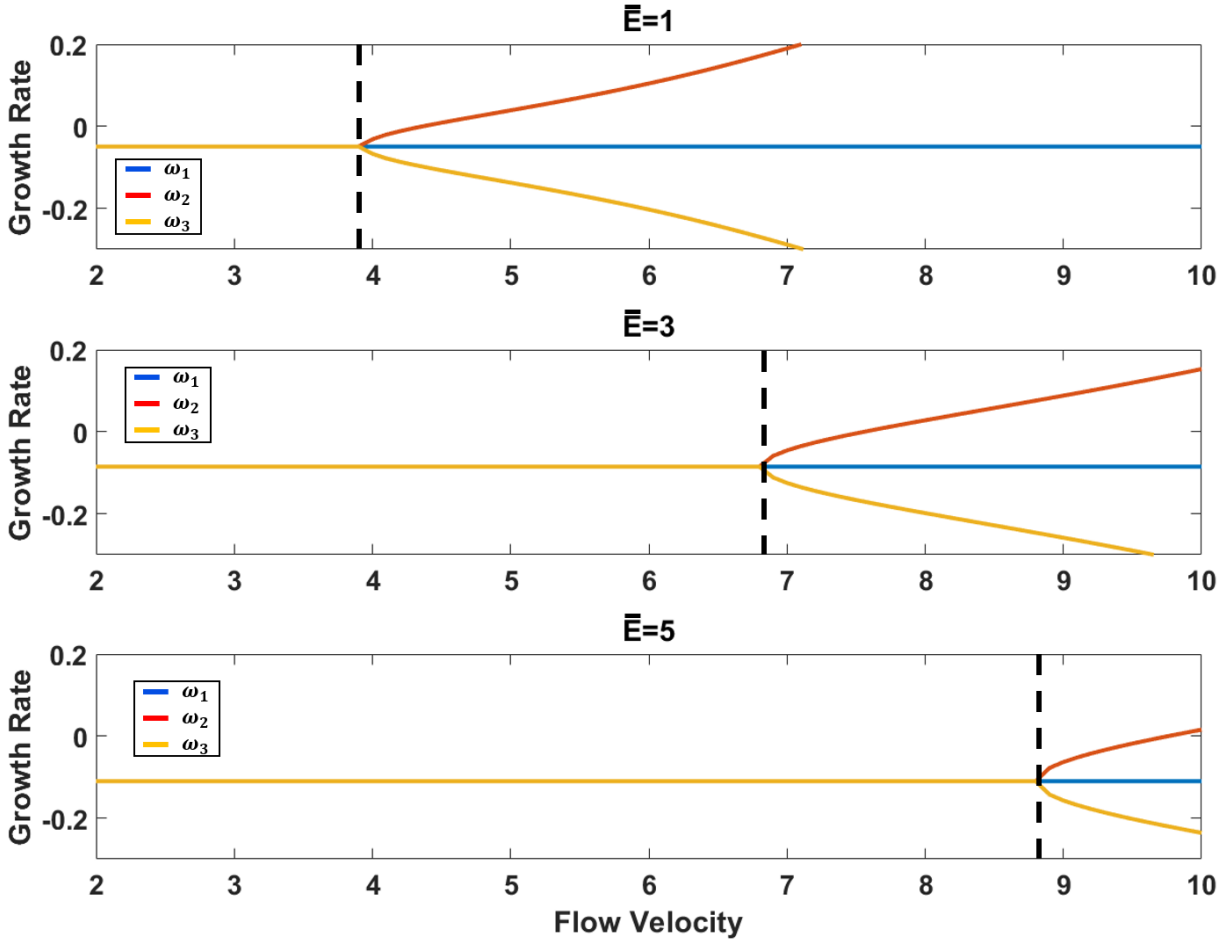

Figure 3.6: Illustration of the changing growth rates due to the varying flow velocities and vocal fold structural parameters. The Poisson ratio was kept constant at 0.47 for each of the three structural conditions. The bifurcation location indicates phonation onset for the given structural and flow parameters.

3.4 Excised Porcine Larynx Test Methodology

The following section highlights the steps taken to prepare porcine larynx samples as well as the methods used for establishing test parameters and methods for data collection during excised porcine larynx phonation experiments.

3.4.1 Sample Preparation

Six excised porcine larynx samples were obtained following IACUC protocol no. #18–222 from an on-campus abattoir in the Virginia Tech Meat Science Center. After collection, samples were transported to the laboratory while immersed in a Phosphate-Buffered Saline (PBS) solution (PBS, pH 7.4, Fisher Scientific, USA). The samples were then stored prior to testing for a maximum duration of two weeks at a temperature of -20 °C with each sample in an individual container and a folded piece of PBS soaked gauze placed between the left and right vocal folds to prevent tissue dehydration. After thawing the tissue slowly on the day of the experiment, sample preparation was conducted following a similar procedure to the study presented in [52].

As illustrated in Figure 3.7, saggital plane dissection cuts were made through the thyroid cartilage from the superior side of the thyroid to the location of the vocal fold attachment. Further, a dissection cut was made in the medial-lateral direction in order to remove all tissue superior to the porcine vocal folds. Great care was taken to not cut through the vocal fold attachment to the thyroid cartilage while removing extraneous tissue. Although the function of the porcine superior vocal folds has been debated in prior studies [10, 11], this study focused on evaluating phonation only due to the inferior vocal folds in order to better relate the changing elastic tissue properties as characterized in [15] to the vocal fold dynamics. Additionally, evaluating only the motion of the inferior porcine vocal folds also results in a more appropriate comparison to human voice production where the true vocal folds are the primary source of vibrations and the false vocal folds are not active oscillators. Therefore, the superior vocal folds were carefully extricated from the porcine larynx samples. In all larynx samples a 3-5 cm section of the trachea was left intact and used to attach the porcine samples to an airflow source via a 1 inch diameter pipe as described in more detail in the next section.

After following the procedure described above to expose the porcine inferior vocal folds, the trachea was mounted on a 1 inch PVC pipe as can be seen in Figure 3.8. The *in situ* length of the inferior vocal folds were measured and recorded using a digital caliper for each sample in a similar manner

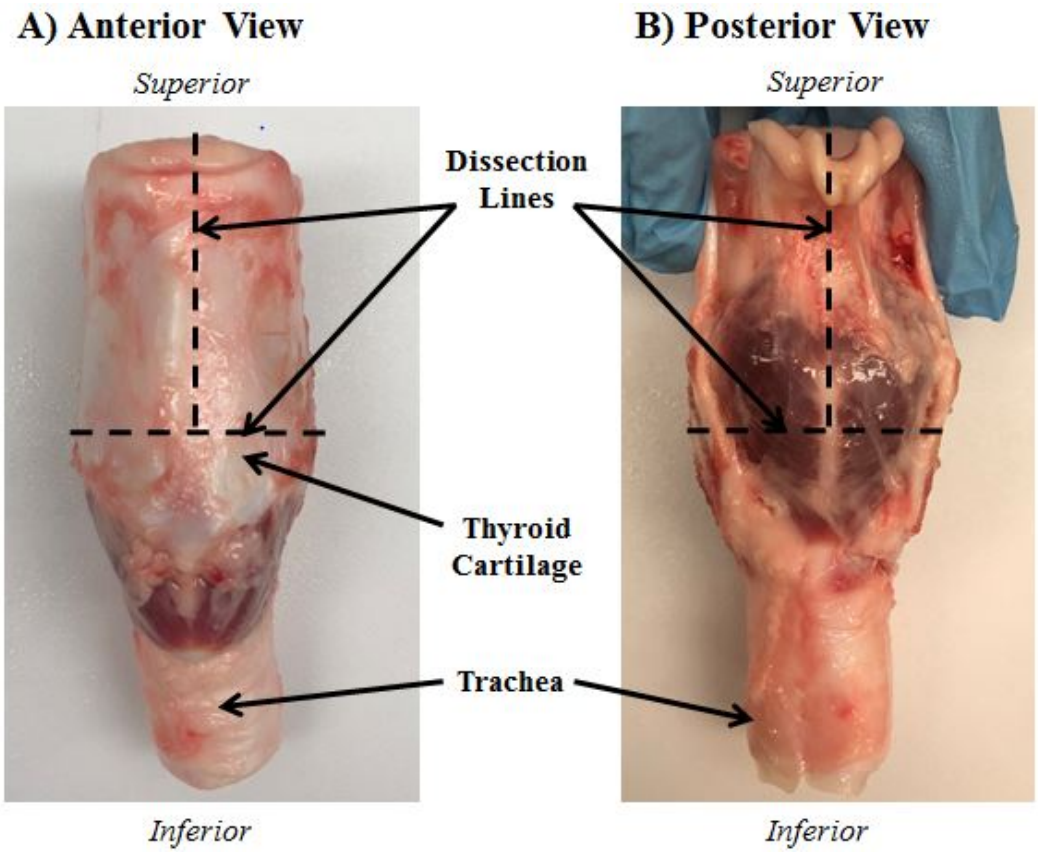

Figure 3.7: A) Anterior view of excised porcine larynx sample highlighting the location of cuts along dissection line through the thyroid cartilage; B) The dissection cut lines on the porcine larynx sample are highlighted from the posterior view of the sample.

to [15]. A braided silk suture was then used to tie the arytenoids together following the suture path which is also highlighted in Figure 3.8. The sutures were tied around a 1×1 inch piece of gauze which was saturated in PBS. Since the epiglottis and other surrounding tissue was removed during the dissection, the saturated gauze helped to ensure airflow was forced through the vocal fold opening instead of between the arytenoids and cricoid cartilage. Using a methylene blue 1% aqueous solution (Fisher Science Education, USA) the inferior vocal folds were dyed before being speckle coated with an aerosol fast dry gloss white paint (McMaster-Carr, USA) following a similar protocol to [15]. Finally, hooks were attached to the anterior side of the thyroid cartilage using a 10 lb test fishing line.

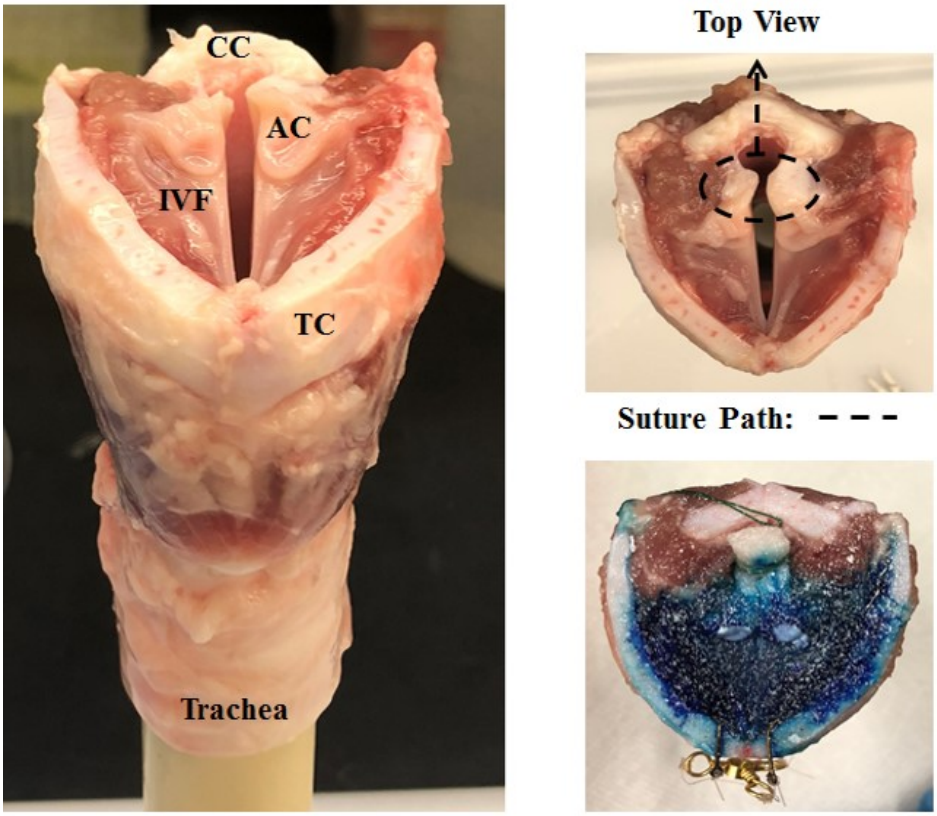

Figure 3.8: Excised porcine larynx sample with exposed inferior vocal folds (IVF). The location of the trachea, thyroid cartilage (TC), arytenoid cartilage (AC), and cricoid cartilage (CC) are also illustrated in the figure. In addition, the top view illustrates the dissection path around the arytenoids as well as the sample after being dyed and speckled.

3.4.2 Excised Larynx Testing Protocol

Each of the excised porcine larynx samples was mounted on a custom built experimental setup as shown in Figures 3.9 and 3.10. As mentioned previously, the trachea was mounted on a 1 inch PVC pipe and secured using a circle clamp. The thyroid cartilage was clamped to prevent movement of the sample in the medial-lateral and inferior-superior directions during testing as seen in the bottom image in Figure 3.9. As mentioned previously, sutures were tied around the arytenoids to bring the vocal folds together medially. On the posterior side of the sample, the sutures were secured to a servo motor (Dynamixel RX-24F) which applied a sinusoidal stretch (frequency = 0.125 Hz, amplitude = 10 mm) in the anterior-posterior direction as shown in Figure 3.9.

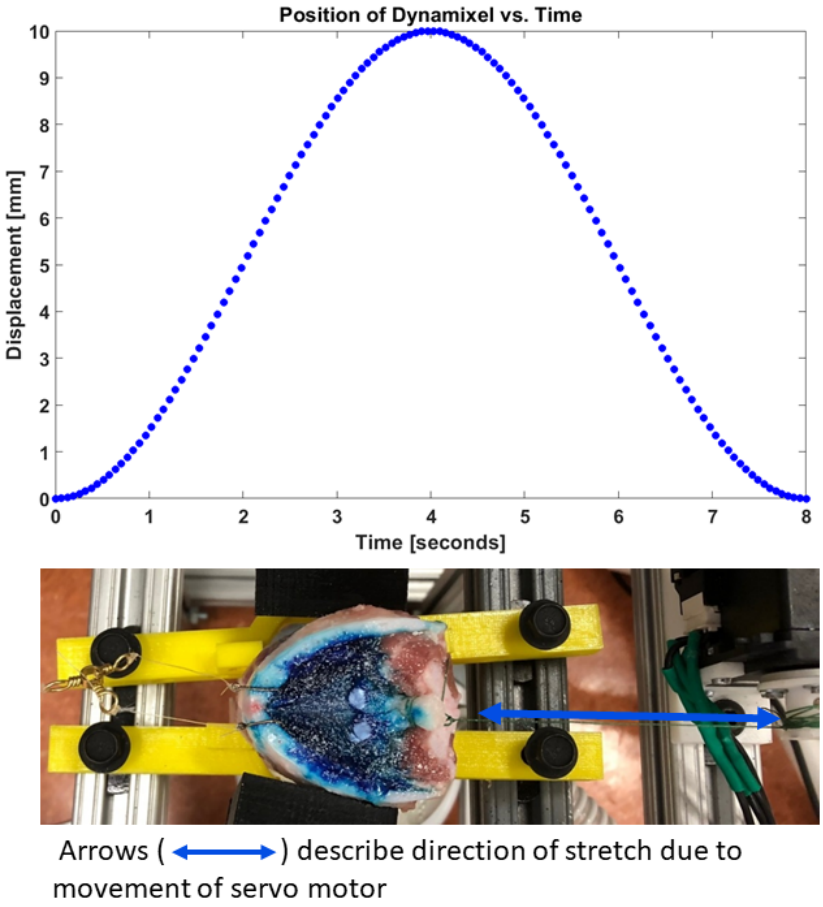

Figure 3.9: Top graph illustrates the sinusoidal movement (frequency = 0.125 Hz, amplitude = 10 mm), of the Dynamixel over an entire test. The bottom image displays a top view of the sample and direction of stretch applied by the Dynamixel servo motor.

The schematic shown in Figure 3.10, further illustrates the testing setup. A muffler was used to reduce both flow fluctuations and excessive noise in air flow from a compressed air source. The airflow was then heated to 90-95 °F and humidified to approximately 85-95% using a humidifier (Fisher & Paykel, HC150 Heated Humidifier) to better simulate airflow through the trachea coming from the lungs. Airflow was adjusted until vocal fold vibration was observed. A flow meter (PCE Instruments) was used to record air flow velocity and temperature approximately 2-4 cm below the clamped sample. As discussed in the previous section, the superior surface of the inferior porcine vocal folds was exposed to better observe vocal fold dynamics during self-oscillation and sound

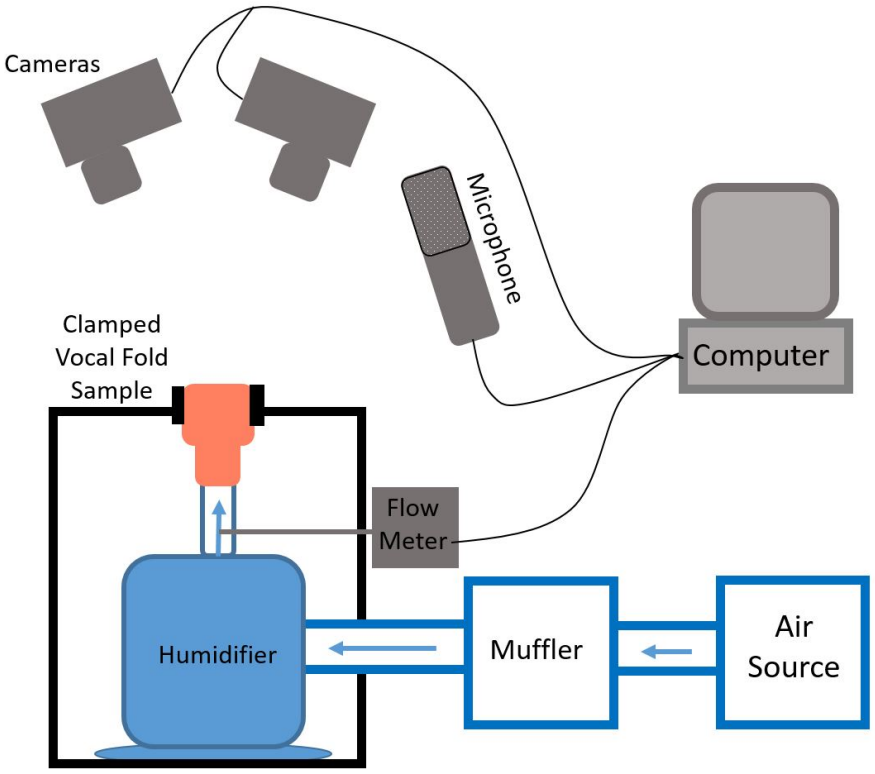

Figure 3.10: Setup of experimental setup used for dynamic test. The setup includes high-speed cameras which were positioned above a vocal fold sample that was connected to a humidified air source. A microphone was used to record the frequencies of sounds produced during testing while a servo motor was used to actuate the vocal fold sample and change the sound produced.

production. A microphone (Nady, USB-1C Condenser Microphone) recording at 44100 Hz and two high-speed cameras (The Slow Motion Camera Company, FPS 1000 HD) collecting images at 4000 frames per second with a pixel resolution of 640×320, were used to continuously record data throughout testing. An image tracking technique was employed using the DLTdv7 software reported in [85] to track the 3D movement of the vocal folds. Following a similar method used in [15], the engineering strain in the anterior-posterior direction (due to the movement of the dynamixel servo motor) was then determined by averaging the engineering strain values computed from 8 points on the surface of the porcine inferior vocal folds. Effort was made to track the most central and medially located points on the porcine vocal folds between the thyroid and arytenoid cartilage attachment points. In addition to determining the engineering strain of the vocal folds

in the anterior-posterior directions, the flow-induced motion of the vocal folds was evaluated by analyzing 100 frames (at a sampling frequency of 4000 Hz) every 0.5 seconds when self-oscillation was observed. Figure 3.11 illustrates an example of the 3D vocal fold kinematic data collected 4 seconds into testing. As Figure 11 shows, the majority of the flow induced motion occurs in the medial-lateral (X) and inferior-superior directions (Z). The collected data was then analyzed to provide insight into the the relationship between the measured frequency and the anterior-posterior strain which was related to the changing elastic tissue properties [15].

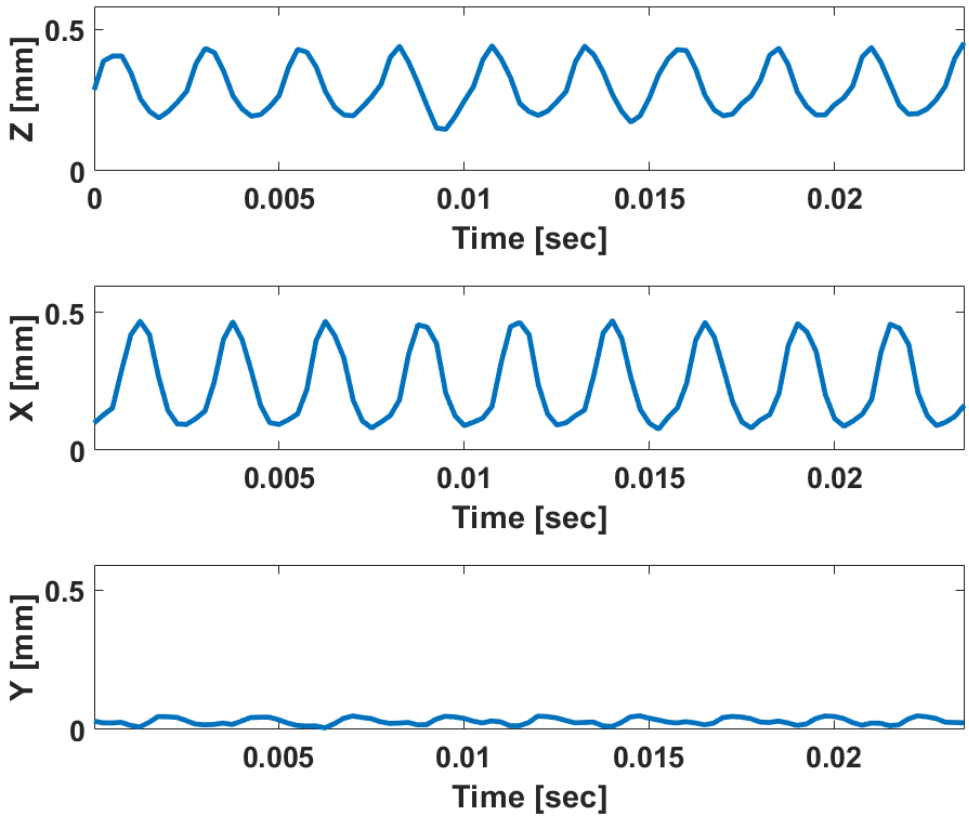

Figure 3.11: Highlights the 3D motion of the vocal folds. The collected data was taken for 0.25 seconds at peak of the dynamixel motion (4 seconds into testing). The majority of the motion occurs in the medial-lateral (X) and inferior-superior directions (Z) due to the flow induced forces on the tissue.

3.5 Excised Larynx Test Results

Following the methodology described in the previous section, both sound and video data were collected throughout the excised larynx testing. The recorded sound data was further analyzed to better understand how the frequencies of the sound produced by the porcine vocal folds changed during testing. Analysis of sound data collected from the six porcine larynx samples showed that phonation onset occurred at an average stretch value of 6.2 ± 1.2 mm based on the position the Dynamixel servo motor which resulted in an average onset frequency of 258.5 ± 12.6 Hz. Additionally, the average peak frequency was found to be 383.7 ± 31.3 Hz at the maximum displacement of the Dynamixel (10 mm). While sound and video data was recorded for all six samples, in many of the tests the speckle pattern did not yield accurate tracking results throughout the duration of the test. After collecting all of the data, the 3D motion tracking was only possible for one sample. The difficulty with speckle adherence to the vocal fold tissue will be discussed in more detail in the discussion section of this paper and has been previously discussed by other authors in [52]. Furthermore, the following results highlight the collected data from the sample which was able to be tracked and resulted in an onset frequency of 247 Hz and a peak frequency of 404 Hz. The spectrogram shown in Figure 3.12 highlights the full period of the sinusoidal motion (0-8 seconds) of the Dynamixel servo motor. In Figure 3.12 the y-axis represents changes in frequency, the x-axis represents changes in time, and changes in color illustrate the relative power spectral density levels at different frequencies and times. As can be seen in the figure, no sound was produced by the vocal folds at the beginning of this test. About 2 seconds into the experiment, however, the vocal folds began vibrating with the produced sound continuing to change frequencies until reaching a maximum value at the greatest displacement of the servo motor (at 4 seconds). Throughout the tests, the airflow velocity was kept constant at approximately 350 cm^3/s. At low strains the vocal folds' lower modulus values are not large enough for phonation onset to occur given the vocal fold adduction levels and airflow characteristics used throughout the test. Table 3.1 displays measured fundamental frequency values evaluated between engineering strain values of 0.20 to 0.35 in the

anterior-posterior direction. The modulus, E, was determined based on the previously reported mean elastic modulus parameters for porcine vocal folds in [15] at the measured strains.

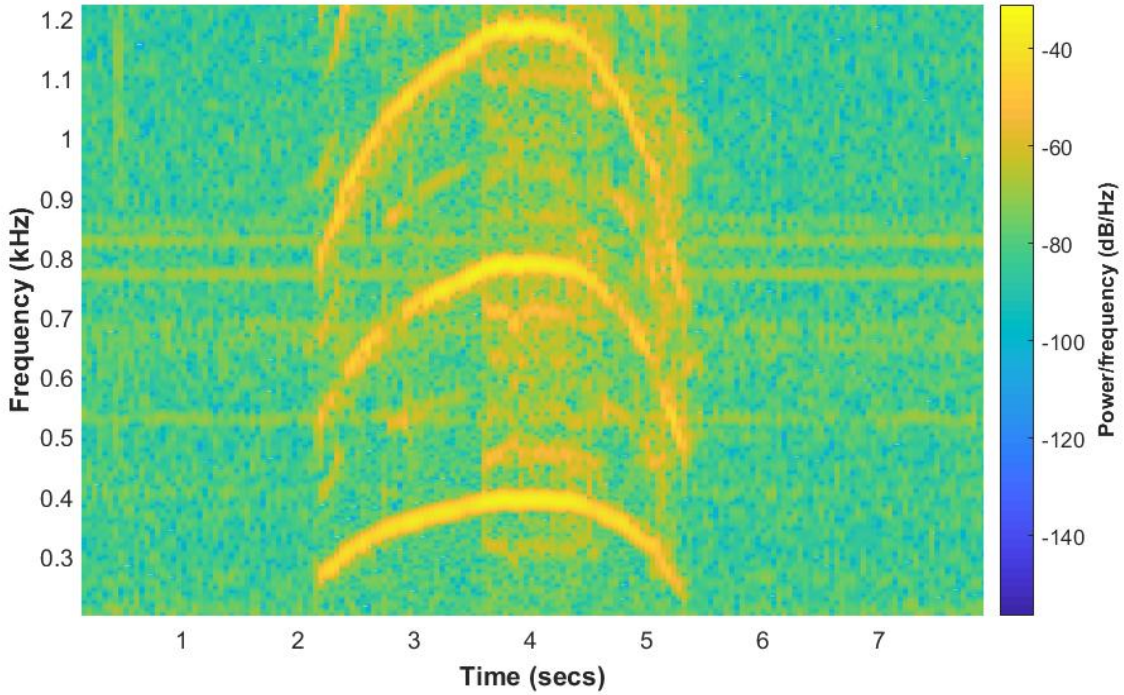

Figure 3.12: Spectrogram of porcine vocal folds during the first period of the sinusoidal motion of the Dynamixel servo motor.

Table 3.1: Measured frequencies of vibration produced during excised porcine larynx testing. The frequencies were determined from sound data collected at 44100 Hz. The modulus values were determined based on the measured strain values and previous reported mean elastic model parameters for porcine vocal folds.

Strain, ϵ [mm/mm]	0.20	0.25	0.30	0.35
Modulus, E [kPa]	76.5	200.8	527.5	609.7
Frequency [Hz]	251	290	330	396

In addition to analyzing the change in frequency from the recorded sound data, the video data was evaluated by computing the fast Fourier transform (FFT) of the resulting vocal fold kinematic data. Figure 4.7 further highlights the change in frequency of the vocal fold. An FFT was computed over the measured medial-lateral vocal fold motion every 0.5 seconds from 2.5 seconds (shortly after

sound production occurred) to 4 seconds (peak dynamixel movement).

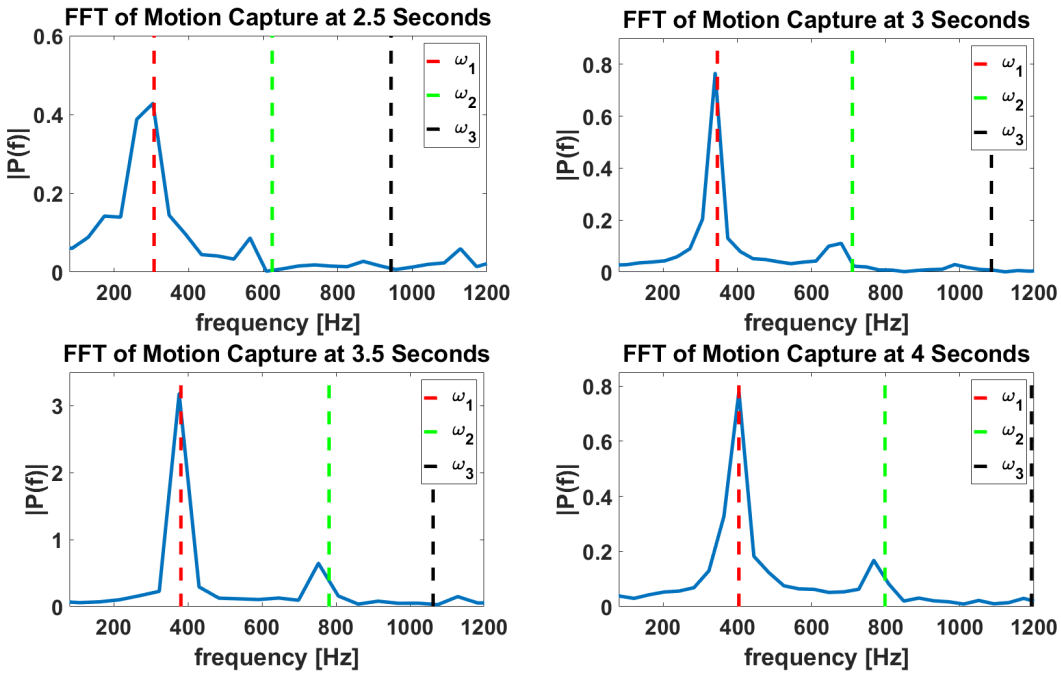

Figure 3.13: Illustrates the change in frequency during testing. The FFT was computed using medial-lateral motion from the vocal fold kinematic data every 0.5 seconds during sound production. The vertical dotted lines represent ω_1, ω_2, and ω_3 from the measured porcine vocal fold sound at the appropriate time interval.

As mentioned earlier and shown in Table 3.1, the change in frequencies was related to the anterior-posterior strain and subsequently to the previously reported tissue elasticity [15]. The measured frequency was also compared the simulated results using the aeroelastic model of phonation shown in Figures 3.4 and 3.5. Figure 3.14 illustrates the relationship between the measured results, simulating findings, and previously report tissue elasticity. The red shaded region highlights the previously reported mean modulus values [15] at the measured anterior-posterior strains which correspond to the lowest and highest measured frequencies. Additionally, the dashed lines represent the measured frequencies, ω_1 and ω_2, and the corresponding modulus values at a Poisson ratio of $\nu = 0.4$ which were calculated using the simulated results from the aeroelastic model shown in Figures 3.4 and 3.5.

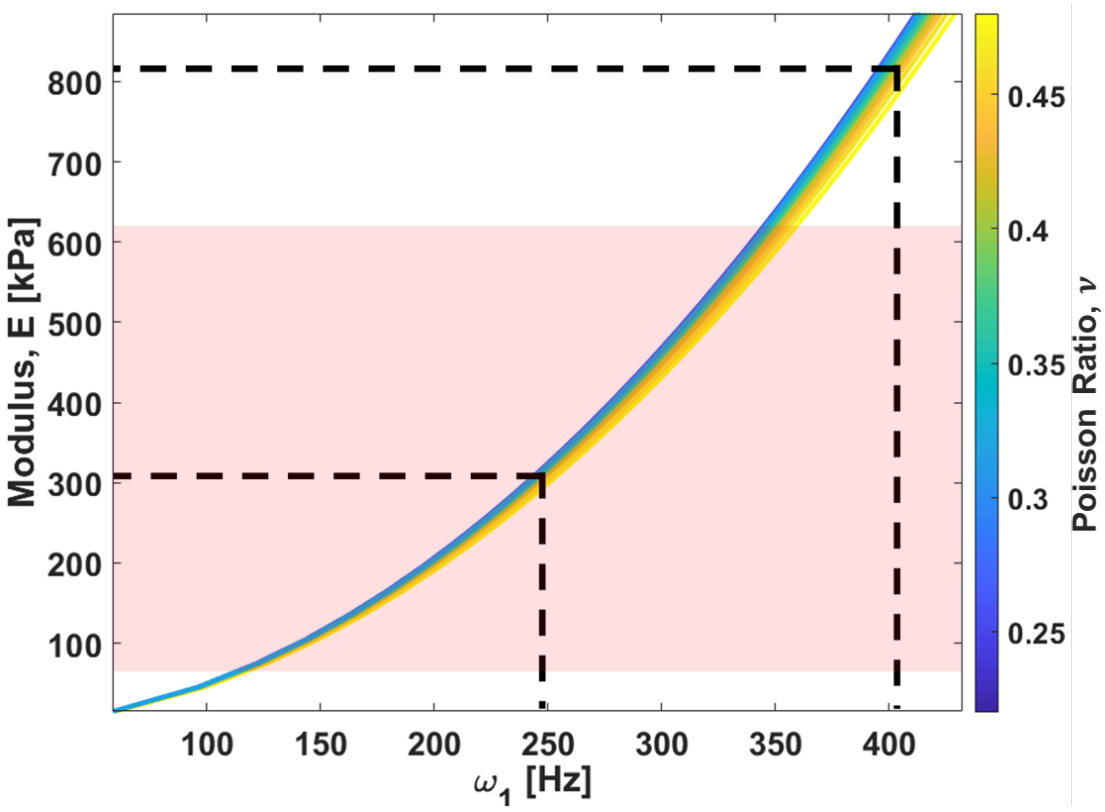

Figure 3.14: Plot of measured fundamental frequency in relation to elastic parameters, E and ν. Plot of second eigenfrequency in relation to elastic parameters, E and ν. The shaded red region highlights the mean modulus values reported at the lowest and highest strain values sound production. The dotted line represent the lowest and highest measured ω_1 and ω_2 values and the corresponding modulus values at $\nu = 0.4$.

3.6 Discussion

The results shown in Figure 3.12 and Figure 3.14 highlight the significant impact that the changing elastic parameters have on the frequencies of vibration during sound production. As reported in previous studies, porcine vocal folds as well as human vocal folds exhibit significant nonlinear elasticity, particularly at higher strains. Thus, the applied anterior-posterior strain results in significant frequency changes. While tissue dehydration and time constraints make it difficult to accurately measure the elastic properties of the excised porcine larynges used in these dynamic tests, the mean previously reported elastic parameters were found to overlap with the simulated results from

the aeroelastic model. Although an effort was made to use similar geometric parameters to the actual vocal fold tissue, differences in vocal fold geometry, varying tissue elasticity from the mean previously reported elastic parameters, as well as spatially varying vocal fold elasticity could likely be attributed to the differences in measured and simulated results.

Similar to the challenges reported in previous studies [52], collecting the motion capture data proved to be difficult. Specifically, during sound production a significant number of potential markers or speckles did not adhere to the vocal fold surface, particularly along the medial edge of the tissue. Additionally, the need to capture at high frame rates in order to prevent motion blur furthered the challenges by decreasing the available pixel resolution. The methylene blue dye helped to improve contrast between the white paint markers and tissue surface, however, in many cases there were not enough markers left on the vocal fold surface or the image quality was not high enough (often due to motion blur caused by a frame rate that was too low or by lowered pixel resolutions) to obtain accurate tracking results. While 8 porcine larynges were tested, only one resulted in an image quality sufficient to yield 3D marker tracking data. In future studies, improved speckle techniques could result in higher quality strain maps and provide insight into how vocal fold medial-lateral and inferior-superior strains change during changing vocal fold vibration frequencies.

This study focused only on the relationship between porcine vocal fold phonation frequencies and changes in anterior-posterior strain which result in varying elastic properties of the tissue as reported by previous studies [15, 44]. As highlighted in previous studies [44], the elasticity of porcine vocal folds is likely strain rate dependent. While future studies are still needed to fully explore the viscoelastic behavior of the tissue across the full vocal range, additional experiments investigating the relationship between phonation frequency and strain rate will also be needed.

As mentioned previously, the results of this study shed light on how the changing vocal fold tissue elasticity due to anterior-posterior strain impacts vocal fold vibration frequency during phonation. The combination of the previously reported vocal fold elastic parameters, measured porcine vocal fold frequency response, and simulated vocal fold dynamics using the aeroelastic model of phonation

can be used as a guide during the manufacturing of synthetic vocal folds. Using the results presented in this report, structural parameters of synthetic vocal folds can be adjusted in an effort to achieve a desired dynamic response and more closely approximate the frequency range of vocal fold tissue.

Chapter 4

Synthetic Vocal Fold Manufacturing and Testing

Garret Burks, Manjot Singh, Blake Johnson, Raffaella De Vita, Alexander Leonessa. Effect of Mechanical Properties on the Dynamics of Self-Oscillating Synthetic Vocal Folds. (2019)

Abstract

This study focuses on the measured changes in dynamic behavior exhibited by eight synthetic vocal fold models with varying mechanical properties. Uniaxial tensile testing was conducted to determine changes in mechanical properties between materials made from silicone rubber and polydimethylsiloxane (PDMS) with varying mixing ratios. The results of the mechanical testing showed that the elastic modulus, E, varied from 20.6 kPa to 437.4 kPa, the measured Poisson ratios, ν, spanned the range of 0.43 to 0.48, and the density, ρ_{VF}, varied from 0.86 to 1.02 g/cm^3 across the eight samples. Vocal fold models were dynamically tested using a custom built experimental setup that supplied a heated and humidified airflow to the synthetic vocal folds. The resulting sounds were recorded and analyzed in order to identify the change in fundamental frequency which spanned 66.8 Hz to 342.6 Hz across the eight samples. Additionally, a mathematical aeroelastic model of phonation was implemented to further investigate the relationship between the mechanical properties and phonation frequency. Finally, a proof-of-concept magnetic actuation method was

demonstrated by using magnetic elastomers to deform the synthetic vocal folds through the use of an electromagnet.

4.1 Introduction

Situated directly between the lungs and oral and nasal passageways, the vocal folds play a critical role in speech production, respiration, and airway protection. Due to the importance of the vocal fold tissue, damage to or loss of control of the vocal folds due to trauma, neuromuscular disorders, or laryngeal cancer can have significant detrimental impacts on an individual's quality of life. While treatment options have improved for some voice disorders, many of 7.5 million individuals in the United States who are annually affected by voice-related disorders still face serious challenges related to dysphonia and dysphagia [86, 87]. The desire to improve treatment options for those individuals has led to numerous researchers conducting studies in order to better understand vocal fold tissue properties and anatomy [4, 6, 7], investigate vocal fold tissue dynamics during sound production [10, 11, 48, 51, 52], as well as efforts related to the creation of synthetic vocal fold models [54, 57, 58].

Due to the difficulty of studying and measuring vocal fold dynamics *in vivo*, many researchers have conducted studies using excised larynx samples. In several early studies, canine larynges were used as a common model of phonation and studied to investigate flow characteristics through the glottal channel as well as canine vocal fold impact stresses [48, 51]. More recently, researchers have opted to use excised porcine larynges [10, 11, 52] which are thought to have more similar vocal fold structure to human vocal folds than other species [6, 7]. Additionally, the use of porcine larynges was further supported by studies which evaluated vocal fold elasticity and found similarities between human and porcine elastic properties across the full vocal range [15, 44, 47]. In particular, in [15, 44] both human and porcine vocal folds were found to have highly nonlinear elasticity at higher anterior-posterior strains. This important characteristic, which results in an increase in vocal fold stiffness from low to high strains, is generally thought to be responsible for the great range of frequencies

that can be produced by the voice-box which is often considered to span about 80 to 160 Hz for males and 140 to 260 Hz for females [88].

Although canine, porcine, or other species larynx samples are more easily obtained and less expensive than cadaveric samples, they are also limited by a relatively short time frame (minutes after thawing) during which the samples are usable for experimental testing. Additionally, it is often difficult to account for changes in mechanical properties or in geometry between samples during the analysis of experimental results. These reasons, among others, have led some researchers to investigate the development and use of synthetic vocal folds as models of phonation. In early synthetic vocal fold studies, researchers in [53] used polyester resin models of a simplified rectangular glottal channel to better understand and compare results to a mathematical models describing the fluid flow through the larynx. Building on that work, researchers in [54], identified phonation onset threshold pressures using a synthetic vocal fold cover layer made of silicone that was attached to a rigid (metal) body layer. In other studies such as in [55, 56, 57], researchers have used rubber models to represent an isotropic cover layer of the vocal folds and investigate how vocal fold dynamics change with varying air flow characteristics and vocal fold geometry. More recently, researchers in [58], described the methodology used to produce a multi-layer synthetic vocal fold model which could more closely approximate the spatially varying mechanical properties of human vocal folds. In the study presented in [58], the researchers showed that the multi-layer vocal fold model exhibited a lower phonation onset pressure than single-layer synthetic models and, in turn, more closely approximated human vocal fold dynamics. Lastly, researchers have built on that work by investigating the differences in synthetic vocal fold dynamics due to both linear and nonlinearly elastic materials used in the cover layer [89]. While the study in [89] illustrated that the dynamics of synthetic vocal folds made with nonlinearly elastic materials could be changed through stretching the models in the anterior-posterior direction, the study did not highlight specifically the correlation between the material properties and the measured vocal fold dynamics. Further, although the use of nonlinearly elastic materials demonstrated the ability to change vocal fold dynamics, the models presented in [89] required manual adjustment between experiments to change the length

of the vocal folds. To our knowledge, there are no other current studies that have investigated actuation methods which could be used to control the dynamic response of synthetic vocal folds during sound production.

While progress has been made by the researchers highlighted above and others to improve the manufacturing of synthetic vocal fold models, there is still work needed to more closely approximate vocal fold dynamics across the full vocal range. Specifically, there is a need to further investigate the impact of the varying elastic properties across the full elastic range, as previously reported in [15, 47], on vocal fold dynamics and the frequencies of vibration during sound production. Further, there is also a need to investigate actuation methods which could be used to control the dynamic response of the synthetic vocal folds during sound production. This paper focuses on the manufacturing of synthetic vocal folds with varying mechanical properties and experimental measurements quantifying synthetic vocal fold dynamics. The following sections will describe in more detail how manufacturing parameters were adjusted with the goal of changing the dynamic behavior of the synthetic vocal fold models to better simulate vocal fold dynamics across the full vocal range. Lastly, a proof of concept vocal fold actuation method will be described.

4.2 Methodology

The following section highlights the materials and process used to manufacture the synthetic vocal fold models, the mechanical testing protocol used to quantify the elasticity of the synthetic vocal fold materials, and the methods used to experimentally test and evaluate the dynamic behavior of each vocal fold model.

4.2.1 Materials

Synthetic vocal fold models were manufactured using the three different materials: polydimethylsiloxane (PDMS) using SYLGARD™ 184 silicone elastomers from Dow Corning Corporation, sil-

icone rubber made using Ecoflex™ 00-30 (EF) from Smooth-On, Inc., and silicone rubber made using Dragon Skin™ 20A (DS) from Smooth-On, Inc. Additionally, black iron oxide microparticles (diameter $= 30-45\mu$m) were purchased from Alpha Chemicals, Inc. and used in the manufacturing of magnetic elastomers. The mixing ratios and manufacturing process will be described further in the following sections.

4.2.2 Manufacturing Synthetic Vocal Fold Models

Vocal fold models were manufactured using a casting method where the geometry of the synthetic vocal folds was based on anatomical measurements of inferior porcine vocal folds as reported in [15, 83]. Figure 4.1 illustrates a frontal-plane cross-section of the vocal folds along with the 3D printed mold cavity used to create the synthetic models. The relevant cross-section dimensions can also be seen in Figure 4.1 while the full vocal fold models were generated to have a length, $L = 4$ cm, representing the anterior-posterior length of the tissue.

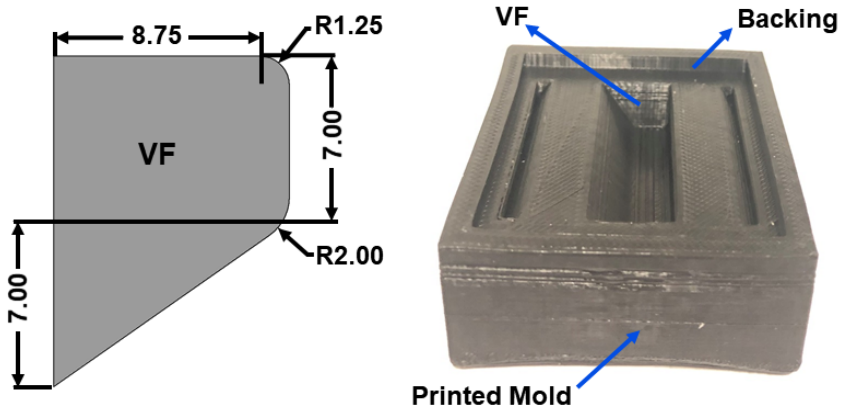

Figure 4.1: Frontal plane vocal fold cross-section (left) based on previously reported anatomical measurements of porcine vocal folds. Additionally, a 3D printed mold is shown (right) which was based on the cross-sectional geometry and used to create the synthetic vocal fold models. All dimension values are displayed in mm.

As mentioned previously, three different materials, polydimethylsiloxane (PDMS), Ecoflex 00-30 (EF), and Dragon Skin 20A (DS), were mixed at various mixing ratios for one minute before being

placed in a vacuum chamber in order to remove any entrapped air in the mixture. Mixing ratios of all three materials were varied with the goal of varying the structural properties of the material. Specifically, the elastic modulus was varied with the goal of approximating the elastic range of porcine inferior vocal folds which has been previously reported to span the range of approximately 17 kPa at low strains to over 600 kPa at higher strains [15]. The specific mixing ratios for each sample will be highlighted in more detail in the results section of this report. The fully homogenized samples were allowed to sit in the vacuum chamber at -20 Bar for 3 minutes or until all air bubbles were removed. Next, the material was poured into the mold cavity shown in Figure 4.1 before being placed into an oven and allowed to cure at 100°C for 30 minutes. After removing the model from the oven, an additional mold with a dovetail geometry was placed on the backing and filled with additional material before being allowed to cure for an additional 30 minutes in the oven at 100°C. The cured dovetail joint was then carefully pulled through the backing mold and the fully cured vocal fold model was removed from the mold. Extra care was taken and a silicone mold release agent was applied when removing the parts to ensure no tears were created in either the dovetail joint or the vocal fold model. Finally, extraneous backing material was removed by cutting along the inferior and superior edges of the model.

In addition to varying the mixing ratios used to create the synthetic vocal fold models, an additional vocal fold model was created using magnetic elastomers in order to investigate a proof-of-concept magnetic actuation method. Magnetic black Iron Oxide microparticles (Alpha Chemicals) were added to the Dragon Skin material prior to being homogenized and following the procedure describe above to cure the model. The mixing ratios will be described in more detail in the results section. In this way, a magnetic vocal fold model was created which could be manipulated with an electromagnet as will be described in more detail in the following sections.

4.2.3 Mechanical Testing

For every vocal fold model, additional samples were created and used to measure the mechanical properties of each material by performing uniaxial tensile tests. After following the same protocol described previously to remove entrapped air and fully cure the sample in a rectangular mold cavity, a digital caliper (accuracy ±0.05 mm, Mitutoyo Absolute Low Force Calipers Series 573, Japan) was used to record the length, width, and thickness dimensions of each sample. The average measurements across all samples was found to be 40.82 ± 0.70 mm, 5.96 ± 0.06 mm, and 2.62 ± 0.11 mm, for the length, width, and thickness, respectively. A total of five measurements for both the width and thickness were collected for each sample and used later to compute an average cross-sectional area. A uniaxial mechanical tensile testing protocol similar to the methods described in [15] was followed to evaluate the elastic properties of each sample. After recording the sample measurements, each sample was speckled using an aerosol fast dry gloss black paint in order to create a high contrast pattern on the sample surface to be used for non-contact strain measurements. 200 grit sand paper was folded over ends of samples before mechanically clamping the samples in two custom 3D printed clamps. The left and right clamps with the secured sample were then carefully secured to a 2 lbf load cell (Jr. S-Beam Miniature Load Cell, FUTEK Advanced Sensor Technology, Inc.) as well as two microscale linear actuators (25 mm travel, RS-232 plus manual control, Zaber Technologies Inc.) as shown in Figure 4.2. A data acquisition module (NI cDAQ-9172, National Instruments) and LabVIEW program (LabVIEW, National Instruments) were used to control the position of the actuators and record force measurements and actuator position data at a sampling rate of 4 Hz. A preload of 0.01 N was applied to remove any slack in the samples prior to the start of testing. The samples were then evaluated using displacement controlled ramp tests with a constant displacement rate of 0.1 mm/s and a maximum displacement of 20 mm.

During each test, two CMOS cameras (Basler ace acA2440-75 um, Basler, Inc., Exton, Pa) were also used to record images at a resolution of 2448×2048 pixels and a frame rate of 4 Hz as the samples were stretched. All of the stress and strain values were determined based on the preloaded

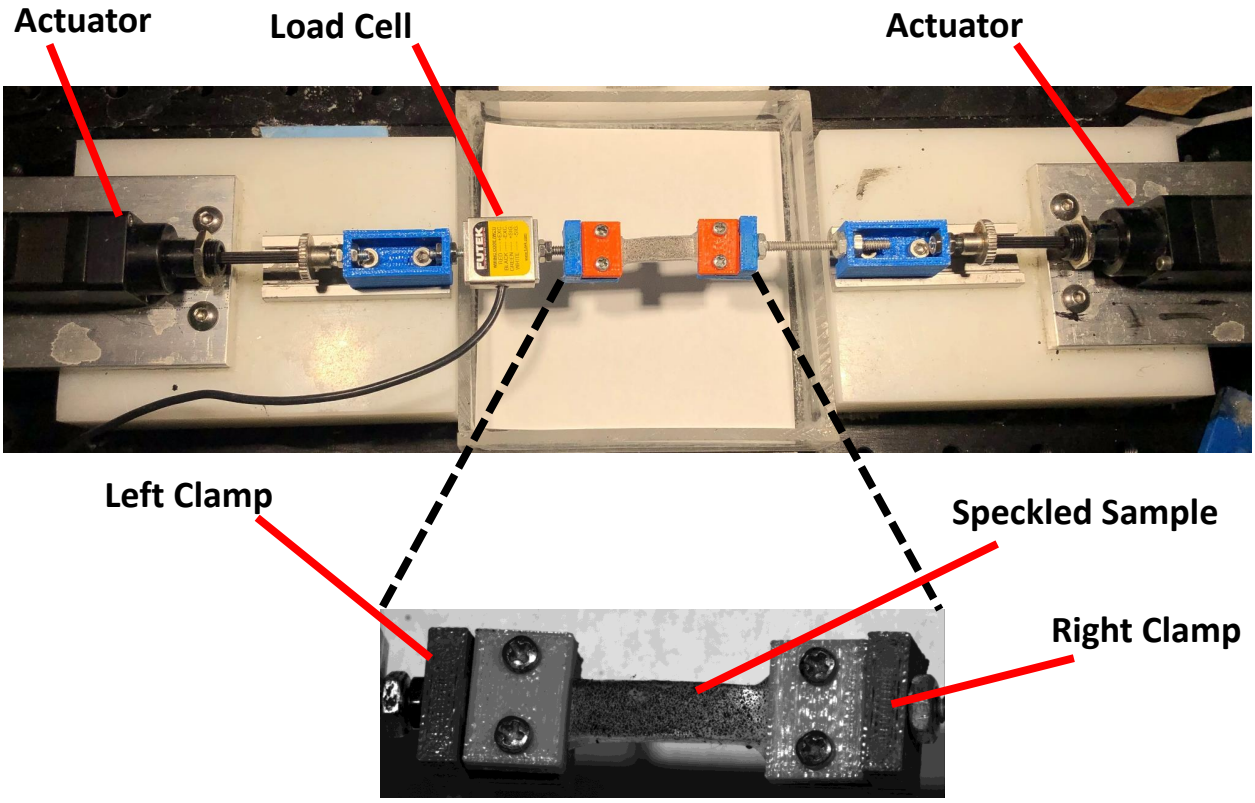

Figure 4.2: Top view of the custom-built experimental mechanical test setup used to evaluate elastic properties of samples through uniaxial tensile tests.

sample configuration. Non-contact strain measurements were determined in the center region of each sample as the sample was stretched via a Digital Image Correlation (DIC) 3D system (Vic-3D 8, Correlated Solutions) as shown in Figure 4.3. For each sample, engineering strain values were averaged over the middle region of the sample as shown in figure. Additionally, the nominal stress, σ, was calculated based on the data collected via the force sensor during the uniaxial tensile tests and the initial measured cross-sectional area of the sample.

The stress and strain values were then analyzed to determine the low-strain elastic modulus for each sample as shown in Figure 4.4. Although all samples were found to exhibit slightly nonlinear elasticity at higher strains, all samples were found to be effectively modeled ($R^2 > 0.99$) with

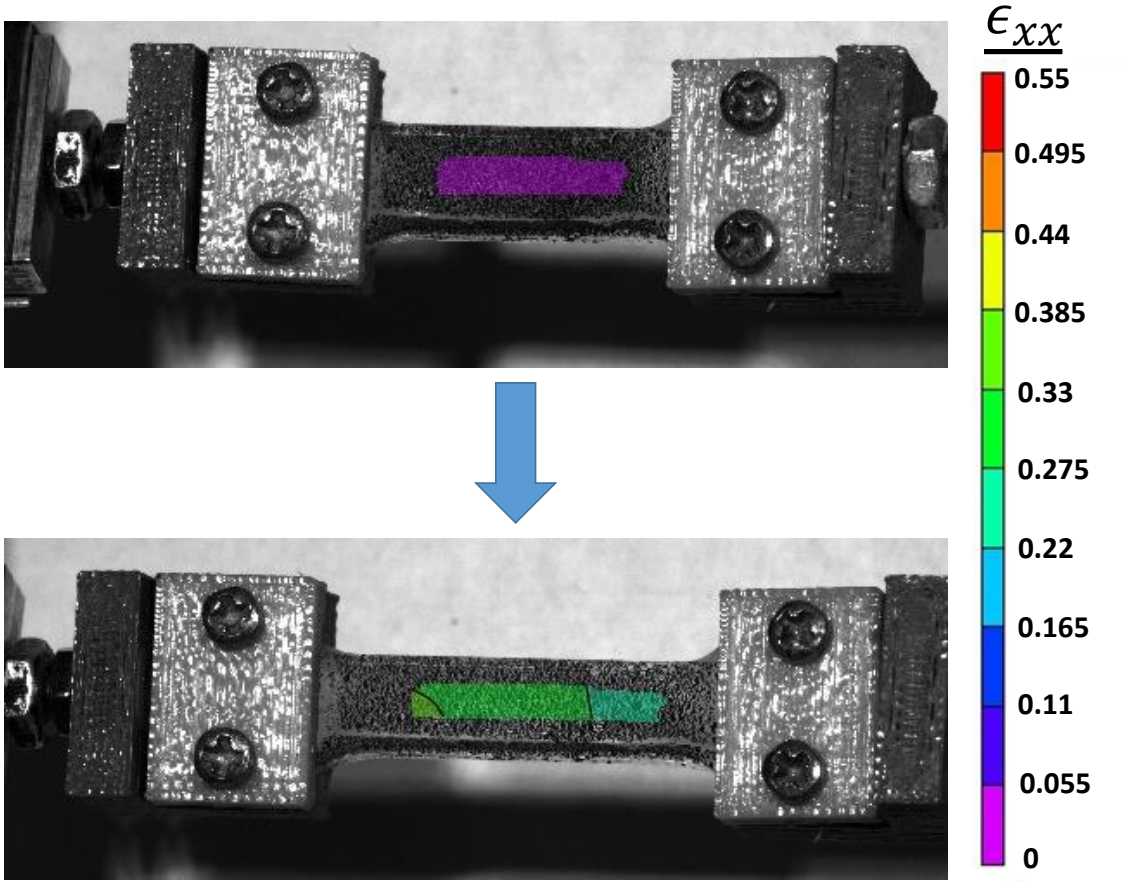

Figure 4.3: The highlighted region represents the area used to calculate non-contact strain measurements using the DIC system (VIC-3D 8, Correlated Solutions).

a linear fit at low strains ($\epsilon_{xx} < 0.15$) as highlighted in Figure 4.4. Thus, the elastic modulus, E, for each sample was considered as the slope of the low-strain linear region. Additionally, the characterization of the modulus at low-strains is further supported by the small flow-induced motion relative to size of the synthetic vocal folds. In addition to determining the modulus, the Poisson ratio for each sample was also determined based on the measured transverse and axial strain data. Similar to the elastic modulus highlighted in Figure 4.4, the Poisson ratio was also found to vary with strain especially at higher strain values. Therefore, the Poisson ratios were similarly computed as the average value across the measured engineering strain from 0 to 0.15. Lastly, each sample's density, ρ_{VF}, was determined using a digital scale (Gemini-20, American Weigh Scales, Inc.) to

record the sample mass and recorded geometric measurements using a digital caliper (Mitutoyo Absolute Low Force Calipers Series 573, Japan) to compute the volume of each sample.

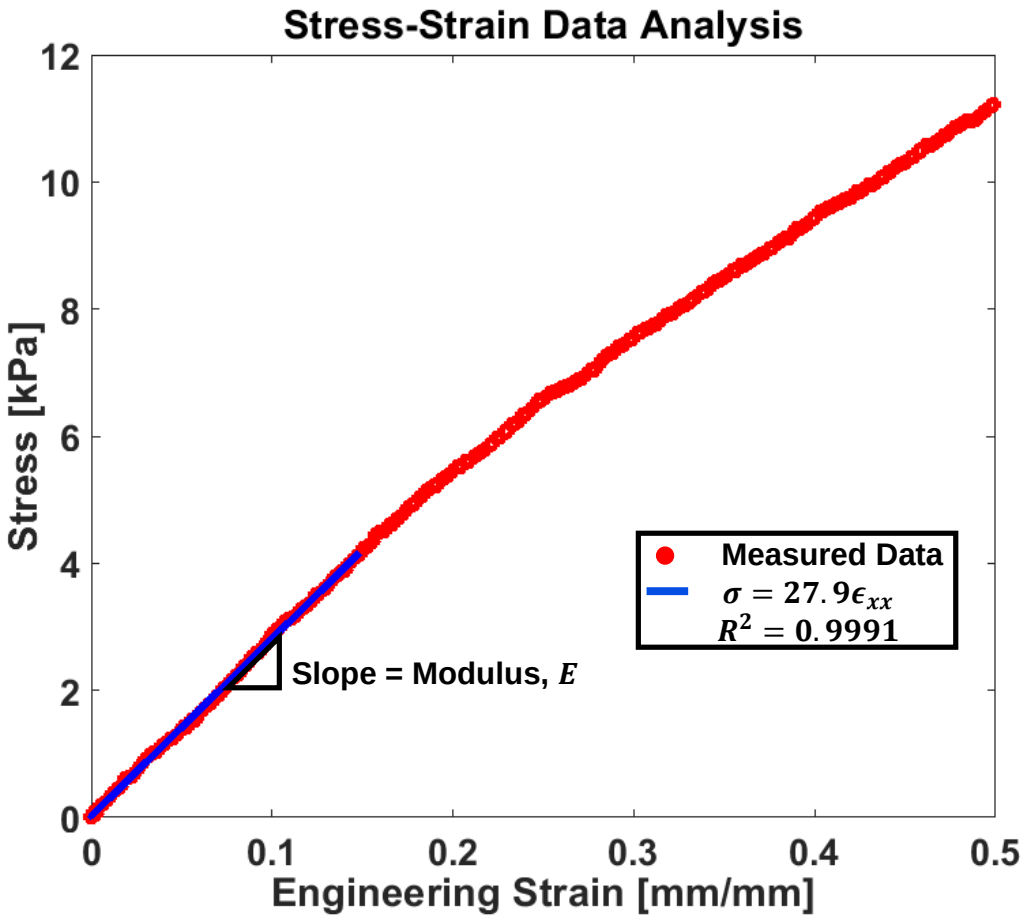

Figure 4.4: Representative stress-strain response illustrating how the low-strain Young's Modulus, E, was determined.

4.2.4 Dynamic Testing of Synthetic Vocal Fold Models

The dynamic behavior of each of the synthetic vocal fold models was evaluated using a custom built experimental setup as illustrated by the schematic in Figure 4.5. A muffler was used to reduce variations in flow rate being supplied by a compressed air source and to reduce excessive noise from the air source. The air flow was then heated and humidified to approximately 90 °F

and 90% using a humidifier (HC150 Heated Humidifier, Fisher & Paykel) to better simulate airflow conditions coming out of the lungs. A 1 inch PVC pipe was then used to connect the humidifier to a mounting plate on which the synthetic vocal folds were secured. A flow meter (PCE Instruments) was also used to measure the flow rate through the PVC pipe approximately 2 inches below the mounting plate.

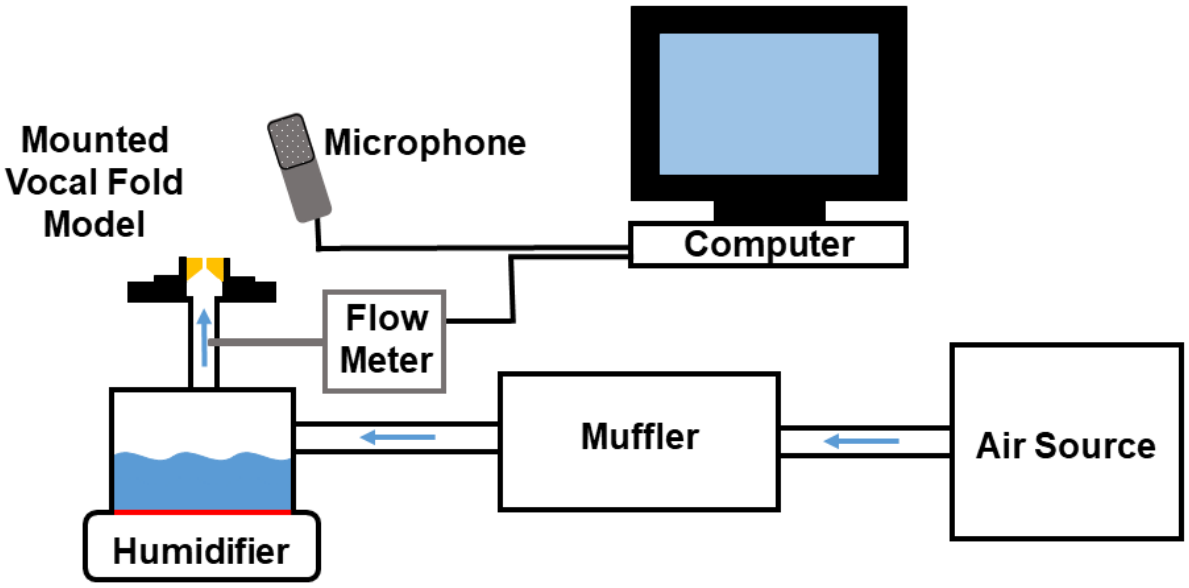

Figure 4.5: Schematic of the experimental setup used for dynamic tests which includes the flow of heated and humidified air that was supplied to the synthetic vocal fold models as well as a flow meter and microphone used to measure flow conditions and vocal fold vibrations.

The synthetic vocal fold samples were secured to lateral side walls via the dovetail joints as shown in Figure 4.6. The two lateral side wall were then fastened onto a mounting plate along sliding tracks that allowed for the width between the vocal folds or the glottal channel to be adjusted. Additional walls were adhered to the anterior and posterior sides of the synthetic vocal folds using silicone and clamped to the mounting plate during testing. A 1/8 inch rubber gasket was also used under both the lateral side walls and anterior and posterior walls to prevent airflow leaks. Further, silicone was used to seal any leaks or gaps between the walls of the synthetic vocal fold model and the mounting plate during testing.

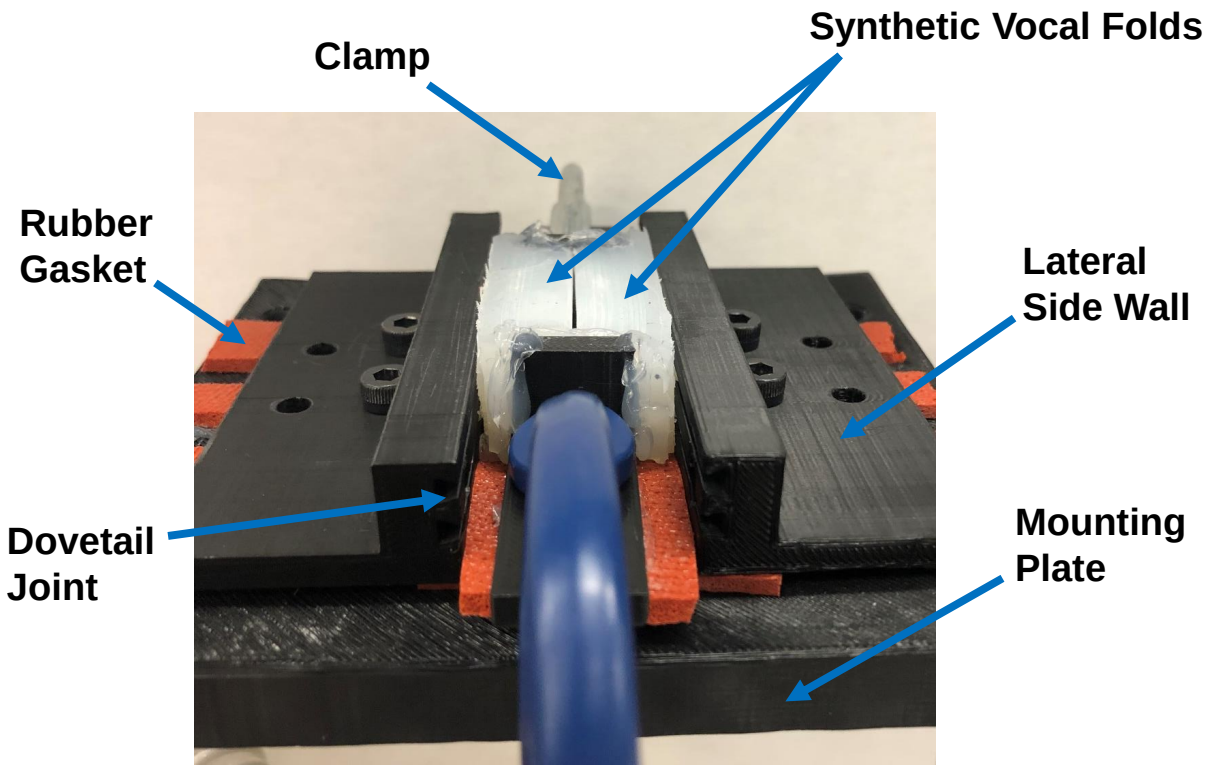

Figure 4.6: Image of the mounting plate and experimental setup used to support and adjust the synthetic vocal fold models including the clamps, rubber gasket, lateral side walls, as well as the vocal fold model.

For each sample the air flow rate and glottal opening was adjusted until self-sustained oscillations were observed. Following the onset of phonation, sound data was collected via a microphone (Nady microphone) for 8 seconds while the synthetic vocal folds vibrated at a constant tone. The sound data was then analyzed in MATLAB through the use of a fast Fourier transform (FFT) based on the middle 4 seconds of collected sound data. The fundamental frequency was then identified as the first peak frequency as shown in the example FFT highlighted in Figure 4.7. No changes to the flow rate or vocal fold position via clamp conditions were made during the sound recording of the synthetic vocal fold vibration.

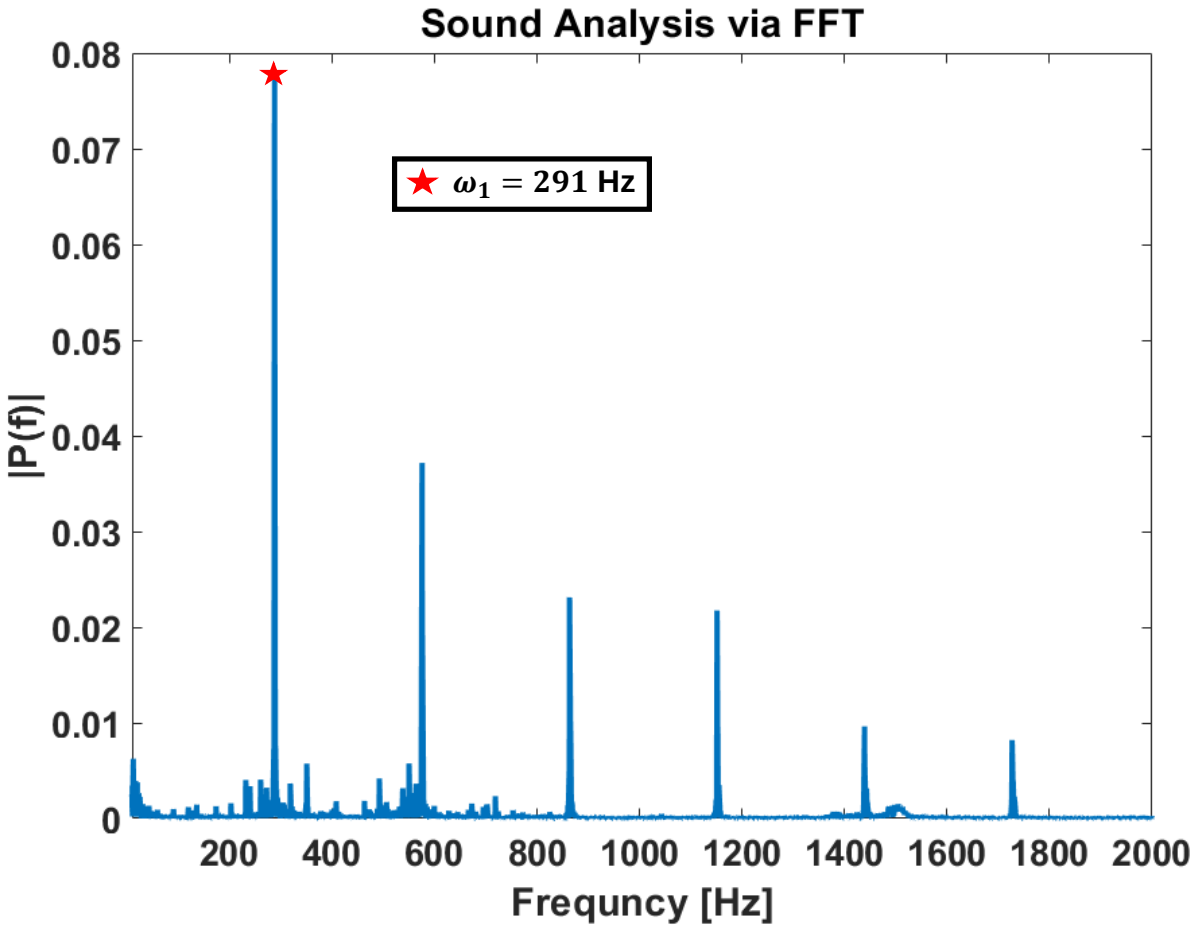

Figure 4.7: Example of sound analysis via FFT which was used to identify the fundamental frequency for each synthetic vocal fold model.

In addition to testing the synthetic vocal fold models with varying mixing ratios, a proof-of-concept magnetic actuation method was investigated using the dynamic experimental setup. As shown in the schematic in Figure 4.8, only one of the two vocal folds was made magnetic with the black iron oxide particles. An electromagnet (12V DC, 500 N, uxcell) was then positioned on the lateral side of the magnetic vocal fold. In order to ensure the magnetic field would effectively reach the vocal fold model, the lateral side wall was modified so that the electromagnet could be placed within a cutout section of the wall and positioned directly against the magnetic vocal fold. Any gaps between the electromagnet, vocal fold, and side wall were then sealed using silicone. A square wave was then generated using a myDAQ (National Instruments) and a LabVIEW program (LabVIEW, National

Instruments). The signal which had an offset of 5V, amplitude of 5V, and frequency of 0.5Hz was designed to alternate between 0V and 10V thus turn the electromagnet on and off. Before being sent to the electromagnet, the generated signal was supplied to a power amplifier (TOE 7610-10, Toellner Systems, Inc) to ensure the power requirements (approximately 5 Watts) of the electromagnet were met. A similar dynamic testing protocol was followed as described previously where the flow rate and glottal width was adjusted until self-sustained oscillations were observed before sending the square wave to the electromagnet.

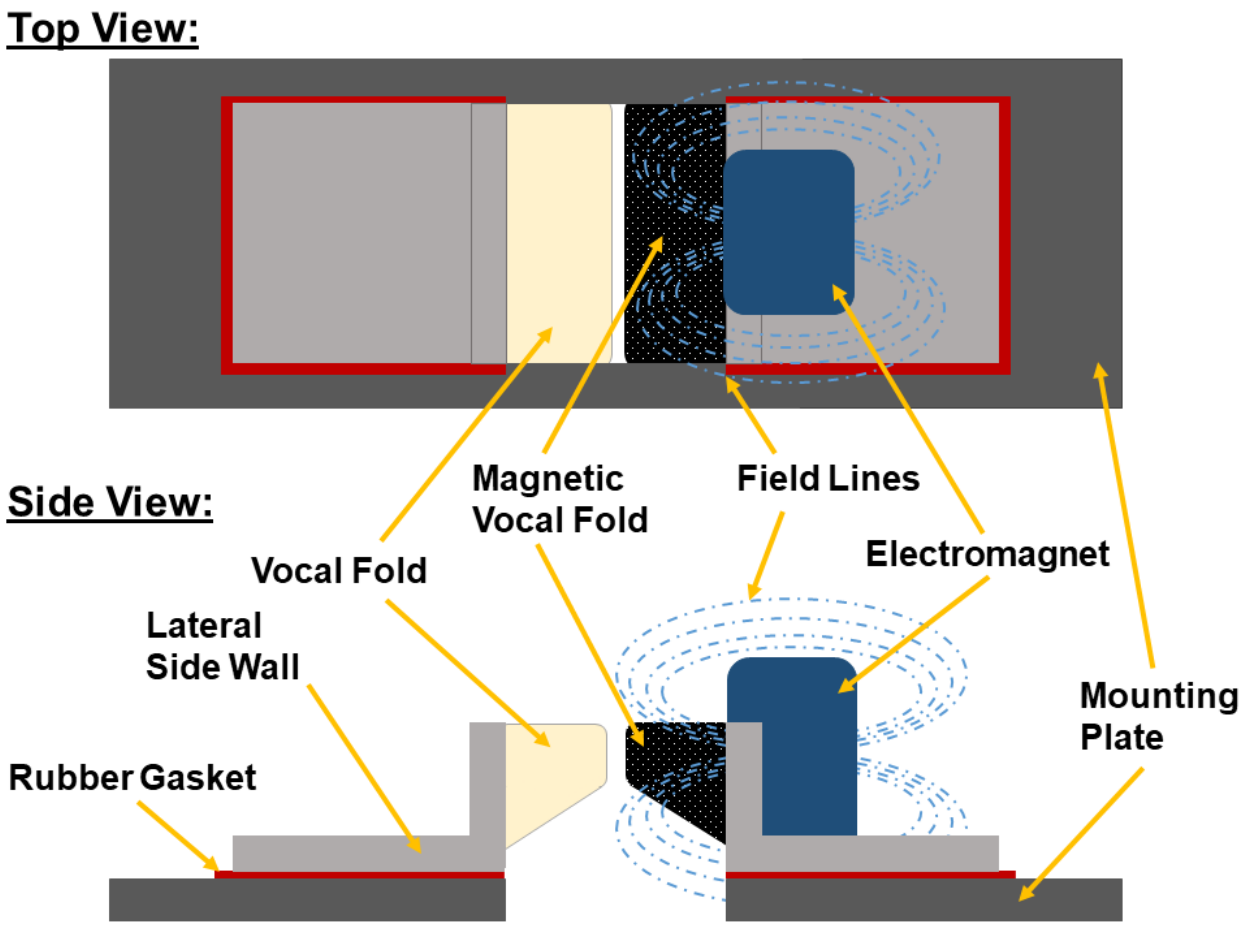

Figure 4.8: Schematic illustrating the experimental setup used to demonstrate the proof-of-concept electromagnetic actuation method.

4.2.5 Aeroelastic Model of Phonation Description

In order to better understand the dynamic behavior of the synthetic vocal fold models, a mathematical aeroelastic model of phonation based on the work first described in [9] and depicted in the flowchart shown in Figure 4.10 was implemented. The model, which begins with an assumed 2D geometry of the vocal folds such as cross-section shown in Figure 4.1, is a coupled fluid-structure model that was selected due to its incorporation of vocal fold material properties such as the elastic modulus, E, density, ρ_{VF}, and Poisson's ratio, ν, as well as airflow characteristics through the glottal channel such as the flow rate and fluid density. The mathematical model begins by utilizing the Ritz method to approximate the displacement fields of the 2D vocal fold structure through the decomposition of the spatial variables, x and z, and temporal variables, q_r. The width of glottal channel was similarly approximated and based on the displacement of each vocal fold in the x-direction along the lateral edges. The displacement fields were then used to determine the vocal fold stresses and strains while the fluctuating glottal width was incorporated into linearized continuity and linearized Bernoulli's equations to determine the changing flow velocity and flow pressures through the glottal channel. The vocal fold stresses and strains were then used to calculate the potential and kinetic energy before being used to calculate the Lagrangian and ultimately to form Lagrange's equation. Lagrange's equation could then be reorganized into matrix form where each element of the mass and stiffness matrices, M and K, was determined based on the coefficients of the Lagrangian. On the fluid side, the fluctuating pressure through the glottal channel can then be related to the forces exerted on the vocal folds and similarly reorganized to yield force matrices Q_0, Q_1, and Q_2. Lastly, a structural damping matrix, C, can be written as a matrix proportional to the mass matrix, M. The general differential equation as shown at the bottom of Figure 4.10, can then expressed in state space form as,

$$\begin{bmatrix} \dot{q}_r \\ \ddot{q}_r \end{bmatrix} = \begin{bmatrix} 0 & I \\ -(M-Q_2)^{-1}(K-Q_0) & -(M-Q_2)^{-1}(C-Q_1) \end{bmatrix} \begin{bmatrix} q_r \\ \dot{q}_r \end{bmatrix}, \tag{4.1}$$

with the corresponding eigenvalue problem written as

$$A\mathbf{v} = \lambda\mathbf{v}, \tag{4.2}$$

where A is a matrix comprised of all of the fluid and structural terms. As described in [9], the resulting eigenvalues of the matrix, A, can then provide information on both phonation onset and phonation frequency. In this report, the model-predicted frequencies were used to provide a comparison to the experimentally measured synthetic vocal fold phonation frequencies. For a more detailed description please refer to [9] where the original model was reported.

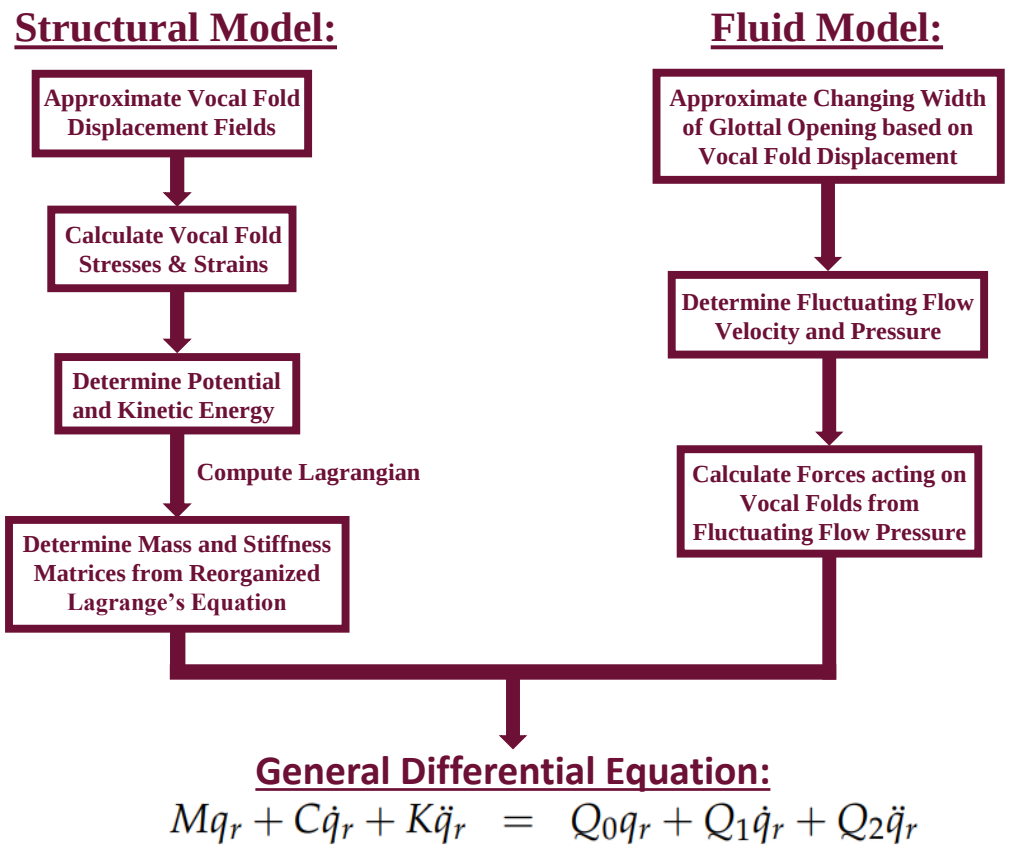

Figure 4.9: This flowchart details the aeroelastic model of phonation first described in [9] used to evaluate vocal fold dynamics.

4.3 Results

Following the methodology described in the previous section, eight synthetic vocal fold models were constructed and tested using the dynamic experimental testing protocol. The mixing ratios of each material were varied with the goal of approximating the range of modulus values of the vocal folds as previously reported in [15, 44, 47]. The results of the mechanical testing for each material and corresponding mixing ratios are shown in Table 4.1. As the table shows the elastic modulus was found to vary from 20.6 kPa using the softer Ecoflex 00-30 (EF) material up to a modulus of 437.4 kPa using the Dragon Skin 20A (DS) material. The mixing ratios shown in Table 4.1 are displayed in the format A:B:T, where A and B represent the weight percentage of the base and hardener agents, respectively, while the T represents the weight percentage of a silicone thinner which was used to reduce the viscosity and ultimately the modulus of the vocal fold models. Additionally, the Poisson's ratio for each material, ν, which was calculated based on the DIC strain measurements ($\epsilon_{xx} < 0.15$) was found to be between 0.43 and 0.48 for all samples. As highlighted in the Table 4.1, all sample densities were measured between 0.86 and 1.02 g/cm^3. After analyzing the results of the dynamic testing, the measured fundamental frequency was found to span the range of 66.8 Hz to 342.6 Hz and to increase significantly with an increase in modulus across the eight synthetic vocal fold models.

Table 4.1: Table highlighting the differences in mixing ratios, elastic modulus, and frequency between each of the synthetic vocal fold models. The materials are listed using the following notation: Ecoflex 00-30 (EF), Dragon Skin 20A (DS), polydimethlysiloxane (PDMS)

Sample	1	2	3	4	5	6	7	8
Material	EF	EF	EF	DS	DS	DS	PDMS	DS
Ratio [A:B:T]	1:1:1	1:1:0.5	1:1:0	1:1:0.5	1:1:0.33	1:1:0.2	20:1:0	1:1:0
E **[kPa]**	20.6	27.9	42.9	187.6	210.2	221.2	234.5	437.4
ν	0.44	0.45	0.46	0.46	0.47	0.46	0.48	0.43
ρ_{VF} [g/cm^3]	0.92	0.91	1.02	0.86	0.92	0.94	0.95	0.96
f_{measured} **[Hz]**	66.8	78.5	108.4	244.3	261.7	273.4	291.5	342.6
$f_{\text{predicted}}$ **[Hz]**	71.8	81.6	96.9	214.6	223.5	223.7	230.0	316.2
Difference	6.9%	3.8%	11.9%	13.8%	17.1%	22.2%	26.7%	8.3%

As mentioned previously, a mathematical aeroelastic model model of phonation, which was originally reported in [9], was implemented to further evaluate the change in the vocal fold elasticity on the frequencies during phonation. The results of Figure **??**, highlight both the measured experimental data as indicated by individual red markers as well as the simulated results shown by the contour lines. The top plot in Figure **??**, displays contour lines at different Poisson's ratios, ν, based on the measured values shown in Table 4.1 and a constant vocal fold density of $\rho_{\text{VF}} = 0.94$ g/cm^3. Similarly, the bottom graph displays contour lines at variable vocal fold densities and a constant Poisson ratio of $\nu = 0.46$. As the figure shows, the range of vocal fold densities had a more significant impact on the frequency than the range of Poisson's ratios over the measured values. Furthermore, as expected, the change in elastic modulus played the most significant role on the predicted frequency across the range of values tested. As shown in the figures, the experimentally measured results were found to exhibit a similar parabolic relationship to the aeroelastic model. Table 4.1 further highlights the percent difference between the experimental and simulated results which were determined for the measured elastic modulus, Poisson ratio, and density for each sample. As the results in the table show, the differences between model predicted results and experimental findings were relatively small ($< 12\%$) when evaluating the three samples with the lowest modulus values. Generally, with the exception of sample 8, the % difference seemed to rise slightly as the modulus of the of the synthetic vocal fold increased. Possible explanations for this discrepancy will be discussed further in the discussion section.

In addition to the dynamic testing of the synthetic models with variable mixing ratios, sound produced by a magnetic vocal fold model was also measured and analyzed as shown by the spectrogram in Figure 4.11. The nonmagnetic vocal fold shown in Figure 4.8, was created using the Dragonskin 20A material with a mixing ratio of 1:1:0.5 for the base, hardener, and silicone thinner parts, respectively. An equal part (by weight percentage) of the black iron oxide particles was added prior to homogenizing the mixture. As the spectrogram in Figure 4.11 illustrates, the vocal folds initially produced sound at a constant frequency which is indicated by the higher power spectral density around 265 Hz shown between 0 and 1 seconds which corresponds to the period of time the electro-

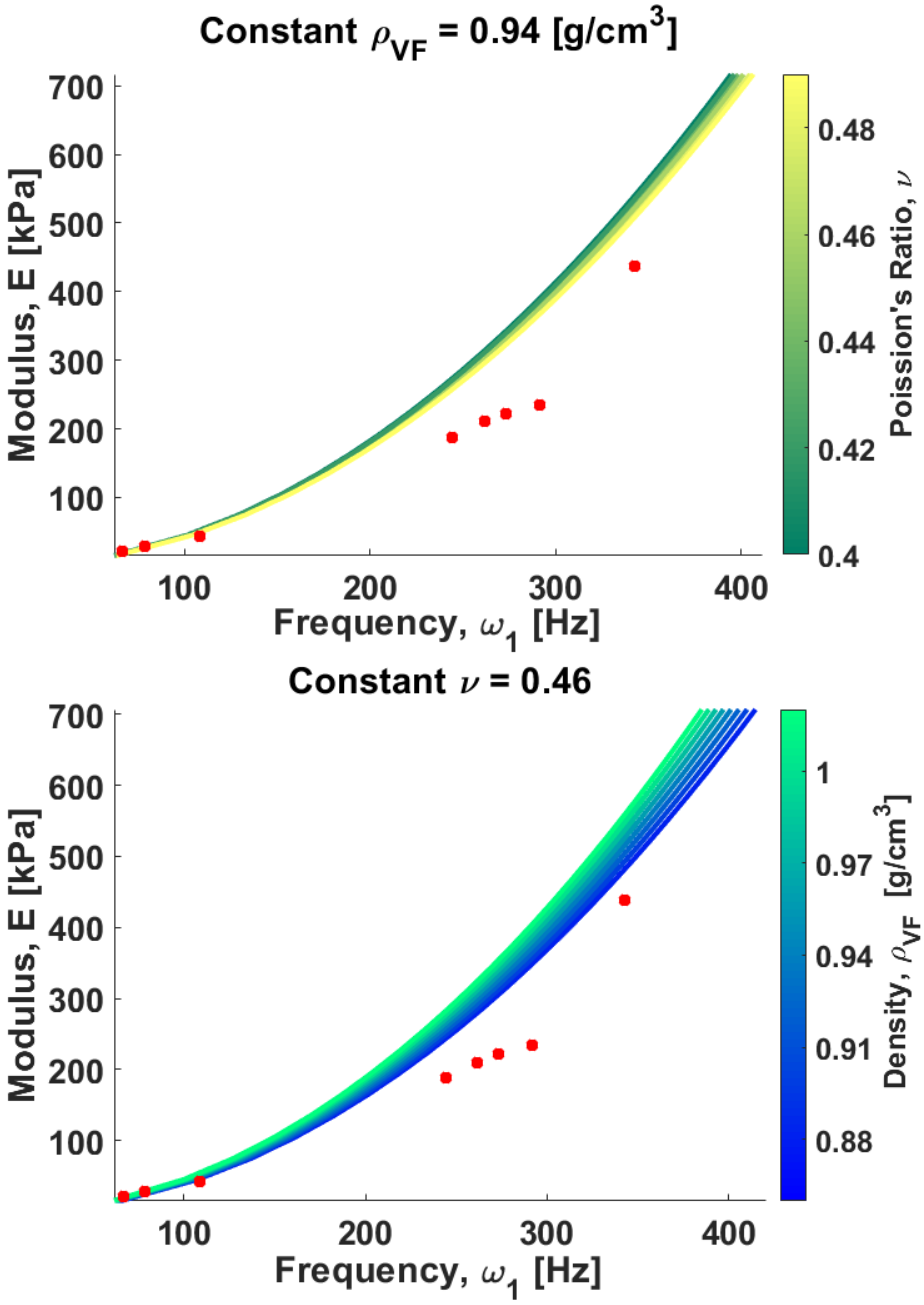

Figure 4.10: These plots highlight both the measured experimental data collected on the eight synthetic vocal fold models (red markers) as well as the simulated findings (contour lines) using the aeroelastic model of phonation [9].

magnet was off (0V). When the electromagnet was turned on (10V), the electromagnet pulled the magnetic vocal fold laterally and, in turn, stopped the vibration of the vocal folds. Any remaining

noise that can be seen via the spectrogram between 1 and 2 seconds reflects the measured sound caused by the air flowing through the wider glottal opening. Figure 4.11, continues to highlight three full periods of the 0.5 Hz square wave sent to the electromagnet and the resulting changes in dynamic behavior of the vocal folds.

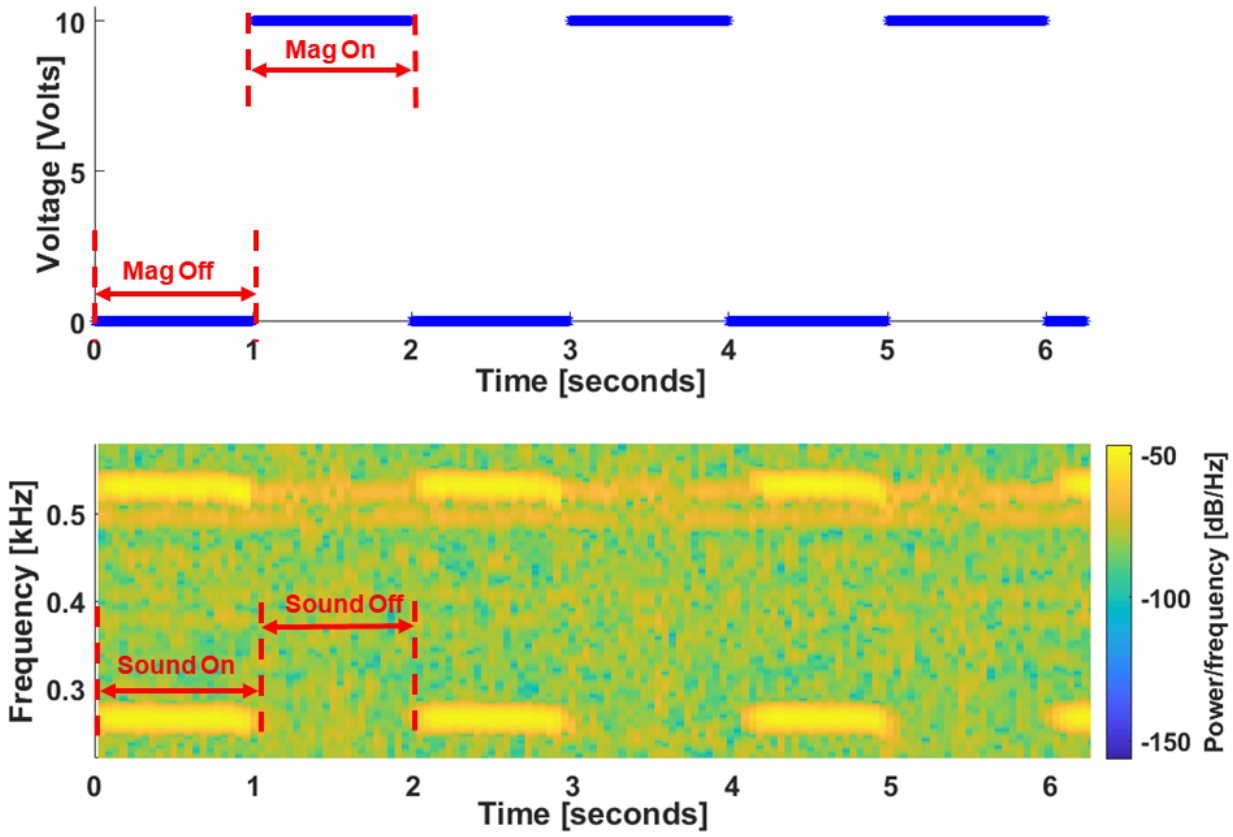

Figure 4.11: Proof of concept electromagnetic actuation test where the synthetic vocal folds produced sounds when the electromagnet was off (0 Volts) and the self-sustained oscillations stopped when the electromagnet was turned on (10 Volts)

4.4 Discussion

This paper highlights the significant impact of changing material properties of synthetic vocal folds on the vocal fold dynamics during sound production. Specifically, the relationship between

phonation frequency and the elastic modulus was evaluated through both experimental as well as simulated results. Additionally, a proof-of-concept magnetic actuation method was explored as a means of adjusting vocal fold dynamics during sound production.

As the results shown in Figure **??** and Table 4.1 highlight, the experimental results were found to generally exhibit similar trends as the aeroelastic model, especially at low modulus values where the percent difference was found to be less than 7% for the two lowest synthetic vocal folds. As highlighted by Table 4.1, as the modulus of the synthetic vocal folds increased, the % difference also seemed to rise. The discrepancies between the experimental results and aeroelastic model simulations can likely be attributed to a combination of both uncertainty in some experimental measurements as well as assumptions related to the mathematical model. For example, the aeroelastic model was based on a 2D frontal-plane cross section of the vocal folds. While the synthetic vocal folds were manufactured with the same cross-section as shown in Figure 4.1, it is important to note that the fixed boundary conditions along the anterior and posterior edges likely impacted the vocal fold dynamics, especially as the stiffness of the materials increased. Additionally, the aeroelastic model assumes that the flow of air through the glottal channel is one-dimensional and irrotational which may not be valid assumptions, particularly, at higher flow velocities and thus could impact simulated phonation results. Further, although great care was taken to fully mix the materials (PDMS, EF, DS), it is possible that the synthetic vocal folds were not completely homogeneous and therefore had variable structural properties within each sample. Any potential variations in material properties and the measurements of those properties could have also played a role in the discrepancy between the experimental and simulated findings.

As mentioned previously, the geometric dimensions of the synthetic vocal fold models were based on previously reported porcine vocal fold anatomical measurements [6, 7, 15]. While the cross-sectional geometry does represent a simplified frontal plane geometry of the porcine vocal folds, it is worth noting that the further geometry changes could be made to more accurately represent the porcine or human vocal folds. Specifically, future studies could investigate the impact of variations in the anterior-posterior geometry of the vocal fold model. The synthetic models created in this paper

had a constant cross-sectional geometry, however, it is known that the frontal plane geometry of both porcine and human vocal folds change between the thyroid and arytenoid attachment points. Geometric changes to more accurately reflect the tissue geometry especially anterior-posterior variations could be useful in future studies of vocal fold dynamics or in the design of an improved vocal fold prosthesis.

This paper focused only on the dynamic changes in single-layer homogeneous, symmetric, vocal fold models due to change in mechanical properties between models. Other researchers have shown that multi-layered synthetic models can more accurately match the phonation onset pressures exhibited by healthy human vocal fold tissue [58], however these studies did not evaluate the impact of changes in the elastic modulus within each layer across the full vocal range. As mentioned previously, the elastic properties of the vocal fold cover layers have been described as highly nonlinear especially at high strains [15, 44, 47]. Future studies could use a multilayered vocal fold model to investigate the impact of changes in the vocal fold cover layer elasticity as well as changes in the body layer properties across the range of active and passive properties of the thyroarytenoid muscle on the dynamics of tissue during sound production.

As shown in previous studies [44, 47, 90], the mechanical properties of the vocal fold tissue is likely strain rate dependent and thus likely change as the frequencies of vibration are changed across the full vocal range. While the viscoelastic properties of the materials used in this paper were not investigated, it could be of interest in future studies to evaluate materials with varying viscoelastic properties, such as materials described in [91], and their corresponding impact on vocal fold dynamics. Additionally, it could be beneficial to account for material visceoelasticity in mathematical models describing vocal fold dynamics, such as the aeroelastic model implemented in this report, in order to provide more accurate simulations of phonation and vocal fold dynamics.

Lastly, this paper demonstrated a proof-of-concept actuation method by embedding magnetic microparticles into the synthetic vocal folds and using an electromagnet placed on the lateral side of the magnetic vocal fold. Although this method of actuation only provided the ability to stop and

start sound production by pulling one of the vocal folds laterally, future studies could investigate improved methods of actuation through changes in coil location relative to the vocal fold model, electromagnetic field strength, as well as controlling the location where the magnetic microparticles were deposited within the vocal folds. Additionally, the electromagnet used in this study required that the magnetic material was either touching or in very close proximity (< 1 cm). Future studies looking to employ this method of actuation could focus more on coil design to produce stronger electromagnet fields and generate a farther electromagnetic reach. In addition to refining the actuation method, the use of nonlinearly elastic materials could be used in future studies to provide control of the sound frequency produced by the synthetic vocal folds. The use of materials with nonlinear elasticity such as those described in [60] could allow for the change of frequencies of vocal fold vibration due to changes in strain. The combination of all of these changes could ultimately provide more robust control of synthetic vocal fold dynamics which could be used to better design effective treatment options and improve the understanding of voice-related disorders.

Chapter 5

Conclusions

In conclusion, this dissertation focuses on quantifying the elastic properties of porcine vocal folds across the full vocal range, investigating the impact of those elastic properties on vocal fold dynamics during sound production through both experimental dynamic tests as well as through the implementation of a mathematical aeroelastic model of phonation, and exploring manufacturing techniques which could be used to create synthetic vocal folds.

The second chapter describes the experimental work focused on identifying quasi-static continuous model parameters for the elastic properties of porcine vocal folds using DIC methods to calculate strain values during uniaxial tension tests. 16 porcine inferior vocal fold (IVF) samples were extricated after identifying and marking the cartilaginous attachment points and carefully removing extraneous muscle fibers from the folds. The samples were mechanical clamped and mounted on a custom built uniaxial tensile setup. After applying a preload, the samples were stretched to approximately 40% strain while force data was collected via a load cell and images of the speckled superior surface of the samples were captured throughout testing. Engineering strain values were determined by tracking the deformation of the speckle points on the surface of the vocal fold using a digital image correlation (DIC) protocol implemented in MATLAB. The stress-strain results were then modeled by finding the optimized continuous elastic parameters using a similar method as described in [70].

The third chapter details the 2D mathematical fluid-structure model used to better understand the role of vocal fold mechanical properties on the dynamics of tissue during sound production as well as the results of experimental dynamic tests using excised porcine larynges. The 2D aeroelastic model

of phonation was based on the work presented in [9] which investigates how changes in the the vocal fold geometry, tissue properties, and flow characteristics impact vocal fold dynamics. The dynamic experimental tests studied the impact of applying an anterior-posterior strain on porcine larynx samples on the vocal fold dynamic response and especially on the frequency of produced sounds. These tests involved subjecting the porcine larynx samples to a heated and humidified air source which was adjusted to simulate airflow through the trachea and laryngeal cavity. The superior surface of the vocal fold tissue was exposed through dissection while two high-speed cameras (4000 FPS) and a microphone (44100 Hz) were used to continuously record data throughout the tests. The results of the dynamic testing was then compared to the simulated results produced by the aeroelastic model with the goal of better understanding the correlation between varying vocal fold stiffness or elastic modulus (changing with anterior-posterior strain) and the dynamic behavior of the vocal folds during phonation.

The fourth chapter describes the process used to manufacture of synthetic vocal fold models and highlights the dynamic experimental test results using those models. The synthetic models were mounted on the same experimental setup and be subjected to an air source with similar flow characteristics. Manufacturing parameters were iteratively adjusted to span the elastic modulus or stiffness range of the porcine vocal folds as found in the mechanical tensile testing described in Chapter 2. The dynamic results of the synthetic models were also discussed in relation to the porcine vocal folds and the simulated results from the aeroelastic model of phonation.

5.1 Significance of Work

While some prior work has been conducted to investigate porcine vocal fold elasticity [44], the quasi-static elastic parameters in the anterior-posterior direction have not yet been fully described for both the low and higher strain regions. Further, no studies have identified the location of transition points between linear and nonlinear elastic regions of vocal fold properties. Through the uniaxial tension testing, it was found that the stress-strain results indicated that the elastic modulus

of the tissue could be closely modeled by a low-strain linear region followed by an exponential nonlinear region and then a higher strain linear region. The results obtained from this work further the available information on porcine vocal fold elasticity and can be incorporated into models of phonation where the frequency of sound produced changes with strain in the anterior-posterior direction and, as a result, with the vocal fold tissue properties.

Additionally, the dynamic experimental work using excised porcine larynges provides valuable insight into the impact of the nonlinear elastic properties of porcine vocal fold tissue on the frequencies of sound produced during phonation. While other researchers have used porcine and other species larynx samples to investigate vocal fold impact stresses or airflow characteristics which correspond to vocal fold vibration onset, the study presented in this dissertation focuses primarily on the frequency changes produced by porcine vocal folds and sheds new light on relationship between changes in the frequency of vocal fold vibration and changes in elastic properties due to anterior-posterior tissue strain. Furthermore, the experimental results were compared to the simulated vocal fold dynamics using the previously proposed aeroelastic model of phonation in an effort to determine the model's effectiveness at predicting frequency changes across the full vocal range.

Also, this work utilizes additive manufacturing techniques to produce synthetic vocal fold models with the goal of achieving a desired dynamic response across the vocal range of the porcine vocal folds. While progress has been made by other researchers to improve the manufacturing of synthetic vocal fold models, there is still a need to more closely approximate vocal fold dynamics across the full vocal range. The studies presented in this dissertation investigate the impact of the varying elastic properties across the full range of vocal fold elasticity on the frequencies of vibration during sound production and also begin exploring potential actuation methods which could be used to control the dynamic response of the synthetic vocal folds during phonation. While there is still much work need to continue refining the design and control, an improved synthetic vocal fold model has the potential to increase the understanding and possible treatments of numerous voice-related disorders. Finally, the work in this dissertation continues taking steps toward the long-term goal of developing a synthetic vocal fold model that can fully recreate the dynamics of healthy tissue

and can be used as an improved vocal fold prosthesis for total laryngectomy patients.

5.2 Future Work

As highlighted in the previous sections, the work described in this dissertation helps to advance the understanding of vocal fold elastic properties, the role of those elastic properties on vocal fold dynamics, and the manufacturing techniques that can be used to produce synthetic vocal fold models. Despite these advancements, there is still a great deal of work needed to continue understanding vocal fold mechanics and ultimately to work that is required to improve treatment options for individuals struggling with voice-related disorders. The following section highlights some of the work still needed and some of the open questions that still exist.

First, although the work in the dissertation improves the understanding of porcine vocal fold elasticity across the full vocal range, there is still a great deal of work necessary to further understand the strain rate dependency of the tissue, spatially varying properties, and tissue anistropic properties. The study presented in the second chapter focused on only quasi-static uniaxial elastic tensile tests of porcine inferior vocal folds. Generally, biaxial tension tests are preferred to characterize tissue elasticity as they are able to shed light on the isotropic or anisotropic properties of the tissue. Due to geometric constraints which usually require tissue samples to be at least 3×3 cm, many researchers looking to quantify the mechanical properties of the vocal folds have not been able to conduct biaxial tests. Only one study has reported using biaxial tensile tests in [46] where two human cadaveric vocal fold cover layers were tested. Further studies will be needed to not only validate the reported results for the human vocal fold cover layer, but also to investigate inter-species differences in isotropic or anisotropic behavior across the full vocal range. Additionally, as indicated in previous studies [44], porcine vocal folds and likely other species vocal folds are likely strain rate dependent and the nonlinear stress-strain curves, including the elastic parameters of the proposed model, may change at different strain rates. For this reason, future experiments should be conducted to further explore the viscoelasticity of the tissue with regard to the nonlinear elastic

properties. Further, additional tests exploring the spatially varying properties of the vocal folds could also useful. Future studies could explore spatial variations of the tissue through the use of non-contact means of strain measurement such as the DIC methods described in chapter 2.

Next, the impact of the viscoelastic properties, spatially-varying properties, and isotropic or anisotropic behavior could be further explored through additional excised larynx dynamic testing. Using the improved understanding of the tissue properties could also better inform mathematical models such as the one presented in the third chapter which could then be used to improve the accuracy of model predicted vocal fold dynamics. In order to more easily obtain data while studying vocal fold dynamics, more work will be required to improve speckle adherence during dynamic tests. As described previously, improved speckle patterns through the use of different dyes, powders, or other marker techniques could result in higher quality strain maps and provide insight into how vocal fold medial-lateral and inferior-superior strains change during changing vocal fold vibration frequencies. Improving the understanding of vocal fold dynamics through additional excised dynamic larynx testing, could also lead into new manufacturing methods for synthetic vocal folds which can more accurately replicate the dynamics across the full vocal range. Improved models could employ multi-layer techniques and also investigate the use of nonlinearly elastic materials to more closely approximately the dynamics of the vocal fold tissue.

Finally, additional actuation methods for the synthetic vocal folds will need to be explored. While the use of magnetically actuated soft materials shows promise, further work is required to enable frequency modulation and closed-loop control of the vocal fold models. Furthermore, other actuation methods such as the use of embedded shape memory alloys or other smart materials could enable more robust control over the synthetic vocal folds dynamic behavior. In addition, the use of biofeedback as a means of prosthetic control specifically related to voice-production needs to be produced. While some researchers have investigated the neurological mechanisms underlying speech production and communication [92, 93, 94], conventional augmentative and alternative communication (AAC) devices still depend on voluntary motor control by the user in order to provide information to the communication interface, hence they fail for individuals with severe speech and

physical impairments (SSPI) [95]. In the work presented in [92, 93, 94, 96, 97, 98] has advanced the development of brain-machine interfaces for controlled AAC devices using electrocortical electrodes in order to restore more natural control over artificial speech synthesis. More recently, the work in [99] extended the research efforts by investigating non-invasive brain computer interface based control of artificial speech synthesis. In particular, the study in [99] demonstrates the ability to decode EEG signals to provide continuous formant frequency control and allow the user to be directly in control of acoustic speech output. Non-invasive methods such as these combined with a synthetic vocal fold prosthesis that can be actuated to achieve desired the frequency response has the potential to significantly improve treatment options for individuals requiring a laryngectomy or other individuals suffering from voice-related disorders.

The work in this dissertation builds off the work of others and continues improving our understanding of vocal fold mechanical properties and the impact of those properties on the dynamics of sound production. Additionally, preliminary efforts were made to manufacture synthetic vocal fold models that exhibited a desired dynamic behavior. The knowledge gained from these studies can be used to further improve the design of synthetic vocal fold models as well as improve the understanding of vocal fold dynamics, causes of voice disorders, and ultimately to improve the treatment options for individuals struggling with voice-related disorders.

Appendices

Appendix A

Excised Porcine Larynx Spectrograms

A.1 Excised Porcine Sample Test 1

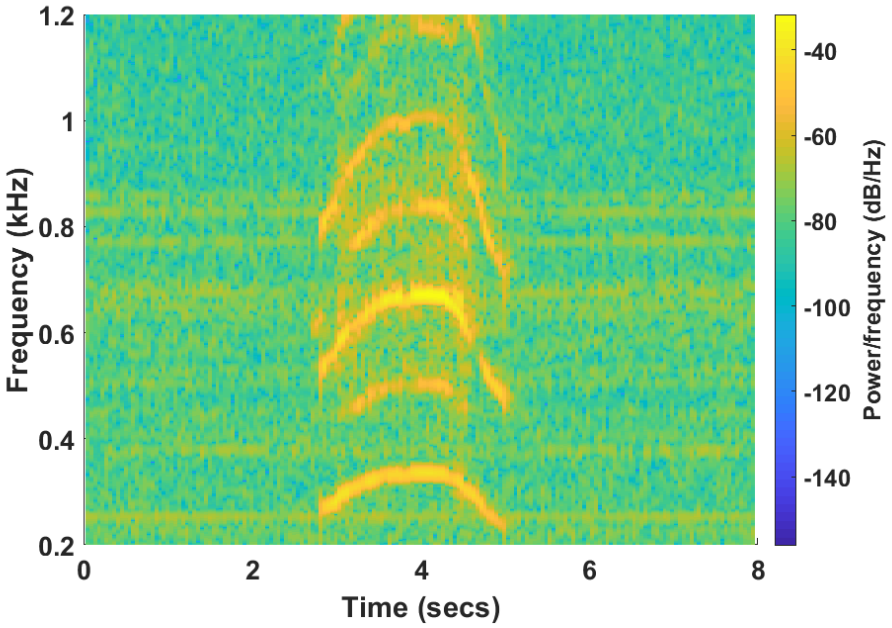

Figure A.1: Spectrogram of an excised porcine larynx when subjected to a sinusoidal dynamixel stretch with an amplitude of 10 mm and a period of 8 seconds.

A.2 Excised Porcine Sample Test 2

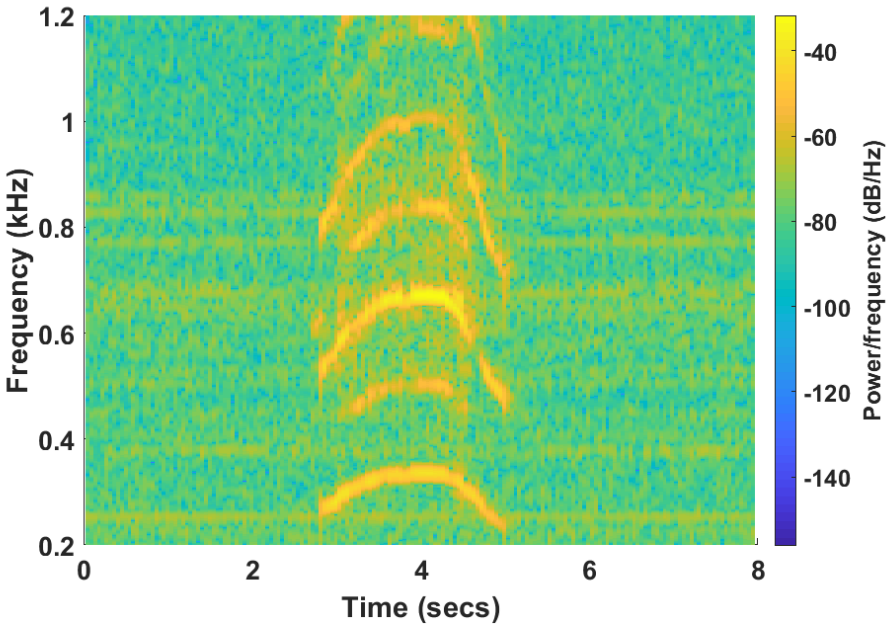

Figure A.2: Spectrogram of an excised porcine larynx when subjected to a sinusoidal dynamixel stretch with an amplitude of 10 mm and a period of 8 seconds.

A.3 Excised Porcine Sample Test 3

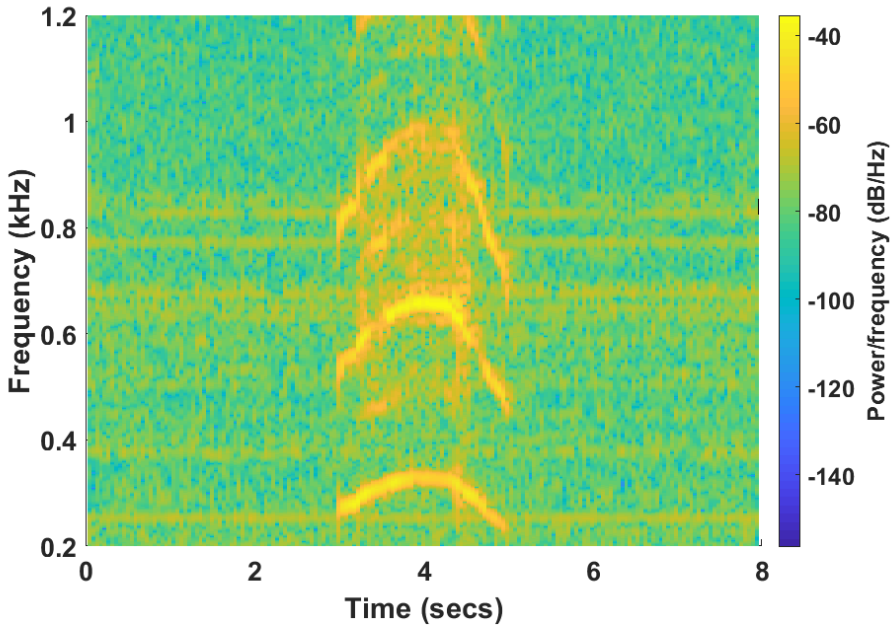

Figure A.3: Spectrogram of an excised porcine larynx when subjected to a sinusoidal dynamixel stretch with an amplitude of 10 mm and a period of 8 seconds.

A.4 Excised Porcine Sample Test 4

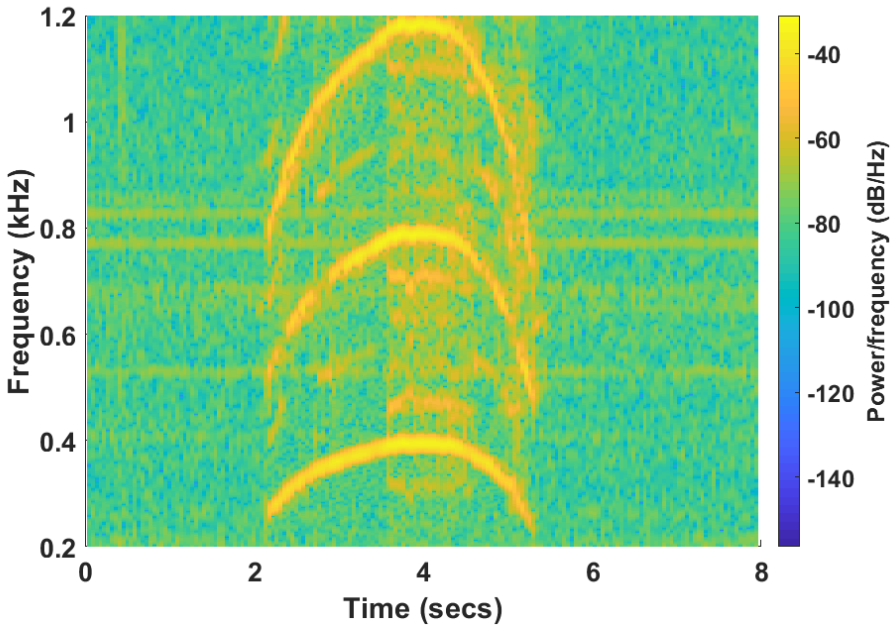

Figure A.4: Spectrogram of an excised porcine larynx when subjected to a sinusoidal dynamixel stretch with an amplitude of 10 mm and a period of 8 seconds.

A.5 Excised Porcine Sample Test 5

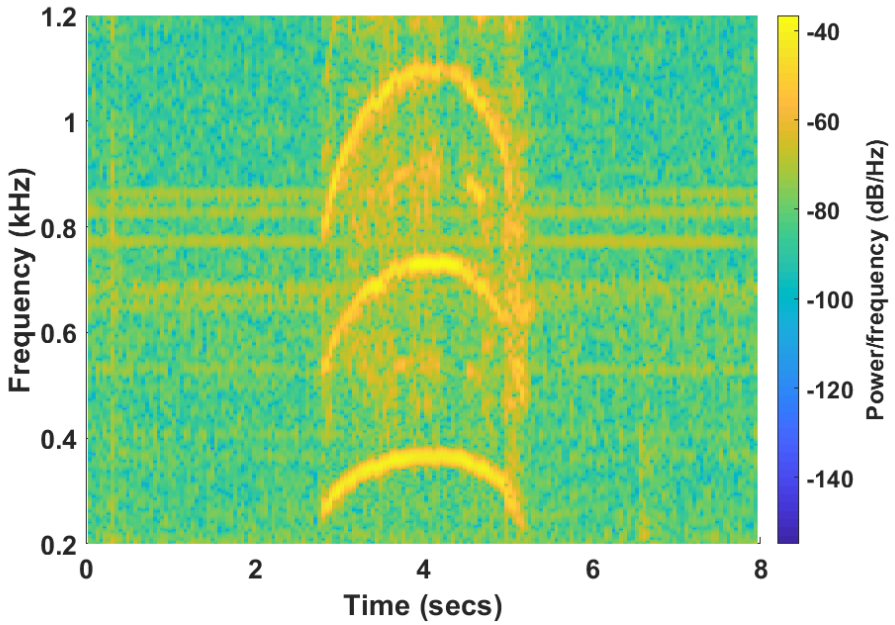

Figure A.5: Spectrogram of an excised porcine larynx when subjected to a sinusoidal dynamixel stretch with an amplitude of 10 mm and a period of 8 seconds.

A.6 Excised Porcine Sample Test 6

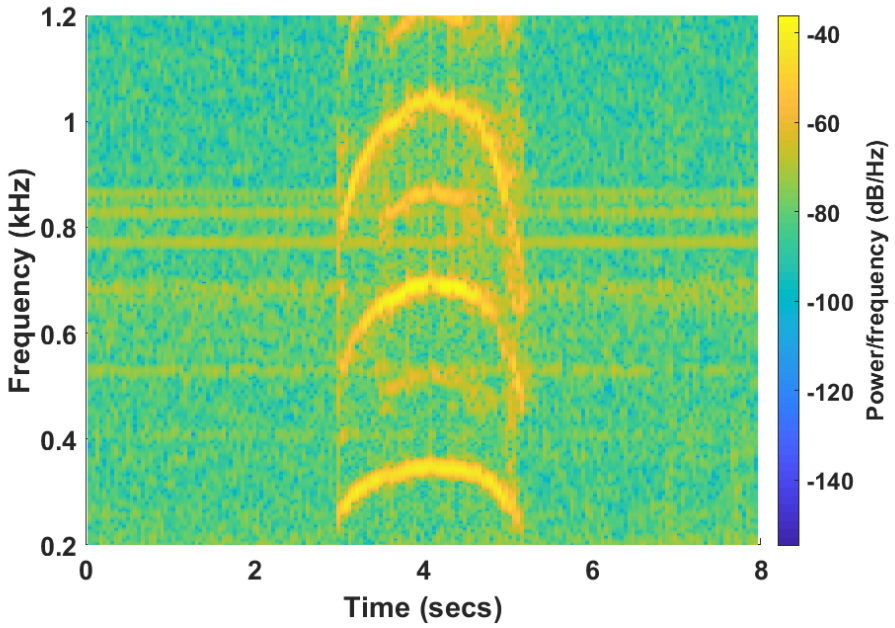

Figure A.6: Spectrogram of an excised porcine larynx when subjected to a sinusoidal dynamixel stretch with an amplitude of 10 mm and a period of 8 seconds.

A.7 Excised Porcine Sample Test 6with 6 second sinusoidal period

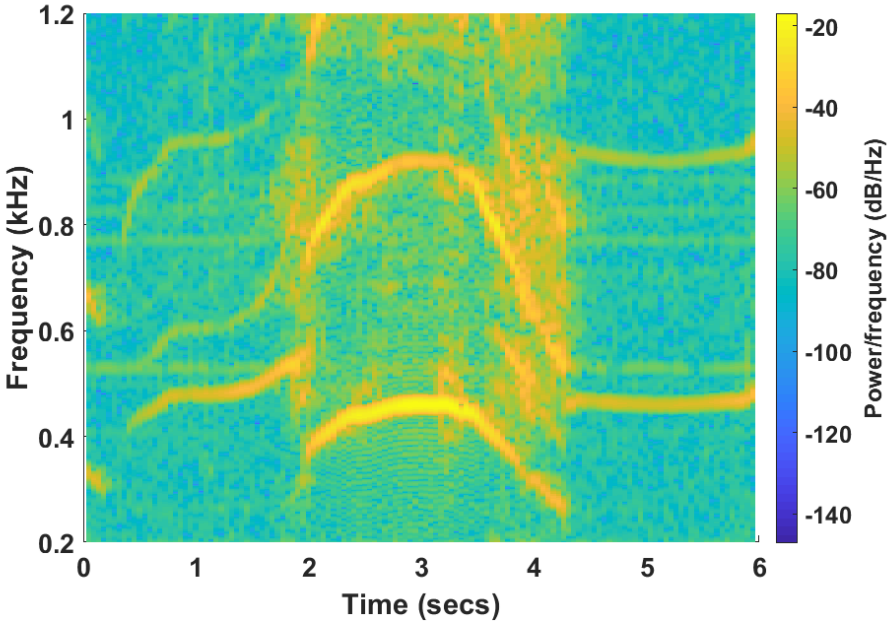

Figure A.7: Spectrogram of an excised porcine larynx when subjected to a sinusoidal dynamixel stretch with an amplitude of 10 mm and a period of 6 seconds.

Appendix B

Excised Porcine Larynx Spectrograms

B.1 Comparison of Aeroelastic Model and Experimental Results

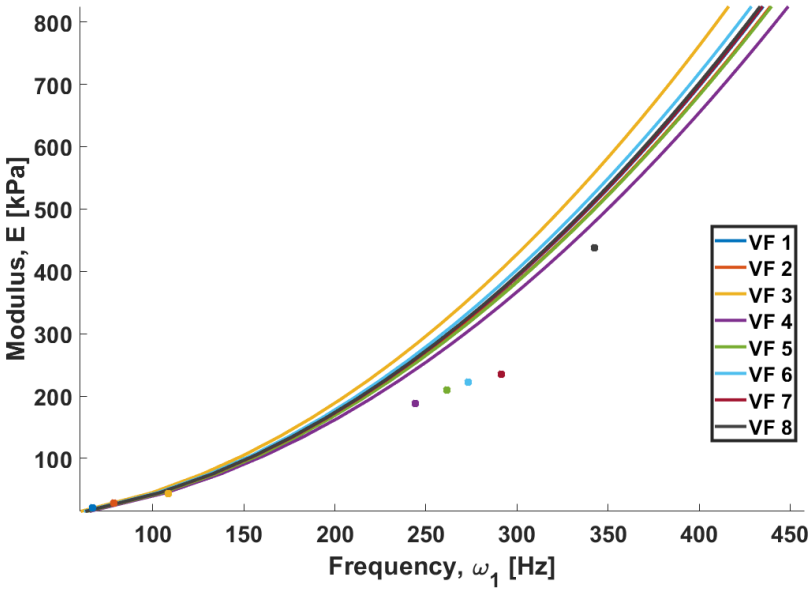

Figure B.1: Comparison of experimental results and aeroelastic model simulated results when evaluated at measured density, Poisson ratio and modulus values.

Bibliography

[1] Lumen Learning, "Overview of body systems - respiratory system." [Online; accessed Sept 16, 2019].

[2] Nucleus Medical Media, "Left thyroid lobectomy with severed left recurrent laryngeal nerve," 2015. [Online; accessed Feb 22, 2019].

[3] R. Arrangoiz, F. Cordera, D. Caba, M. Muñoz, E. Moreno, and E. L. de León, "Comprehensive review of thyroid embryology, anatomy, histology, and physiology for surgeons," *International Journal of Otolaryngology and Head & Neck Surgery*, vol. 7, no. 04, p. 160, 2018.

[4] M. Hirano, "Morphological structure of the vocal cord as a vibrator and its variations," *Folia Phoniatrica et Logopaedica*, vol. 26, no. 2, pp. 89–94, 1974.

[5] B. H. Story, "An overview of the physiology, physics and modeling of the sound source for vowels," *Acoustical Science and Technology*, vol. 23, no. 4, pp. 195–206, 2002.

[6] M. S. Hahn, J. B. Kobler, B. C. Starcher, S. M. Zeitels, and R. Langer, "Quantitative and comparative studies of the vocal fold extracellular matrix i: elastic fibers and hyaluronic acid," *Annals of Otology, Rhinology & Laryngology*, vol. 115, no. 2, pp. 156–164, 2006.

[7] M. S. Hahn, J. B. Kobler, S. M. Zeitels, and R. Langer, "Quantitative and comparative studies of the vocal fold extracellular matrix ii: collagen," *Annals of Otology, Rhinology & Laryngology*, vol. 115, no. 3, pp. 225–232, 2006.

[8] A. K. Miri, "Mechanical characterization of vocal fold tissue: a review study," *Journal of Voice*, vol. 28, no. 6, pp. 657–667, 2014.

[9] Z. Zhang, J. Neubauer, and D. A. Berry, "Physical mechanisms of phonation onset: A lin-

ear stability analysis of an aeroelastic continuum model of phonation," *The Journal of the Acoustical Society of America*, vol. 122, no. 4, pp. 2279–2295, 2007.

[10] F. Alipour and S. Jaiswal, "Glottal airflow resistance in excised pig, sheep, and cow larynges," *Journal of Voice*, vol. 23, no. 1, pp. 40–50, 2009.

[11] F. Alipour and S. Jaiswal, "Phonatory characteristics of excised pig, sheep, and cow larynges," *The Journal of the Acoustical Society of America*, vol. 123, no. 6, pp. 4572–4581, 2008.

[12] F. Alipour, R. C. Scherer, and E. Finnegan, "Pressure-flow relationships during phonation as afunction of adduction," *Journal of Voice*, vol. 11, no. 2, pp. 187–194, 1997.

[13] M. Hirano, Y. Kakita, K. Ohmaru, and S. Kurita, "Structure and mechanical properties of the vocal fold," *Speech Lang*, vol. 7, pp. 271–297, 1982.

[14] F. Alipour-Haghighi and I. R. Titze, "Elastic models of vocal fold tissues," *The Journal of the Acoustical Society of America*, vol. 90, no. 3, pp. 1326–1331, 1991.

[15] G. Burks, R. De Vita, and A. Leonessa, "Characterization of the continuous elastic parameters of porcine vocal folds," *Journal of Voice*, 2018.

[16] H. Liu and M. L. Ng, "Electrolarynx in voice rehabilitation," *Auris Nasus Larynx*, vol. 34, no. 3, pp. 327–332, 2007.

[17] K. Matsui, K. Kimura, A. Pérez, S. Rodríguez, and J. M. Corchado, "Development of electrolarynx by multi-agent technology and mobile devices for prosody control," in *International Conference on Practical Applications of Agents and Multi-Agent Systems*, pp. 54–65, Springer, 2014.

[18] G. S. Meltzner and R. E. Hillman, "Impact of aberrant acoustic properties on the perception of sound quality in electrolarynx speech," *Journal of Speech, Language, and Hearing Research*, vol. 48, no. 4, pp. 766–779, 2005.

[19] R. F. Knight, "Tracheoesophageal voice prosthesis," Feb. 21 1995. US Patent 5,391,205.

[20] L. D'Alatri, F. Bussu, E. Scarano, G. Paludetti, and M. R. Marchese, "Objective and subjective assessment of tracheoesophageal prosthesis voice outcome," *Journal of Voice*, vol. 26, no. 5, pp. 607–613, 2012.

[21] A. Ackerstaff, F. Hilgers, N. Aaronson, and A. Balm, "Communication, functional disorders and lifestyle changes after total laryngectomy," *Clinical Otolaryngology & Allied Sciences*, vol. 19, no. 4, pp. 295–300, 1994.

[22] T. D. Woodard, A. Oplatek, and G. J. Petruzzelli, "Life after total laryngectomy: a measure of long-term survival, function, and quality of life," *Archives of Otolaryngology–Head & Neck Surgery*, vol. 133, no. 6, pp. 526–532, 2007.

[23] S. M. Robertson, J. C. Yeo, C. Dunnet, D. Young, and K. MacKenzie, "Voice, swallowing, and quality of life after total laryngectomy—results of the west of scotland laryngectomy audit," *Head & neck*, vol. 34, no. 1, pp. 59–65, 2012.

[24] K. Izdebski, J. C. Ross, and S. Lee, "Fungal colonization of tracheoesophageal voice prosthesis," *The Laryngoscope*, vol. 97, no. 5, pp. 594–597, 1987.

[25] M. A. Morris, S. K. Meier, J. M. Griffin, M. E. Branda, and S. M. Phelan, "Prevalence and etiologies of adult communication disabilities in the united states: Results from the 2012 national health interview survey," *Disability and health journal*, vol. 9, no. 1, pp. 140–144, 2016.

[26] N. Bhattacharyya, "The prevalence of voice problems among adults in the united states," *The Laryngoscope*, vol. 124, no. 10, pp. 2359–2362, 2014.

[27] P. Carding, M. Bos-Clark, S. Fu, P. Gillivan-Murphy, S. Jones, and C. Walton, "Evaluating the efficacy of voice therapy for functional, organic and neurological voice disorders," *Clinical Otolaryngology*, vol. 42, no. 2, p. 201, 2017.

[28] Y. S. Lee, D. H. Lee, G.-E. Jeong, J. W. Kim, J.-L. Roh, S.-H. Choi, S. Y. Kim, and S. Y. Nam, "Treatment efficacy of voice therapy for vocal fold polyps and factors predictive of its efficacy," *Journal of Voice*, vol. 31, no. 1, pp. 120–e9, 2017.

[29] A. Perry, E. Casey, and S. Cotton, "Quality of life after total laryngectomy: functioning, psychological well-being and self-efficacy," *International journal of language & communication disorders*, vol. 50, no. 4, pp. 467–475, 2015.

[30] I. Titze, *Principles of Voice Production*. Iowa City, IA: The National Center for Voice and Speech, 2000.

[31] S. Kurita, "A comparative study of the layer structure of the vocal fold," *Vocal fold physiology*, pp. 3–21, 1981.

[32] G. Marioni, R. Marchese-Ragona, G. Cartei, F. Marchese, and A. Staffieri, "Current opinion in diagnosis and treatment of laryngeal carcinoma," *Cancer treatment reviews*, vol. 32, no. 7, pp. 504–515, 2006.

[33] S. L. Parker, T. Tong, S. Bolden, and P. A. Wingo, "Cancer statistics, 1997," *CA: A cancer journal for clinicians*, vol. 47, no. 1, pp. 5–27, 1997.

[34] F. L. Ampil, C. A. O. Nathan, G. Caldito, T. F. Lian, R. F. Aarstad, and R. M. Krishnamsetty, "Total laryngectomy and postoperative radiotherapy for t4 laryngeal cancer: a 14-year review," *American journal of otolaryngology*, vol. 25, no. 2, pp. 88–93, 2004.

[35] E. A. Chu and Y. J. Kim, "Laryngeal cancer: diagnosis and preoperative work-up," *Otolaryngologic Clinics of North America*, vol. 41, no. 4, pp. 673–695, 2008.

[36] T. Most, Y. Tobin, and R. C. Mimran, "Acoustic and perceptual characteristics of esophageal and tracheoesophageal speech production," *Journal of communication disorders*, vol. 33, no. 2, pp. 165–181, 2000.

[37] R. E. Hillman, M. J. Walsh, G. T. Wolf, S. G. Fisher, and W. K. Hong, "Functional outcomes following treatment for advanced laryngeal cancer. part i–voice preservation in advanced laryngeal cancer. part ii–laryngectomy rehabilitation: the state of the art in the va system. research speech-language pathologists. department of veterans affairs laryngeal cancer study group.," *The Annals of otology, rhinology & laryngology. Supplement*, vol. 172, pp. 1–27, 1998.

[38] H. Liu, Q. Zhao, M. Wan, and S. Wang, "Enhancement of electrolarynx speech based on auditory masking," *IEEE Transactions on Biomedical Engineering*, vol. 53, no. 5, pp. 865–874, 2006.

[39] E. A. Goldstein, J. T. Heaton, J. B. Kobler, G. B. Stanley, and R. E. Hillman, "Design and implementation of a hands-free electrolarynx device controlled by neck strap muscle electromyographic activity," *IEEE Transactions on Biomedical Engineering*, vol. 51, no. 2, pp. 325–332, 2004.

[40] S. M. Zeitels, A. Blitzer, R. E. Hillman, and R. R. Anderson, "Foresight in laryngology and laryngeal surgery: a 2020 vision," *Annals of Otology, Rhinology & Laryngology*, vol. 116, no. 9, pp. 1–16, 2007.

[41] C. E. Stepp, J. T. Heaton, R. G. Rolland, and R. E. Hillman, "Neck and face surface electromyography for prosthetic voice control after total laryngectomy," *IEEE Transactions on Neural Systems and Rehabilitation Engineering*, vol. 17, no. 2, pp. 146–155, 2009.

[42] J. T. Heaton, M. Robertson, and C. Griffin, "Development of a wireless electromyographically controlled electrolarynx voice prosthesis," in *Engineering in Medicine and Biology Society, EMBC, 2011 Annual International Conference of the IEEE*, pp. 5352–5355, IEEE, 2011.

[43] K. S. Clements, C. H. Rassekh, H. Seikaly, J. A. Hokanson, and K. H. Calhoun, "Communication after laryngectomy: an assessment of patient satisfaction," *Archives of Otolaryngology–Head & Neck Surgery*, vol. 123, no. 5, pp. 493–496, 1997.

[44] F. Alipour, S. Jaiswal, and S. Vigmostad, "Vocal fold elasticity in the pig, sheep, and cow larynges," *Journal of Voice*, vol. 25, no. 2, pp. 130–136, 2011.

[45] J. Kelleher, K. Zhang, T. Siegmund, and R. Chan, "Spatially varying properties of the vocal ligament contribute to its eigenfrequency response," *Journal of the mechanical behavior of biomedical materials*, vol. 3, no. 8, pp. 600–609, 2010.

[46] Z. Zhang, H. Samajder, and J. L. Long, "Biaxial mechanical properties of human vocal fold cover under vocal fold elongation," *The Journal of the Acoustical Society of America*, vol. 142, no. 4, pp. EL356–EL361, 2017.

[47] F. Alipour and S. Vigmostad, "Measurement of vocal folds elastic properties for continuum modeling," *Journal of Voice*, vol. 26, no. 6, pp. 816–e21, 2012.

[48] K. Verdolini, R. Chan, I. R. Titze, M. Hess, and W. Bierhals, "Correspondence of electroglottographic closed quotient to vocal fold impact stress in excised canine larynges," *Journal of Voice*, vol. 12, no. 4, pp. 415–423, 1998.

[49] J. J. Jiang and I. R. Titze, "A methodological study of hemilaryngeal phonation," *The Laryngoscope*, vol. 103, no. 8, pp. 872–882, 1993.

[50] N. P. Solomon, K. Liu, T.-Y. Hsiao, E. S. Luschei, T.-C. Fu, I. R. Titze, and M.-M. Hsu, "Effect of subglottic pressure on fundamental frequency of the canine larynx with active muscle tensions," *Annals of Otology, Rhinology & Laryngology*, vol. 103, no. 10, pp. 817–821, 1994.

[51] D. H. Slavit, R. J. Lipton, and T. V. McCaffrey, "Glottographic analysis of phonation in the excised canine larynx," *Annals of Otology, Rhinology & Laryngology*, vol. 99, no. 5, pp. 396–402, 1990.

[52] H. Bakhshaee, J. Young, J. C. Yang, L. Mongeau, and A. K. Miri, "Determination of strain field on the superior surface of excised larynx vocal folds using dic," *Journal of Voice*, vol. 27, no. 6, pp. 659–667, 2013.

[53] R. C. Scherer, I. R. Titze, and J. F. Curtis, "Pressure-flow relationships in two models of the larynx having rectangular glottal shapes," *The Journal of the Acoustical Society of America*, vol. 73, no. 2, pp. 668–676, 1983.

[54] I. R. Titze, S. S. Schmidt, and M. R. Titze, "Phonation threshold pressure in a physical model of the vocal fold mucosa," *The Journal of the Acoustical Society of America*, vol. 97, no. 5, pp. 3080–3084, 1995.

[55] Z. Zhang, J. Neubauer, and D. A. Berry, "Aerodynamically and acoustically driven modes of vibration in a physical model of the vocal folds," *The Journal of the Acoustical Society of America*, vol. 120, no. 5, pp. 2841–2849, 2006.

[56] Z. Zhang, J. Neubauer, and D. A. Berry, "The influence of subglottal acoustics on laboratory models of phonation," *The Journal of the Acoustical Society of America*, vol. 120, no. 3, pp. 1558–1569, 2006.

[57] S. L. Thomson, L. Mongeau, and S. H. Frankel, "Aerodynamic transfer of energy to the vocal folds," *The Journal of the Acoustical Society of America*, vol. 118, no. 3, pp. 1689–1700, 2005.

[58] P. R. Murray and S. L. Thomson, "Synthetic, multi-layer, self-oscillating vocal fold model fabrication," *JoVE (Journal of Visualized Experiments)*, no. 58, p. e3498, 2011.

[59] B. Pickup and S. Thomson, "Influence of asymmetric stiffness on the structural and aerodynamic response of synthetic vocal fold models," *Journal of biomechanics*, vol. 42, no. 14, pp. 2219–2225, 2009.

[60] P. R. Murray, S. L. Thomson, and M. E. Smith, "A synthetic, self-oscillating vocal fold model platform for studying augmentation injection," *Journal of Voice*, vol. 28, no. 2, pp. 133–143, 2014.

[61] K. Zhang, T. Siegmund, R. W. Chan, and M. Fu, "Predictions of fundamental frequency

changes during phonation based on a biomechanical model of the vocal fold lamina propria," *Journal of Voice*, vol. 23, no. 3, pp. 277–282, 2009.

[62] K. Zhang, T. Siegmund, and R. W. Chan, "A two-layer composite model of the vocal fold lamina propria for fundamental frequency regulation," *The Journal of the Acoustical Society of America*, vol. 122, no. 2, pp. 1090–1101, 2007.

[63] K. Zhang, T. Siegmund, and R. W. Chan, "A constitutive model of the human vocal fold cover for fundamental frequency regulation," *The Journal of the Acoustical Society of America*, vol. 119, no. 2, pp. 1050–1062, 2006.

[64] I. R. Titze and D. W. Martin, "Principles of voice production," 1998.

[65] I. R. Titze, "The physics of small-amplitude oscillation of the vocal folds," *The Journal of the Acoustical Society of America*, vol. 83, no. 4, pp. 1536–1552, 1988.

[66] I. R. Titze, "On the relation between subglottal pressure and fundamental frequency in phonation," *The Journal of the Acoustical Society of America*, vol. 85, no. 2, pp. 901–906, 1989.

[67] Z. Zhang, J. Neubauer, and D. A. Berry, "Influence of vocal fold stiffness and acoustic loading on flow-induced vibration of a single-layer vocal fold model," *Journal of sound and vibration*, vol. 322, no. 1-2, pp. 299–313, 2009.

[68] Z. Zhang, "Characteristics of phonation onset in a two-layer vocal fold model," *The Journal of the Acoustical Society of America*, vol. 125, no. 2, pp. 1091–1102, 2009.

[69] I. R. Titze, "Vocal fold mass is not a useful quantity for describing f0 in vocalization," *Journal of Speech, Language, and Hearing Research*, vol. 54, no. 2, pp. 520–522, 2011.

[70] M. L. Tanaka, C. A. Weisenbach, M. C. Miller, and L. Kuxhaus, "A continuous method to compute model parameters for soft biological materials," *Journal of biomechanical engineering*, vol. 133, no. 7, p. 074502, 2011.

[71] A. H. Lee and D. M. Elliott, "Freezing does not alter multiscale tendon mechanics and damage mechanisms in tension," *Annals of the New York Academy of Sciences*, vol. 1409, no. 1, pp. 85–94, 2017.

[72] G. Lionello, C. Sirieix, and M. Baleani, "An effective procedure to create a speckle pattern on biological soft tissue for digital image correlation measurements," *Journal of the mechanical behavior of biomedical materials*, vol. 39, pp. 1–8, 2014.

[73] C. Eberl, R. Thompson, and D. Gianola, "Digital image correlation and tracking with matlab, matlab file exchange," 2006.

[74] D. Zhang and D. D. Arola, "Applications of digital image correlation to biological tissues," *Journal of Biomedical Optics*, vol. 9, no. 4, pp. 691–699, 2004.

[75] J. D. Humphrey, *Cardiovascular solid mechanics: cells, tissues, and organs*. Springer Science & Business Media, 2013.

[76] F. Alipour-Haghighi and I. R. Titze, "Viscoelastic modeling of canine vocalis muscle in relaxation," *The Journal of the Acoustical Society of America*, vol. 78, no. 6, pp. 1939–1943, 1985.

[77] A. L. Perlman, I. R. Titze, and D. S. Cooper, "Elasticity of canine vocal fold tissue," *Journal of Speech, Language, and Hearing Research*, vol. 27, no. 2, pp. 212–219, 1984.

[78] Z. Zhang and T. Hieu Luu, "Asymmetric vibration in a two-layer vocal fold model with left-right stiffness asymmetry: Experiment and simulation," *The Journal of the Acoustical Society of America*, vol. 132, no. 3, pp. 1626–1635, 2012.

[79] S. H. Gould, *Variational methods for eigenvalue problems: an introduction to the methods of Rayleigh, Ritz, Weinstein, and Aronszajn*. Courier Corporation, 1995.

[80] K. Ishizaka and J. L. Flanagan, "Synthesis of voiced sounds from a two-mass model of the vocal cords," *Bell system technical journal*, vol. 51, no. 6, pp. 1233–1268, 1972.

[81] B. H. Story and I. R. Titze, "Voice simulation with a body-cover model of the vocal folds," *The Journal of the Acoustical Society of America*, vol. 97, no. 2, pp. 1249–1260, 1995.

[82] J. Horáček and J. Švec, "Aeroelastic model of vocal-fold-shaped vibrating element for studying the phonation threshold," *Journal of Fluids and Structures*, vol. 16, no. 7, pp. 931–955, 2002.

[83] K. A. Stevens, S. L. Thomson, M. E. Jetté, and S. L. Thibeault, "Quantification of porcine vocal fold geometry," *Journal of Voice*, vol. 30, no. 4, pp. 416–426, 2016.

[84] J. N. Reddy, "An introduction to the finite element method," *New York*, 1993.

[85] T. L. Hedrick, "Software techniques for two-and three-dimensional kinematic measurements of biological and biomimetic systems," *Bioinspiration & biomimetics*, vol. 3, no. 3, p. 034001, 2008.

[86] E. van Leer and N. Porcaro, "Pervasive diagnosis and rehabilitation of voice disorders: Current status and future directions," in *Proceedings of the 10th EAI International Conference on Pervasive Computing Technologies for Healthcare*, pp. 295–299, ICST (Institute for Computer Sciences, Social-Informatics and …, 2016.

[87] N. Bhattacharyya, "The prevalence of pediatric voice and swallowing problems in the u nited s tates," *The Laryngoscope*, vol. 125, no. 3, pp. 746–750, 2015.

[88] B. J. Benjamin, "Frequency variability in the aged voice," *Journal of Gerontology*, vol. 36, no. 6, pp. 722–726, 1981.

[89] S. M. Shaw, S. L. Thomson, C. Dromey, and S. Smith, "Frequency response of synthetic vocal fold models with linear and nonlinear material properties," *Journal of Speech, Language, and Hearing Research*, 2012.

[90] R. W. Chan and I. R. Titze, "Viscoelastic shear properties of human vocal fold mucosa: Measurement methodology and empirical results," *The Journal of the Acoustical Society of America*, vol. 106, no. 4, pp. 2008–2021, 1999.

[91] L. A. Bloomfield, "Viscoelastic silicon rubber compositions," July 22 2014. US Patent 8,785,507.

[92] J. S. Brumberg, A. Nieto-Castanon, P. R. Kennedy, and F. H. Guenther, "Brain–computer interfaces for speech communication," *Speech communication*, vol. 52, no. 4, pp. 367–379, 2010.

[93] J. S. Brumberg and F. H. Guenther, "Development of speech prostheses: current status and recent advances," *Expert review of medical devices*, vol. 7, no. 5, pp. 667–679, 2010.

[94] J. S. Brumberg, P. R. Kennedy, and F. H. Guenther, "Artificial speech synthesizer control by brain-computer interface," in *Tenth Annual Conference of the International Speech Communication Association*, 2009.

[95] S. Fager, D. R. Beukelman, M. Fried-Oken, T. Jakobs, and J. Baker, "Access interface strategies," *Assistive Technology*, vol. 24, no. 1, pp. 25–33, 2012.

[96] F. H. Guenther, J. S. Brumberg, E. J. Wright, A. Nieto-Castanon, J. A. Tourville, M. Panko, R. Law, S. A. Siebert, J. L. Bartels, D. S. Andreasen, *et al.*, "A wireless brain-machine interface for real-time speech synthesis," *PloS one*, vol. 4, no. 12, p. e8218, 2009.

[97] F. H. Guenther and J. S. Brumberg, "Brain-machine interfaces for real-time speech synthesis," in *2011 Annual International Conference of the IEEE Engineering in Medicine and Biology Society*, pp. 5360–5363, IEEE, 2011.

[98] B. Denby, T. Schultz, K. Honda, T. Hueber, J. M. Gilbert, and J. S. Brumberg, "Silent speech interfaces," *Speech Communication*, vol. 52, no. 4, pp. 270–287, 2010.

[99] J. S. Brumberg, J. D. Burnison, and K. M. Pitt, "Using motor imagery to control brain-computer interfaces for communication," in *International Conference on Augmented Cognition*, pp. 14–25, Springer, 2016.